TECHNISCHE UNIVERSITÄT DARMSTADT

ULB

Intein mediated high throughput screening for bispecific antibodies

Hofmann, Tim Lothar

(2020)

DOI (TUprints): https://doi.org/10.25534/tuprints-00013280

Lizenz:

CC-BY-SA 4.0 International - Creative Commons, Namensnennung, Weitergabe unter gleichen Bedingungen

Publikationstyp: Dissertation

Fachbereich: 07 Fachbereich Chemie

Quelle des Originals: https://tuprints.ulb.tu-darmstadt.de/13280

Intein mediated high throughput screening for bispecific antibodies

TECHNISCHE UNIVERSITÄT DARMSTADT

Vom Fachbereich Chemie
der Technischen Universität Darmstadt

zur Erlangung des Grades
Doctor rerum naturalium (Dr. rer. nat.)

Dissertation
vorgelegt von
Tim Lothar Hofmann
aus
Paderborn

Referent: Prof. Dr. Harald Kolmar
Korreferent: Prof. Dr. Michael Hust

Tag der Einreichung: 29. Mai 2020
Tag der mündlichen Prüfung: 20. Juli 2020

Darmstadt 2020

Die vorliegende Arbeit wurde unter der Leitung von Herrn Prof. Dr. Harald Kolmar am Clemens-Schöpf-Institut für Organische Chemie und Biochemie der Technischen Universität Darmstadt sowie bei Merck KGaA in Darmstadt von April 2017 bis April 2020 angefertigt.

Lizenz: CC-BY-SA 4.0 International - Creative Commons, Namensnennung
https://creativecommons.org/licenses/

Publications or patents derived from the presented work

Parts of this work have been published

Hofmann T, Schmidt J, Ciesielski E, Becker S, Rysiok T, Schütte M, Toleikis L, Kolmar H, Doerner A. Intein mediated high throughput screening for bispecific antibodies. MAbs 12(1), (2020).

Contributions to conferences

Hofmann T., (September 24th, 2019) SMART mAbs: A technology tailored for high throughput functional NBE screening. *Talk at R&D Day, Merck, Darmstadt, Germany.*

Hofmann T., Schmidt J., Doerner A., Becker S., Rysiok T., Schütte M., Toleikis L., Kolmar H. (*November 19th, 2019)* „Intein mediated high throughput screening for bispecific antibodies." *Poster at Protein and Antibody Engineering Summit Europe Conference (PEGS), Lisbon, Portugal.*

Hofmann T., (February 19th, 2020) The Greatest Hits: Enlarging the target screening space for bispecifics by high throughput combination. *Talk at TU Braunschweig, Germany.*

Hofmann T., Schmidt J., Doerner A., Becker S., Rysiok T., Schütte M., Toleikis L., Kolmar H. (*March 5th, 2020)* „Intein mediated high throughput screening for bispecific antibodies." *Poster at ELRIG Forum, Darmstadt, Germany. "Poster award"*

Table of contents

1. Abstract

1.1. Zusammenfassung

Bispezifische Antikörper können verschiedene molekulare Architekturen umfassen, um Wirkungsmechanismen zu erzeugen, die durch monospezifische Antikörper nicht adressiert werden können. Diese Wirkungsmechanismen beinhalten unter anderem die Rekrutierung von Effektorzellen oder die erhöhte Selektivität durch zielgerichtete gleichzeitige Bindung von zwei Antigenen. Die Antikörperforschung in der Pharmaindustrie ist in den letzten Jahren kontinuierlich gewachsen, besonders bispezifische Antikörper mit ihren besonderen Eigenschaften stehen im Fokus. Allerdings ist deren Entwicklung sehr herausfordernd, da die optimale Kombination aus zwei ursprünglich monospezifischen Antikörpern gefunden werden muss. Daher kommt es zu unerwünscht verlängerten Entwicklungszeiten und erhöhtem Kostenaufwand. Für Identifikation und Charakterisierung von Kleinmolekülen und klassischen monoklonalen Antikörpern ist mittlerweile das Hochdurchsatz-Durchmustern eine ausgereifte Disziplin. Die Bereitstellung der sehr hohen Anzahl möglicher bispezifischer Kombinationen für ein solches Vorgehen stellt bis jetzt jedoch einen sehr limitierenden Faktor dar. Es kann nur ein kleiner Teil des zu durchmusternden Raumes abgedeckt werden, da die verschiedenen Kombinationen erst aufwendig einzeln neu kloniert, exprimiert und gereinigt werden müssen. In der vorliegenden Studie wird daher ein neuartiger Hochdurchsatz-Durchmusterungsansatz für bispezifische Antikörper vorgestellt, der diese Limitierungen umgeht und den Durchmusterungsraum um ein Vielfaches erweitert. Er basiert auf der Fähigkeit des Split Inteins *Npu* DnaE, Proteine in-trans zu spleißen. Antikörperfragmente werden dabei in der *Hinge*-Region an einen Teil des jeweiligen Split Inteins fusioniert, um die zwei Fragmente so *in vitro* kombinatorisch ligieren zu können. Diese Methode erlaubt die Rekonstitution einer großen Anzahl verschiedenster bispezifischer Antikörper in kürzester Zeit unter voll automatisierten Bedingungen ohne aufwendige Einzelklonierungen und Herstellungsarbeiten. Verschiedene in dieser Arbeit durch Rekonstitution hergestellte Antikörper zeigen im Vergleich zu genetisch fusioniert hergestellten Referenzen durchweg vergleichbare Bindeverhalten und funktionelle Eigenschaften. Die erarbeitete Rekonstitutionsmethode ist außerdem voll implementierungsfähig für automatisierte Hochdurchsatz-Durchmusterung. Eine potenzielle Hochdurchsatz Zugänglichkeit für 96-Well und 384-Well Platten wurde untersucht und bestätigt und diente als konzeptioneller Beweis für die Funktionsfähigkeit der Methode. Fab-Fragmente wurden mit verschiedenen Fc-Fragmenten kombiniert, als beispielhafte Screening Anwendung für einen schnellen Wechsel der Effektor-Funktion von monoklonalen als auch bispezifischen Antikörpern. Die beschriebene Methode könnte es ermöglichen, bispezifische Antikörper im Hochdurchsatz auf Bindung und zelluläre Funktionalität zu screenen, um die Entwicklungszeiten stark zu verkürzen und die Wahrscheinlichkeit eine optimale bispezifische Kombination zu finden, erhöhen. Diese Methode dient letztlich zur Herstellung besserer Biotherapeutika.

1.2. Abstract

The plethora of bispecific antibody architectures can be harnessed to elicit a broad variety of specific modes of actions, spanning from enhanced selectivity by simultaneous avid binding to distinct effector cell recruitment, all of which cannot be addressed by monospecific antibodies. Pharmaceutical antibody discovery has been evolving and continuously growing over the past decades, moving towards the field of complex biologics and mostly bispecific antibodies. Despite their high potential value, discovery of bispecific antibodies as the identification of the best possible combination of two parental monospecific antibodies, however, remains challenging. Discovery of two sets of monospecific antibodies followed by cloning, production and functional investigation of combinations is tedious and often resulting in undesired extended development times and increased expenses. But although automated high throughput screening approaches have become increasingly relevant and mature for pharmaceutical small molecule and classical antibody discovery, screening of bispecific antibodies is, however, up to now very limited by laborious preparation of the tremendous number of potential bispecific combinations. Therefore, a novel high throughput screening method for bispecific antibodies was developed in this study, allowing a full coverage of the large combinatorial screening space and bypass the afore mentioned limitations. This achievement is realized by the ability of the split intein *Npu* DnaE, to splice proteins in trans. Antibody fragments are fused within the hinge region to a respective split intein part, capable to reconstitute two antibody fragments back to a full-length antibody format *in vitro*, without extensive cloning and manufacturing work. Throughout the study, all reconstituted antibodies remained similarly biologically active in several biochemical and functional cell assays when compared to genetically fused references. The reconstitution method is furthermore amenable for automated high throughput screening providing the possibility to screen for bispecific combinations by combinatorial mixing of antibody fragments. High throughput amenability was investigated for 96 well and 384 well plates confirming both high reconstitution efficiency and reproducibility. Fab fragments were combined with different Fc fragments as exemplary application for fast switch effector function screenings of monoclonal in addition to bispecific antibodies. The method described could enable bispecific antibody high throughput binding and functional cellular screenings to greatly shorten development times and enhance the probability of identifying the optimal combination, ultimately leading to the generation of better biotherapeutics.

2. Introduction

2.1. Antibodies – The modern era of targeted therapy, hallmarks and challenges

The human immune system is the most powerful natural defensive line against threats like pathogens, differentiated by the innate and adaptive immune system. Once being invaded by threats, the immune system recognizes highly conserved pathogen-associated molecular patterns (PAMPs), resulting in an unspecific immediate immune response.[1,2] PAMPs are bound by toll-like receptors (TLRs) and expressed on the cell surface of macrophages or neutrophilic cells, leading to a distribution of proinflammatory cytokines activating the complement system and serving as initial defense mechanism of the innate immune system.[3,4] A more specific immune response is given by the adaptive immune system, which is more delayed due to specific antibody generation by B-lymphocytes. B-lymphocytes carry unique B-cell receptors (BCRs) specifically recognizing antigens. Once bound to an antigen, B-cells are activated in the spleen and lymph nodes and differentiate into lymphoblasts and subsequently into plasma cells.[5] Plasma cells are generating antibodies for the respective antigen that are secreted into the blood. The immune system has the advantage to access a huge antibody repertoire of 10^{10} to 10^{12} possible variants and is therefore known as nature's own antibody discovery platform. Antibodies are able to recognize their targets with high affinity and specificity on the one hand and furthermore trigger immune responses and recruitment of other immune cells, while bound to these targets.[6,7] These two key functions of antibodies are therefore to protect and prevent intruders to invade the immune system. Intruders are pathogens in form of antigens, bacteria or viruses, recognized specifically by antibodies and being marked for destruction or combated by the immune system. A response can unfold in either neutralizing biological activity, target degradation or inducing effector cascades.[8] Since the progression of monoclonal antibodies (mAbs) by Köhler and Milstein in 1975, mAbs have widely been used as therapeutic agents for cancer treatment and various other deaseases.[9]

The first approved and marketed mAb for humans is named muromonab-CD3 (OKT3), directed against the CD3 receptor, which was derived from mouse immunization in 1985.[10,11] Its murine IgG2a backbone caused high immunogenicity, leading to the production of human anti-mouse antibodies (HAMA) and neutralization of OKT3 antibody. Chimeric mAbs are less sensitive against HAMA recognition, bearing murine variable domains grafted on a human antibody backbone.[12–14] Humanized mAbs generated by grafting murine complementary determining region (CDR) loop structures to a human backbone or fully human antibodies produced by transgenic mice after replacement of the appropriate antibody genes to human genes, are advanced ways to bypass immunogenicity.[15] Rituximab was the first in class approved chimeric mAb for cancer treatment, more specifically for hematologic malignancies and approved by the FDA in 1997. Rituximab targets CD20 on the cell surface of B lymphocytes to treat low grade non-Hodgkin lymphoma and was a pioneer antibody in targeted cancer therapy.[16] Other mAbs like Trastuzumab, targeting the growth factor Her2/neu which is overexpressed in breast cancer and other carcinomas or Cetuximab, which is targeting EGFR and is upregulated in ovarian or colorectal cancer, can specifically address their targets on the cancer cell surface. Not only targets on the cell surface can be addressed by mAbs but also blocking cell signaling interactions of the tumor stroma. The vascular endothelial growth factor (VEGF), which is responsible for increased neo angiogenesis facilitating tumor

growth in metastatic colorectal cancer can be blocked specifically by Bevacizumab, approved in 2004 by the FDA, leading to tumor death.[17,18,19]

2.1.1. Antibodies – Structure and function

The two key functions of antibodies discussed earlier can be differentiated by the modular structure. Antibodies, also known as immunoglobulins (Ig), are secreted into blood serum after activation by identical immune cells (B-cells), derived from a unique parental cell. IgG´s are Y shaped heterodimeric glycoproteins and consist of two identical heavy (~50 kDa) and light chains (~25 kDa). The flexible region of an antibody, known as hinge region, consists of 15 aa, allowing for optimal steric configuration to bind an antigen.[20] The hinge region is located between the constant heavy chain (HC) regions C_H1 and C_H2 and connects the two heavy chains via two interchain disulfide bonds. Furthermore, HC linkage is accomplished by non-covalent interactions in the C_H3 region. The light chain (LC) is connected to its corresponding heavy chain (HC) within the constant region (C_H1) via disulfide bond. In humans, two classes of LC´s can be expressed by B-lymphocytes.[21] The constant region (C_L) is subdivided into lambda (λ) and kappa (κ). The full-length IgG format is a monomer with a size of ~150 kDa forming a two-fold symmetrical axis and most frequently used for clinical applications.[22]

Enzymatic fragmentation by papain for example separates the antibody within the upper hinge region into two identical Fab (Fragment of antigen binding) fragments, responsible for antigen binding and one Fc (Fragment crystallizable) fragment.[23] The Fc portion mediates target specific effector functions by interaction with different immune cells. Binding to immune effector cells is maintained by expression of Fcγ-receptors on the cell surface, allowing the Fc portion to attach.[24] Macrophages or neutrophil cells are recruited as a result of Fcγ-receptor binding releasing an immune response. Target cell lysis is also triggered by antibody-dependent cell-mediated cytotoxicity (ADCC) or complement dependent cytotoxicity (CDC).[25]

The Fc portion can furthermore contribute to solubility and stability of the antibody and facilitates a longer half-life before being recycled by the membrane located Fc receptor FcRn (neonatal Fc receptor).[26] The FcRn is mostly expressed by vascular endothelial cells, protecting the antibody from catabolic degradation.[27] The different effector functions are defined by the constant region (C) of the antibodies HC.

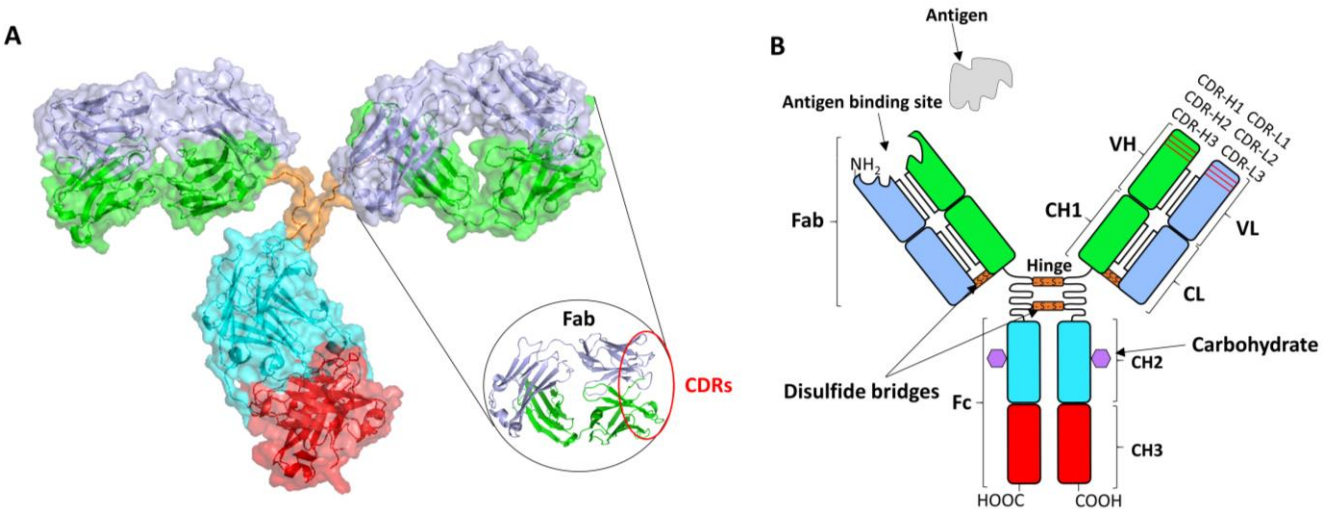

Figure 1: General structure of a full-length IgG antibody depicted as 3D model and illustration including all functional groups.

(A): Cartoon surface model (PDB: 1IGT, colored with PyMOL v. 0.99) of an IgG antibody structure. Variable domains of the heavy chain (V_H) and the C_H1 region is depicted in green. Variable regions of the light chains (V_L) and the corresponding C_H1 domain is depicted in light blue. The flexible hinge region is indicated in orange followed by the C_H2 region in cyan and C_H3 region in red. A ribbon structure of the Fab fragment is highlighted, presenting the complementary determining regions (CDRs) forming loop structures responsible for antigen specific binding. **(B)**: Schematic illustration of an IgG antibody structure following the same color code as A. Additionally the Fc portion is highlighted, triggering Fc effector functions like ADCC or CDC by binding to FcR. Interchain disulfide bonds are depicted in orange within the hinge region and C-terminal between HC and LC. Intrachain disulfide bonds (black square lines) stabilize the domains between the Fab fragment. Glycosylation pattern (lilac hexagon) is illustrated at the C_H2 domain within the Fc portion (Asn297) involved and required for FcγR and complement binding. Red lines N-terminally at the V_H and V_L region indicates the CDRs for antigen recognition.

In general, antibodies belong to the superfamily of immunoglobulins and can be classified into different isotype groups: IgM, IgA, IgG, IgD and IgE. The IgG format can further be subdivided into IgG1-4.[28] Classical antibodies are monospecific and bivalent containing two identical antigen binding sites at the tip of the "Y", known as paratope. The paratope binds specifically a defined epitope of an antigen and is formed N-terminally by combination of variable regions from heavy (V_H) and light chains (V_L) of the Fab fragments. The antibody paratope diversity is generated by random genetic recombination of gene segments encoding for the variable regions (V) of V_H and V_L of germline. Improved diversity (D) is accomplished by random mutations (somatic hypermutations) within the antibody's gene segments (V_H only). The tremendous number of 10^8 to 10^{10} generated variable regions as a result of genetic recombination, called V(D)J recombination.[29,30] More specifically, antigen binding is feasible through the combination of 6 hypervariable loop structures (CDR: Complementary Determining Region) derived from V_H and V_L respectively, flanked and stabilized by 4 constant framework regions (FRs).[31]

2.2. Bispecific antibodies

The idea of bispecific antibodies (bsAbs) was first described in 1960 and it took another 20 years to develop and produce the first monoclonal bsAb by hybridoma technology.[32] Different from monospecific antibodies, the bispecific format consists of two different antigen binding sites and enables the functionality to bind simultaneously two epitopes on one cell surface of tumor cells. Moreover, they can address two different epitopes on two different cells and are therefore mostly used to redirect specific immune effector cells to tumor cells.

Targeting CD3 on $CD8^+$ T cells and EpCAM on human adenocarcinoma cells for example was the first FDA approved bispecific format in 2009, known as catumaxomab.[33] Additionally, the Fc portion is acting as a third binding domain for antigen presenting cells (APC) like macrophages, natural killer cells or dendritic cells via Fc receptor. The ability to form a complex between 3 different cells is called "Triomab".[34] Over 100 bsAb formats have been engineered and since March 2019, 85 bsAbs have been tested in clinical trials, mostly targeting cancer and redirecting immune cells.[35] The bispecific format is a combination of two distinct variable regions derived from the parental monospecific antibodies. The ability to bind simultaneously two different epitopes enables a variety of modes of actions, like an improved cytotoxic potential by bridging cells in-trans, synergistic effects, receptor cross-linking and higher binding specificity. T-cell engagers (TCE), for example, facilitate the redirection of T-cells to tumor cells to engage the formation of an immunological synapse for T-cell activation and target cell killing.[36,37] Other effector cell engagers can be generated, like natural killer cells (NK) for tumor cell killing.[38] Bridging two receptors on one cell surface (in-cis bridging) by biparatopic bsAbs forcing them to crosslink, could lead to either receptor inhibition to reduce tumor growth or receptor activation.[39,40,41] Furthermore, bsAbs can act as immune checkpoint inhibitors by binding to proteins, like PD-1 and PD-L1, on the cell surface like nivolumab or atezolizumab. These checkpoints are key regulators for the immune system and protect the tumor cell from being attacked by effector cells. Inhibition of checkpoints, results in increased antitumor responses.[42] Usually more than one oncogenic signaling pathway needs to be addressed and inhibited, when tackling a cancer disease. Ordinary monoclonal antibodies are restricted to monospecific binding and inhibition of only one signaling pathway, unlike bsAbs or combination therapies.[43–45] However, clinical developments for bsAbs are more time consuming and usually affected by higher manufacturability costs due to the safety and efficacy verification of each mAb and in combination.[46,47]

BsAbs are classified into two major classes. One includes antibodies containing an Fc portion and the other one lacking the Fc region. These classes can hold either a symmetric or asymmetric architecture. Symmetric antibodies contain unmodified assembled heavy chain constant regions. Additional antigen binding sites (valency) at the C- or N-terminus can be included to form a bi- or tetravalent architecture. Dual targeting will influence avidity effects or agonistic properties induced by cross-linking, depending on the valency.[35,48] Asymmetric antibodies contain modifications within the heavy chain constant regions to force correct heterodimerization. Alternatively, antibody fragments like single chain variable fragments (scFv) can be fused together via linker peptide to achieve bispecificity. In general, generating bispecifics requires two heavy and two light chains often resulting in heavy/heavy or heavy/light chain mispairings and homodimerization. Potentially 16 different combinations can occur during antibody expression. Only a theoretical yield of 12.5% for the correctly assembled heterodimer is achieved.[49]

2.2.1. Engineering bispecific antibodies

The first generation of bsAbs was achieved by somatic fusion of two hybridoma cell lines developed by Milstein and Cuello in 1983.[50] Initial issues with correctly assembled heterodimers using these technologies was insufficient. Low yields and heterogeneity through product related impurities, inaccessible for therapeutic applications, required extensive downstream processing. Cognate heavy chain pairing is triggered by the C_H3

domains within an IgG molecule, forming a homodimer interface with high affinity (K_D = 10 pM). Several technologies to avoid chain mispairings have been developed like Knobs into holes, electrostatic steering, DuoBody, BiTE, triomab, common light chains or CrossMabs.[45,51] Pioneer work in forced heterodimerization of two distinct heavy chains was developed by Ridgway and Carter in 1996, inspired by Crick, who proposed a model for packing amino side chains for adjacent coiled coils in 1952.[52,53] The Knobs into holes (KiH) technology is based on the same principle. Traditionally a "knob" is genetically formed by exchanging threonine at position 366 to a bulky amino acid tyrosine within the C_H3 domain of one heavy chain. Additional amino acid exchanges at positions Y407T within the C_H3 domain of the second heavy chain are forming a "hole", forcing both heavy chains to form a sterically complementary interface during expression.[54] The knob and hole forming mutations were refined (T366S, L368A and Y497V) in a rational design in combination with phage display screening, stabilizing the C_H3 heterodimer interface and yielding 92% heterodimer recovery.[55,56] An alternative strategy for Fc mediated heterodimerization embraces the substitution of positively charged lysines at position D339K and E356K in one heavy chain C_H3 domain and negatively charged aspartates at position K409D and K392D located in the other heavy chain C_H3 domain. The altered charged polarity suppresses homodimer formation, although not completely and yielded 90% heterodimer formation.[57,58] Duobodies are IgG-like bsAbs generated by controlled Fab-arm exchange (cFAE) of complementary CH3 mutations. Fab-arm exchange was naturally observed in IgG4 antibodies and the concept was adapted to generate IgG1-like bsAbs. Two antibodies are expressed separately, while destabilizing complementary mutations K409R and F405L within the C_H3 domains favors heterodimerization and reassembly into a bispecific format after mild reduction of the antibodies. However, this technology is limited to a full-length IgG format.[59,60] The strand-exchanged engineered domain (SEED) technology offers the prevention of heavy chain homodimerization during antibody expression. The sequence divergence of the CH3 portion in the Fc region by combining IgG and IgA species yields in 85 to 95% correctly assembled heavy chain pairing.[61] Using heterodimeric Fc platforms, reduces the number of different potential chain combinations from 10 to 4 during antibody expression. Although using the SEED technology often requires an additional purification tag, for instance C-terminally at the C_H3 domain, for purification of homodimer impurities.

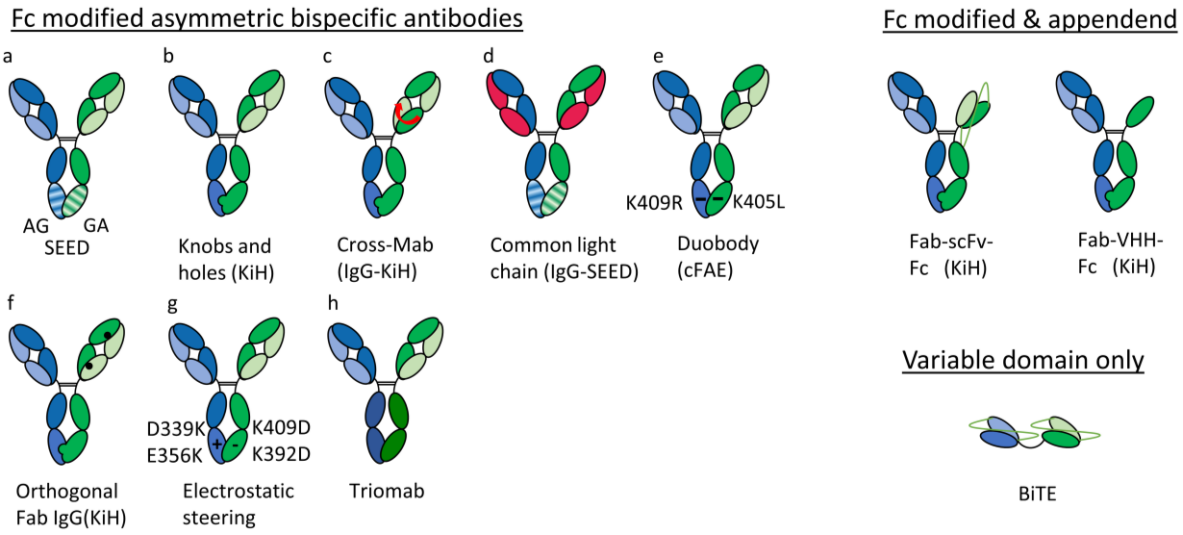

Figure 2: Generation of bispecific antibodies using different technologies for correct heavy chain heterodimerization and light chain pairing for Fc modified or Fc modified and appended asymmetric bsAbs.

Fc modified asymmetric bsAbs; a: Strand exchanged engineered domains (SEED) technology combines IgG and IgA species within the C_H3 portion for correctly assembled heavy chains discovered by David and coworkers in 2010. **b**: Knobs into holes offer correct heterodimerization by bulky amino acid residues forming either a hole or a knob respectively within the C_H3 domain. **c**: CrossMabs relocate the C_H1 domain to the CL region, while the CL is swapped to the C_H1 region for correct LC pairing. V_H and V_L regions are kept consistent. In combination with Knobs into holes, CrossMabs offer both correct HC and LC pairing. **d**: Common light chains (cLCs) can pair with more than one HC. **e**: Duobodies are IgG-like bsAbs generated by controlled Fab-arm exchange (cFAE) of complementary C_H3 mutations. **f**: Lewis and coworkers introduced mutations in the C_H1 and C_L domain of a Fab fragment to ensure correctly assembled LC pairing. **g**: Electrostatic steering introduces oppositely charged amino acids in the C_H3 domain, while forcing a homodimerization to reject. **h**: A Triomab consists of two half-antibodies derived from two different species, typically a rat/mouse hybrid, for correctly species restricted HC and LC pairing. Triomabs can bind to two distinct targets further supported by FcγR binding by the Fc portion, triggering effector functions. **Fc modified and appended bsAbs**: Fab arms can be exchanged to either an scFv or VHH to avoid HC-LC mispairing. **Variable domain only**: BiTEs are lacking the Fc portion and connect dual scFv fragments via peptide linker to avoid all kind of chain mispairings.

Nevertheless, the major bottleneck of all Fc-mediated heterodimerization technologies involves incorrect heavy and light chain pairing. Remedies for correct assembly of heavy and light chains have been achieved by using common light chains, CrossMabs or BiTEs (Bi-specific T-cell engagers). The BiTE technology is lacking the Fc portion and connects dual scFv fragments via peptide linker to avoid all kind of chain mispairings. The first approved BiTE antibody blinatumomab was a milestone in bispecific engineering in 2015 and is one out of two bsAbs on the market for cancer indications.[62,63] CrossMabs consist of an exchanged C_H1 and C_L domain to ensure efficient and specific dimerization of heavy and light chain. The C_H1 domain is relocated in the C_L region, while the C_L is swapped to the C_H1 region. V_H and V_L regions are kept consistent. In combination with KiH, IgG-like bsAbs can be generated without any chain mispairings.[45,64] A simple solution to avoid chain mispairing is to change the format into a less complex architecture like scFvs or single domain antibodies (VHH) instead of Fabs or bsAbs lacking the Fc region. The Fc region can be immunogenic and triggers effector functions like ADCC or CDC through activated Fc receptors, which can be beneficial or disturbing depending on the therapeutic application. However, the Fc region can contribute to solubility and stability of the antibody and facilitates a longer half-life before being recycled by the FcRn receptor. The ability of the Fc region to bind protein A is another advantage while purifying antibodies without the addition of distracting purification tags. A prominent strategy to generate bsAbs and avoid heavy and light chain mispairings are the application of common light chains (cLC). The LC is able to pair with more than one HC and was first described by Merchant *et al.* in 1998,

based on observations that antibodies derived from a phage display campaign, often use the same V_L domain, when directed against several antigens.[54,65] Specific tumor antigen related binders are screened after immunization of transgenic rodents carrying a human HC repertoire with a cLC. Bispecific antibody generation by protein trans splicing (BAPTS) is the most recent described approach, suppressing incorrect heavy and light chain pairing.[66] Split inteins are divided into N- and C-terminal fragments. These fragments are able to form a reconstituted canonical intein complex after reunification, followed by fusion of two antibody fragments and leaving a stable irreversible peptide bond, resulting in correctly paired mAb arms.[67]

In summary, the marketability of bsAbs consumed several billion dollars and the clinical development pipeline expanded from 5 bsAbs in 2010 to 28 bsAbs in 2019.[35] Nevertheless, the right combination of two binding domains must be identified for the right biological activity and results in extensive screening campaigns or empirical selection strategies. Every combination can affect the design parameters for each arm, which effects the affinity, cross-linking and specificity.

2.3. Antibody screening and lead generation

During the last decades, mAbs were applied very successfully as therapeutic modalities.[19] Pharmaceutical mAb discovery typically comprises immunization campaigns in transgenic rodents followed by single B-cell cloning or display of antibody fragments on the surface of yeast or phage.[68] The path of discovering a new therapeutic monoclonal or bispecifc antibody underlies several stages, until entering the clinical trials. A traditional antibody screening approach starting by either phage or yeast display offers a unique antibody selection of potential antibody candidates, typically derived in a scFv or VHH format.[69,70] Phage display is based on a bacterial host system yielding high amounts of target protein and typically yields in a large repertoire of binders. Therefore, high throughput bacterial expression in *E. coli* in combination with high throughput binding and competition assays to their respective antigens leads to a first discrimination of potential antibody hit candidates.[71] The hit candidates are reproduced in medium throughput expression runs followed by purification and another round of binding, competition and first cell-based assays, to further narrow down the best candidates. A re-formatting step into a natural full-length IgG format is essential, as already mentioned before, for further validation of potential lead candidates. The re-formatting step represents a bottleneck in traditional antibody screening campaigns, limited by extensive cloning, expression and purification work of all selected hit candidates.[72,73] Therefore, only a very concise antibody repertoire can be considered to become a final lead candidate.

The full-length IgG candidates are then expressed and purified in low throughput for concluding cell based functional assay validation and finally the generation of the desired lead candidate (Figure 3).[74]

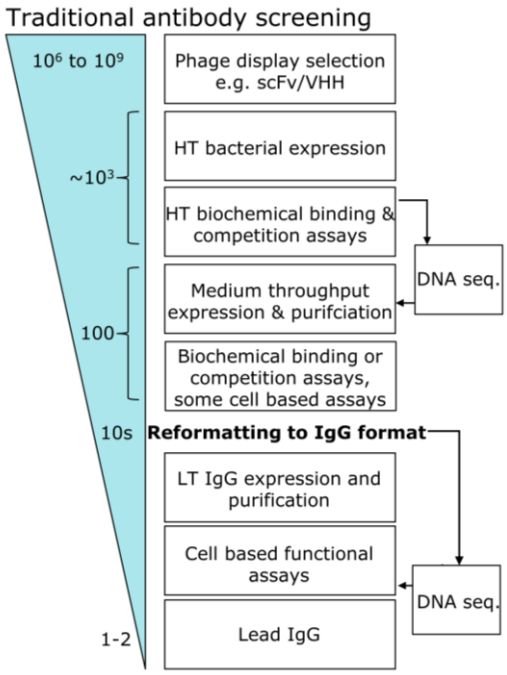

Figure 3: Traditional antibody screening strategy based on a phage display selection until final lead candidate identification.

Unique hits are generated by *in vitro* selection tools like phage display and analyzed in biochemical binding and competition assays. After optimization, expression and purification generated hits are analyzed in functional cell-based assays for effectiveness. Re-formatting into a natural full-length IgG format represents a bottleneck in traditional antibody screening campaigns before the selection of a final lead candidate. HT: High throughput, LT: Low throughput, DNA seq: DNA sequencing. Figure is adapted from Xiao *et al.*[74]

Although antibodies are well investigated and still a rapidly growing field in drug discovery, mAbs lack additional therapeutic potential due to their monospecific nature and limited range of effector functions.[75] Improvements in antibody engineering paved the way for more complex molecules and modified structures for extended therapeutic applications. Effector cell recruitment, enhanced selectivity by avid simultaneous binding, conditional antagonism and targeted delivery of immunomodulators, is broadening the envisioned mode of action to functionalities not supported by mAbs.[32] However, finding hit candidates for complex therapeutic antibody molecules is challenging and requires defined and extended research activities during lead discovery. The next chapter will give insights into bispecific antibody high throughput screening (HTS) for lead discovery.

2.3.1. High throughput screening for bispecific antibodies and complex NBEs

Nowadays antibody hit discovery is linked to modern age technologies like HTS approaches and automation. Since HTS introduction in 1990, a lot of development work was performed and started a new era for improved antibody discovery in pharmaceutical industry.[76] It is important to apply HTS in the early stage of antibody discovery, to increase the chance to enrich hit candidates and selection of lead candidates.[77,78–80] Despite antibodies showing great success in clinical trials, still a tremendous number of 80 to 85% discovered mAbs and also bsAbs are discontinued in lead discovery, due to lack of efficacy. The rate of failing antibodies in clinical trials indicate the importance to enlarge the antibody variety for screening. Screening against biological targets combined with automation, miniaturization and large-scale data analysis became more suitable and cost efficient over the years.[81] This is supported by 74 antibody lead candidates in clinical phases extended by two accredited

marketed drugs discovered by HTS campaigns since 2003.[79,80,82] Nowadays, HTS is the starting point in drug discovery and there is a strong demand in screening the increasing numbers of biological targets to find the optimal lead candidate.[32]

Complex molecules or formats for extended therapeutic applications, like bsAbs, have more clinically relevance compared to mAbs and are more difficult to generate and screen for, due to earlier described reasons. Although elegant approaches for the generation of bsAbs using knob-into-hole, electrostatic steering, DuoMab, SEED, triomab, as well as common light-heavy chain approaches, κλ-bodies or CrossMabs are not suitable for extensive combinatorial screening campaigns.[32,64,83] These technologies are limited to generated combinations of already existing bispecific entities. So far, blinatumomab and emicizumab are only two bsAbs that have been approved by the FDA worldwide during the last decades, indicating the need for new screening attempts.[41,84] Furthermore, the full-length IgG format is still predominantly used in clinical development of candidates. Re-formatting into a full-length IgG-like format, means always a risk in changing the biological and biophysical antibody properties, like decreasing affinity or biological activity, which would lead to further engineering or optimization work.[85] Especially T-cell engagers display a very specific design and need flexibility and space between the two antigen binding arms to redirect T-cells to cancer cells to engage the formation of an immunological synapse for T-cell activation and target cell killing.[86] It would therefore be desirable to use a full-length format already in the early stage of antibody discovery.[74] Unfortunately, the unique hits, created in initial screenings, are usually not based on an IgG like molecule and often derived from bacterial hosts.[87] The production of full-length antibodies in *E. coli* usually results in misfolded protein, low yields and the lack of glycosylation. Therefore, the most common formats for initial hit screenings are antibody fragments like scFvs or VHHs, which fold more efficiently and are being produced in high yields using bacterial hosts.[88] Nevertheless, non-natural surrogate formats like scFv suffer from aggregation and might result in false positive or negative results. Furthermore, they are not compatible to modes of actions, which are dependent on Fc mediated effector functions or bivalent binding.[89]

Screening and therapeutic development of asymmetric full-length IgG bsAbs requires optimization work through molecular engineering for lead candidate generation and selection. To find the best combination of two binding moieties for a bispecific antibody, a large number of monospecific antibodies against their distinct antigen targets must be identified as a first step. Engineering the two best monospecific variants into a bispecific format does not necessarily lead to the best combination for a bsAb approach, to find the final lead candidate. Furthermore, higher binding affinities do not automatically lead to higher bio functional activity. After screening for binding to the respective antigens of both parental monospecific antibodies, a combination into a bispecific format requires antibody engineering methods, like described earlier, for correctly assembled bsAbs. Sampei *et al.* expressed 200 x 200 monospecific antibodies directed against FIXa and FX with different LCs from an immunization campaign to generate 40 000 individual bispecific combinations to find their final lead anti-FIXa/FX bsAb, resulting in massive time-consuming cloning, expression and purification. The full-length asymmetric IgG antibody format was preferred due to the ability to bind both targets in combination enabling long half-life based on the IgG structure and mimic FVIII cofactor activity.

When identifying the single binding moieties of an envisioned bispecific antibody, approaches mainly focus on reduction of individual clone numbers by filters such as affinity, target specificity, optimally domain or epitope mapping. Most intended modes of actions are not conveyed by a single binding moiety, but through the combination to be identified, for example selective effector cell recruitment, target-specific Fc mediated effector functions or enhanced selectivity binding by avidity [25,86]. When attempting to screen a desirable high number of combinations, for example 200 times 200 binding moiety combinations, multiple cloning, expression and purification steps represent a bottleneck for the production, even when multi-parallel small-scale expression methodologies are in place as shown in the study of Sampei *et al.* Therefore, the number of combinations or bsAbs finally generated is usually only a small fraction of the selected repertoire [74]. The group of Sampei *et al.* found 96 bispecific combinations out of 40 000 variants mimicking FVIII activity but suffering from massive chain mispairings tending to undergo multidimensional optimization processes to improve manufacturability and therapeutic potential. This low number of potential variants indicate the importance to screen for the maximum number of combinations to find a lead bsAb.

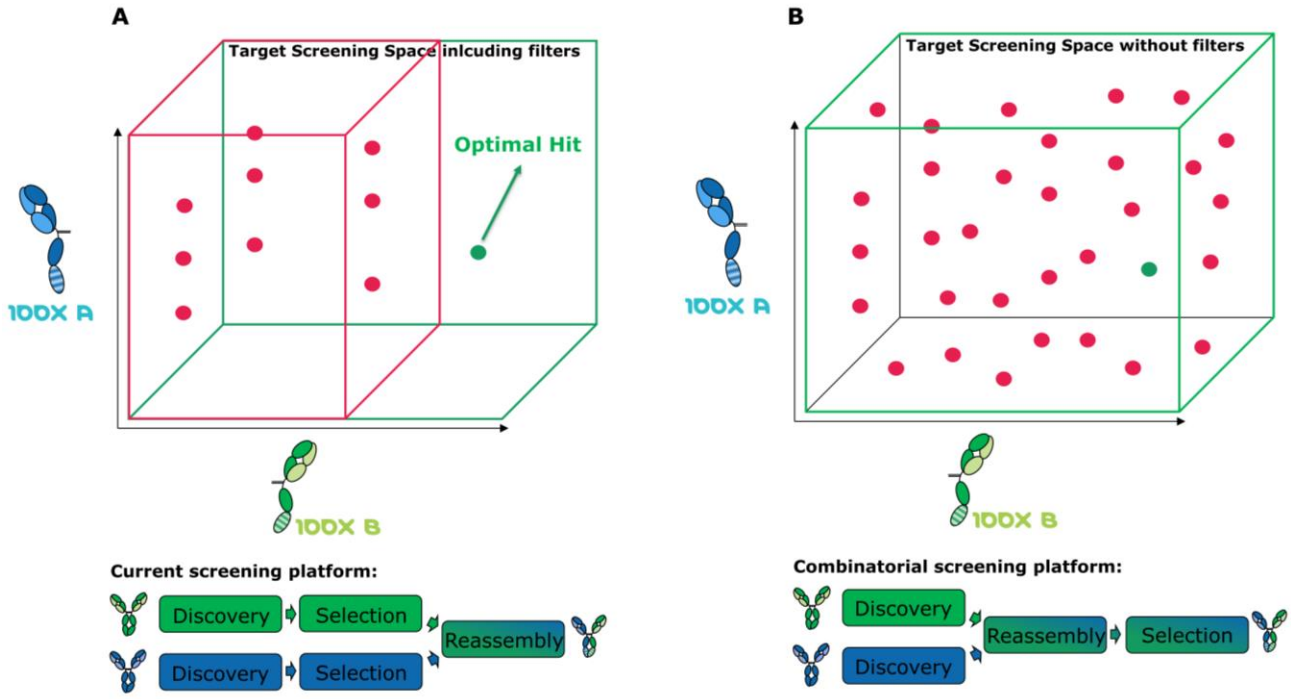

Figure 4: Target screening space during antibody hit discovery for a bispecific format using traditional screening and advanced combinatorial screening methods.

(A) Traditional screening of a bsAb combination filtered and reduced by affinity and target specificity (red box) due to target screening space limitations of a traditional screening platform. Covering the whole target screening space (green box) is a bottleneck and leads to multiple cloning, expression and purification steps after selection. The optimal combination cannot be identified, based on missing screening information of the whole target space. **(B)** Desired combinatorial screening approach to fully cover the whole target screening space with all possible combinations by reassembly both binding moieties directly after discovery. No filters need to be considered. Red dots: Hit candidate identifications for several bispecific combinations with different affinities. Green dot: optimal hit candidate; best affinity and efficacy for the relevant approach.

Finally, most bsAb engineering approaches include comparisons of several formats to further optimize the intended biological mode of action, which in addition enlarge the screening space or efforts, respectively.

A broadly applicable method enabling high throughput binding and functional cellular bsAb screenings has to date not been described but would greatly shorten development times for a wide variety of complex NBEs and enhance the probability of identifying the optimal combination, ultimately leading to the generation of better biotherapeutics (Figure 4).

2.4. Protein conjugation

Molecular engineering is a subtle technology for modifying proteins, improving biophysical properties like thermostability, solubility or tagging biomolecules with fluorophores, drugs and polymers. Since cytotoxic drugs can be efficiently conjugated to antibodies, offering a better safety potential due to the high and specific affinity of antibodies compared to non-targeted cytotoxic molecules, protein conjugation techniques expanded fundamentally.[90] Enzymatic or chemical alteration of biomolecules like antibodies exhibit great potential for new therapeutic approaches in cancer therapy.[91,92] As previously discussed, screening bispecific antibody candidates for the most suitable combination of both binding moieties requires elaborative technologies to gain success. The following chapter deals with protein conjugation technologies predominantly used for antibody engineering.

2.4.1. Microbial Transglutaminase (mTGase)

Transglutaminases (TGs) belong to the group of γ-glutamyltransferases and catalyze the isopeptide bond formation between two proteins. The transamidation reaction involves the crosslinking of γ-glutamyl-glutamine side chains (acyl-donor) and ε-amino groups of lysines (acyl-acceptors) forming a stable inter- or intramolecular isopeptide bond.[93] However, by-products may also occur when glutamine enters a deamidation reaction due to the lack of primary amines or lysine residues forming glutamic acid.[94] The enzyme purity dictates amongst others the content of side reactions, leading to changes in protein charge and therefore protein solubility.[95] The first transglutaminase was discovered in 1989 in *Streptomyces mobaraensis* by Ando and coworkers and was widely used in food industry, to improve functional properties.[96] The enzymatic reaction is well investigated, and transglutaminases are used for cross-linking fibrin in blood coagulation through factor XIII for example. Transglutaminases derived from bacteria (mTGase) can be produced in large quantities in *E. coli* and offer several advantages over TGase found in mammalia.[97,98] mTGase exhibits a smaller molecular weight and is not dependent on any cofactors like calcium, compared to mammalian enzymes. Furthermore, they offer improved stability, performance and reduced deamidation activity. mTGase derived from *Streptomyces mobaraensis* is recombinantly expressed with an amino terminal pro peptide, inhibiting TGase activity and improving the thermostability.[99] The pro peptide is cleaved specifically by metalloproteases supported by a tripeptidyl aminopeptidase, releasing the active form of the enzyme to bypass secretion of inactive enzyme.[100] Transglutaminases accept a variety of substrates and are often used for biotechnological applications like cross-linking heterogeneous polymers or ligation of biomolecules. They became an important tool for site specific conjugation of antibodies to generate antibody drug conjugates (ADCs).[101,102]

However, the glycosylation of an antibody is causing sterically obstruction of the transamidation reaction and either needs to be removed by deglycosylation enzymes or an additional glutamine recognition tag has to be

introduced elsewhere for specific conjugation.[103] A prominent recognition tag for antibody conjugation via mTGase is LLQGA, but this tag is restricted mostly to conjugations C-terminally of the Fc portion or the LC of an antibody. A lot of development work has been performed to engineer the enzyme regarding improved catalytic performance and alternative recognition sequences.[104] One of the major drawbacks of mTGase is its unselective substrate specificity, resulting in unspecific conjugation, making it inaccessible for certain protein ligation reactions.

2.4.2. SpyTag/SpyCatcher

The SpyTag/SpyCatcher system is used as a protein bioconjugation tool derived from the fibronectin binding protein (FbaB) of *Streptococcus pyogenes*. FbaB possesses a collagen adhesin domain (CnaB2) exhibiting an internal isopetide bond between amino acids Lys31 and Asp117.[105] The domain is split between Lys and Asp into two fragments resulting in an N-terminal fragment (SpyCatcher) of 138 aa and a C-terminal fragment (SpyTag) of 13 aa. Reconstitution of these fragments spontaneously form a peptide bond between Lys and Asp bringing the fragments in close proximity and optimal orientation. Reconstitution is initiated by forming a double hydrogen bond between Glu77 and Asp117 facilitating the peptide bond formation by nucleophilic attack and forming a zwitterionic intermediate. Glu77 is transferring protons to form a neutral tetrahedral intermediate, subsequently resolved when water is released. Finally, the peptide bond between Lys31 and Asp117 is formed.[106–108] The reconstitution of SpyTag and SpyCatcher supports a broad range of pH (5 to 8) values and temperatures (4 to 37°C) and works under redox conditions and harsh conditions using solutions with detergents. The ligation reaction rate is described as very fast and efficient with $t_{1/2}$ = 74 s using both fragments and a molar concentration of 10 µM.[109] The technology is a promising tool for biotechnological applications. Recombinant proteins can be ligated through a peptide bond formation, or proteins can be stabilized by protein cyclization. The SpyTag/SpyCatcher fragments can either be fused C- or N-terminally to recombinant proteins or to internal positions within the protein, unlike split inteins, which are restricted to C- or N-terminal fusions.[110] Furthermore, the SpyTag approach can be used to generate site specific conjugated ADCs with high efficiency.[111] However, the SpyTag/SpyCatcher technology is leaving a peptide imprint by incorporation of 151 aa to the protein of interest. A truncated version of an N-terminal SpyCatcher fragment (32 aa shorter) has been developed by Li *et al.* to decrease an immune response in mice and to shorten the incorporated aa between the reconstituted proteins. The truncated SpyCatcher version still remains in the reconstituted protein of interest and modifies the size by addition of 13 kDa and might lead to conformational changes, obstruction or biological functionality.[109]

2.4.3. Sortase

Sortases are membrane associated bacterial enzymes and catalyze a reaction called transpeptidation. They are located in the plasma membrane of gram-positive bacteria and anchor secreted proteins covalently to the cell wall. Sortase A (SrtA) from *Staphylococcus aureus* is the best characterized sortase and was first described in 2004 for biotechnological applications. The transpeptidation reaction is most frequently used for protein ligation or protein labeling and further known as "Sortagging".[112,113] Protein ligation depends on an acyl donor and

acceptor. In presence of a short peptide sequence LPXTG (substrate, acyl donor), while X can refer to any amino acid, a cysteine is activated in the active site and peptide bond cleavage between threonine and glycine is catalyzed forming a linked thioester acyl enzyme intermediate. The enzyme intermediate is then attacked by an amino glycine and resolves in the site-specific ligation of acyl donor and acceptor generating a peptide bond. The transpeptidation reaction of wild type SrtA suffers from poor reaction rates and depends on Ca^{2+} as a cofactor to activate the cysteine in the active side.[114] Engineered versions of SrtA, by incorporating several amino acid exchanges (P94R/D160N/D165A/ K190E/K196T) lead to improved reaction rates up to 120-fold faster, compared to wild type SrtA.[115] Furthermore, the engineered SrtA is Ca^{2+} independent which makes it more interesting for protein tagging. However, the overall total yield of the wild type version for ligation products is still higher and mutated sortase versions tend to higher undesired hydrolytic or oligomeric side products.[114] A significant molar surplus (1:20) of either the acyl donor or acceptor is needed for efficient protein ligation because the reaction is reversible and depends on an equilibrium. Sometimes it can be challenging to produce either the acyl donor or acceptor in large quantities and furthermore, byproducts like accumulated amino glycine peptide fragments are released, forcing a reversed transpeptidation reaction.[116] These byproducts can be removed extensively by dialysis or centrifugal filtration, to limit reversibility of the reaction, allowing to use ligation partners at nearly equimolar ratios. Changing the recognition sequence from LPXTG to LPXTA for example or including an unreactive β-hairpin close to the recognition sequence, can further decrease the reversed transpeptidation or formation of byproducts and expand the substrate range.[117] Sortagging was established for the generation of site specific conjugated antibodies, yet holding notable limitations as mentioned before.[118] Using split inteins with high sequence specificity and no dependency on any cofactors, external energy sources or surplus of reactants, offer a simpler and more elegant way for protein ligation or labeling strategies compared to sortases, transglutaminases or similar ligation techniques described before.

2.4.4. Split Inteins

Inteins are naturally occurring auto catalytic domains found in every organism (archaea, bacteria and eukaryotes) and were first discovered in 1988 and described by Hirata *et al.* and Kane *et al.* in 1990.[119,120] Inteins replicate themselves within genomes and have no other known regulatory or functional role for the host organism and are therefore often described as "selfish" or "parasites".[121] Intein splicing occurs on the protein level and the intervening protein sequences are embedded in host proteins and catalyze the splicing reaction to excise the intein out of the host protein very specifically. Inteins undergo a well-known single turnover reaction, similar to classical enzyme catalysis, that do not depend on co factors like ATP or energy sources. Flanking N- and C-extein sequences are joined together by a native stable peptide bond catalyzed by the intein splicing reaction.[122] Intein splicing replicates the intein within genomes and has no other known regulatory or functional role for the host organism. Therefore, inteins are often described as "selfish" or "parasites", incorporating themselves into the genome and splicing themselves out for replication.[121] They are divided into three different groups. Classical or bifunctional inteins, split inteins and mini inteins varying in length and mode of action. Classical inteins are embedded in their natural host proteins and expressed as one polypeptide chain localized on one gene bearing a splicing domain and a homing endonuclease domain, responsible for the lateral transfer

between genomes.[123] Classic inteins are splicing in *cis* within the same protein. Mini inteins contain only a splicing domain lacking the homing endonuclease domain, while split inteins are localized on two different gene segments and separately encoding for N- and C-inteins, undergoing an autocatalyzed mechanism called protein trans splicing (PTS) after reassembling both intein parts through structural changes of the host protein.[124] Intein splicing is mediated by the N- and C-intein sequences, containing conserved sequence motifs, and the first residue of the C-extein followed by four different coordinated replacement reactions. N-terminal splicing is activated by an N-S or N-O acyl shift mediated by nucleophilic attack of the first amino acid residue (residue 1) of the intein N-terminus and the carbonyl carbon of the flanking N-extein (residue -1), resulting in a linear (thio)ester intermediate.[125] The amino acid at position +1 typically consists of a cysteine or serine side chain. The (thio)ester is then transesterified by nucleophilic attack by the hydroxyl or sulfhydryl group of the first C-extein residue (+1) consisting of either a cysteine, serine or threonine, forming a branched intermediate. The N-terminal intein is cleaved and transferred to the N-extein. The third step is the formation of a succinimide ring by cyclization of the conserved asparagine residue of the intein C-terminus, attacking the previously formed intein-extein junction. Thereby the intein C-terminus is cleaved and finally a spontaneous S-N or O-N acyl shift occurs, resulting in a stable native peptide bond ligation between the two esterified exteins. [126–128]

Natural split inteins with N- (Motif A and B) and C- (Motif F and G) terminal splicing domains have typically a length between 102 – 123 aa and 30 – 50 aa respectively and are flanked by their natural extein sequences.[129] These blocks of consensus sequences are highly conserved and participate in the protein splicing process.[122] In between of the splicing domains is the endonuclease domain (Motif C, E and H) which is not essential for the splicing reaction but for genetic replication within the host protein. While trans splicing inteins are forming an active intein structure, the splicing process can be interrupted due to hydro-/thiolysis of the formed ester-/thioester resolving the Asn cyclization.[130] The N-terminal extein is cleaved off the pre-cursor protein before ligation can occur. Likewise releasing the C-extein and uncoupling the Asn cyclization from step 1 can occur spontaneously.[131] Alternatively, mutations in the conserved parts or the replacement of the intein into a non-native host protein can result in inefficient splicing or uncoupling the splicing reactions, which often results in single site N- or C- terminal cleavage without peptide bond formation.[132] The mutation of the cysteine at position 1 to alanine for example, is blocking the N-terminal cleavage, because alanine is not able to undergo an acyl shift, lacking a hydroxyl side.[133,134] Although inteins show very low sequence homology, splicing is highly efficient because only the terminal regions and the first residues of the N- and C-exteins are needed for the protein splicing.[135] The splicing rate of naturally occurring or artificially designed split inteins is very fast and specific. The best described split inteins are originally from cyanobacteria. *Ssp* DnaB derived from cyanobacterium *synechocystis* is the first discovered naturally occurring split intein.[136] The best characterized split intein is the *Npu* DnaE from cyanobacterium *Nostoc punctiforme* and one of the fastest split inteins known so far and belongs to the category ultra-fast split inteins. The catalyzed trans splicing reaction of *Npu* DnaE is described with $t_{1/2}$ = 1 min at 37°C temperature optimum. *Npu* DnaE consists of a 36 aa Int^C and a 102 aa Int^N fragment.[137–139]

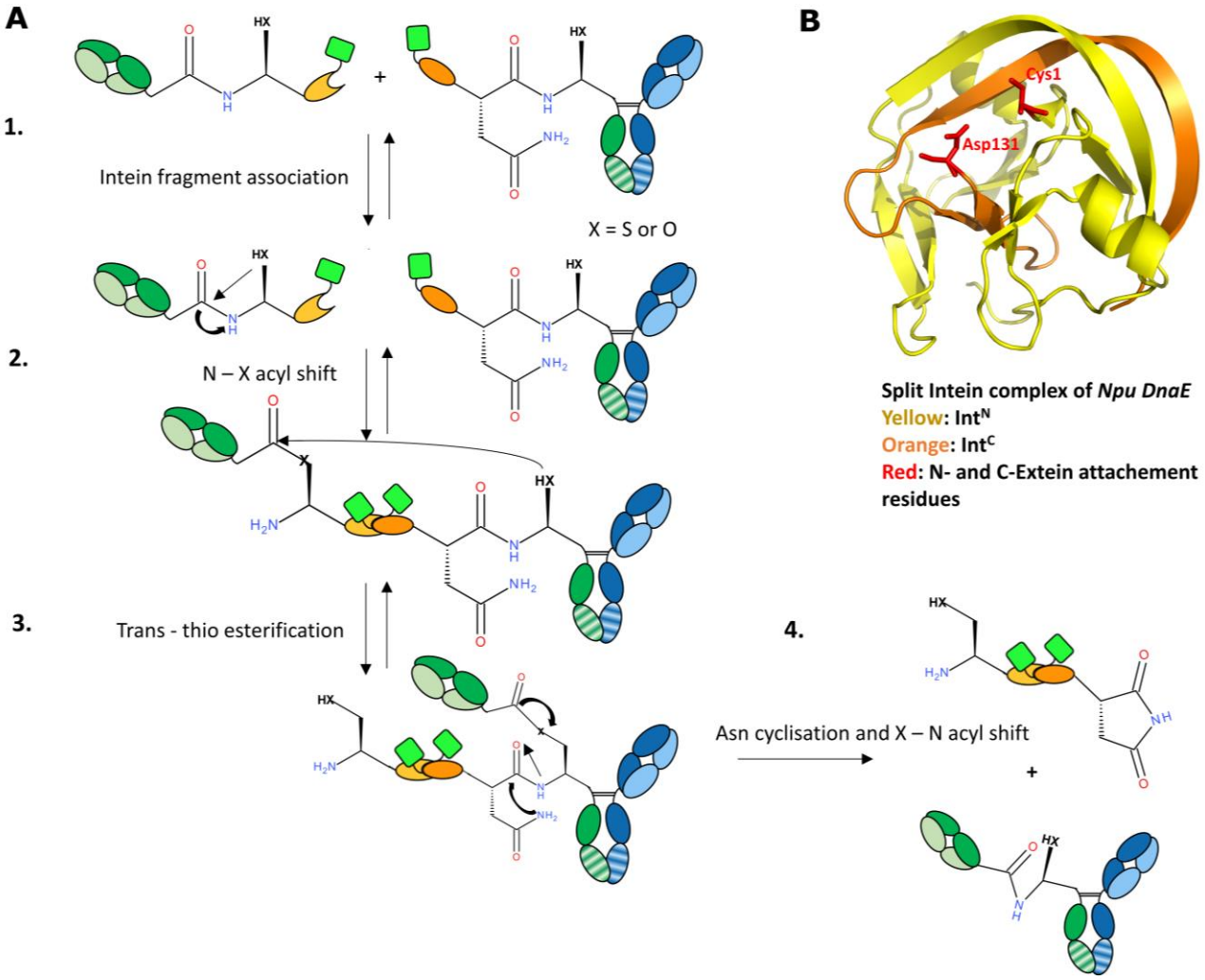

Figure 5: Split intein mode of action and structure of the split intein *Npu* DnaE from *Nostoc punctiforme*.

(A) Illustration of the protein trans splicing (PTS) mechanism of split inteins forming a peptide bond between a one-armed SEED and a Fab fragment. Green squares attached to the intein parts symbolize a hexahistidine tag with glycine serine linker for purification purposes. After reassembly of both intein parts PTS is mediated by four different coordinated replacement reactions. N-terminal splicing is activated by an N-S or N-O acyl shift induced by nucleophilic attack, resulting in a linear (thio)ester intermediate. The (thio)ester is than transesterified by nucleophilic attack by the hydroxyl or sulfhydryl group of the first C-extein residue (+1), forming a branched intermediate. The third step is the formation of a succinimide ring by cyclization of the conserved asparagine residue of the intein C-terminus, attacking the previously formed intein-extein junction. Thereby the intein C-terminus is cleaved and finally a spontaneous S-N or O-N acyl shift occurs, resulting in a stable native peptide bond ligation between the two esterified exteins. **(B)** 3D structure model of the split intein complex *Npu* DnaE from *Nostoc punctiforme* (PDB: 4QFQ, colored with PyMOL v. 0.99). N-terminal intein part (Int^N) is depicted in yellow, while C-terminal intein part (Int^C) is illustrated in orange. Cysteine at position 1 (Int^N) and asparagine at position 131 (Int^C) indicate the first and the last amino acid of both split intein parts and further the attachment point of the extein residues.

Split inteins have become popular for biotechnical applications and many engineering strategies have been described to improve *cis* and *trans* splicing. This powerful toolbox can be used for protein modification or labeling, purification and ligation or furthermore cyclization of peptides to change the conformation and gain new biophysical properties.[140] Expressed protein ligation (EPL) is a classic approach to modify or label proteins with small peptides or peptide tags at the C-terminus of a recombinant protein. The intein is not able to undergo transesterification in *trans*. Therefore, the α-thioester at the C-terminus of the peptide is facilitating the ligation to an N-terminal cysteine.[140,141] The mechanism is similar to native chemical ligation (nCL), although EPL has several disadvantages compared to PTS. PTS is not dependent on additional thiols and large quantities of

recombinant protein or peptides and furthermore not dependent on the fragment size. Either for EPL or PTS, the presence of catalytic cysteines flanking the intein fragments require a reduced state for successful splicing.[142] There are several other reported split inteins described in literature, using a triggered splicing function via pH, temperature or light, achieved through intein modifications making processes more applicable, when they are sensitive to reducing conditions.[143–145] An engineered version of the cysteine free split intein Aes was recently described by Bhagawati and coworkers in 2019, exhibiting improved splicing kinetics and yield applicable for *in vivo* splicing approaches, like chemical labeling of cell surface receptors.[146]

2.5. Aim of the study

Complex NBEs and especially bsAbs with their ability to bind two distinct epitopes on the same or different cells give rise to diverse and potent therapeutic modes of action. Full coverage of the multidimensional screening space of all possible binding moiety combinations and formats to identify candidates with optimal efficiency remains challenging due to excessive cloning, expression and purification steps for bispecific screening. In the presented work, a novel screening methodology for bsAbs should be developed, to overcome the current screening limitations and enlarge the screening space to increase the number of possible bispecific combinations and therefore the chance to find optimal bsAbs. This should be achieved by split intein mediated antibody reconstitution enabling industry scale high throughput combinatorial bsAb screenings. For this, antibody fragments should be generated as fusion proteins using split intein parts derived from *Npu DnaE* and *in vitro* reconstituted within the hinge region resulting in bispecific antibody products in the desired format without additional cloning and expression steps. The specific design of the precursor antibody fragments including hexahistidine tags should allow for a fully automatable high throughput amendable one-pot affinity purification via Ni^{2+} bead addition, resulting in reproducible generation of tag-less high purity bsAb screening candidates (Figure 6). This broadly applicable method should enable high throughput binding and functional cellular bsAb screenings, would greatly shorten development times for a wide variety of complex NBEs and enhance the probability of identifying the optimal combination, ultimately leading to the generation of better biotherapeutics.

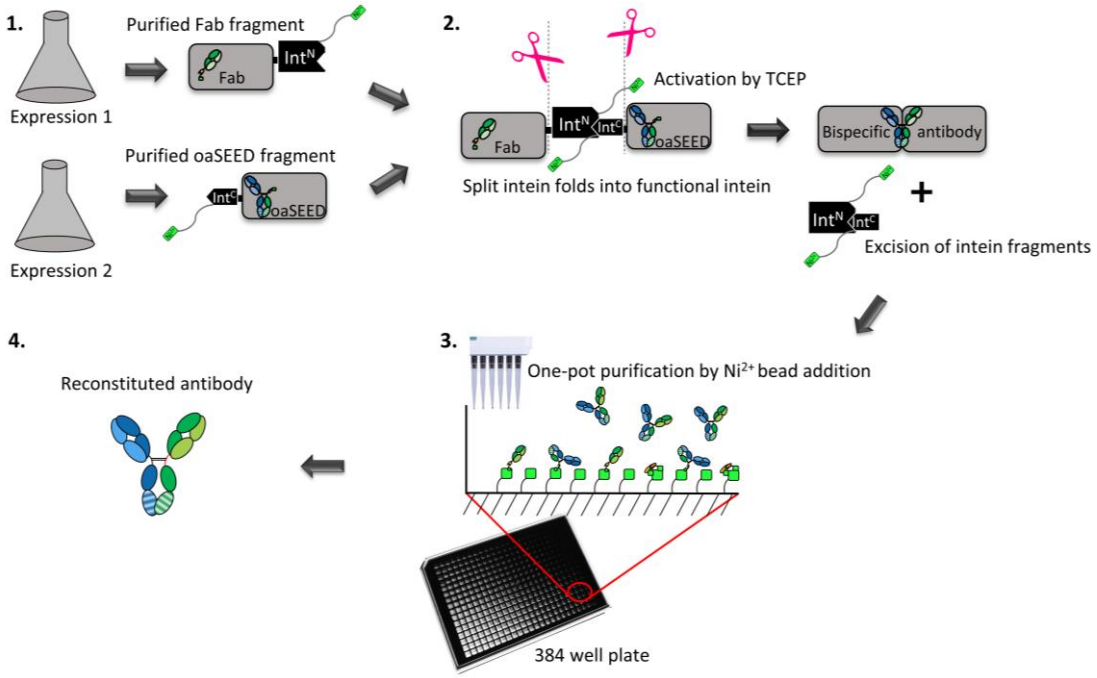

Figure 6: Schematic illustration of bsAb *in vitro* reconstitution mediated by split inteins.

Concept of antibody reconstitution depicting antibody Fab and one-armed (oa) SEED fragments fused N- or C-terminally to their split intein parts. Antibody fragments are expressed in mammalian cells and purified separately before being mixed again in an equimolar ratio for antibody reconstitution. Split intein complex is formed after activation by TCEP and excision of the intein segments takes place after several replacement steps by PTS, leaving a reconstituted newly formed bsAb. Purification tags at the N- and C-terminal parts of the inteins allow for simply removal of non-reconstituted impurities and leftover excised intein complexes. Antibody fragment mix is treated with Ni^{2+} beads after PTS to trap non reconstituted antibody fragments and excised split intein parts via hexahistidine tag based on the specific design. The supernatant containing pure reconstituted antibody is separated from the Ni^{2+} beads and ready for characterization without further treatment. One-pot purification for reconstituted antibodies is applicable for 384 well plates and automated HTS.

3. Materials

3.1. Bacterial strains and human cell lines

Bacterial strains

E. coli One Shot TOP10 chemically competent cells (#C4040-10, Life Technologies, Karlsruhe, Germany); Genotype: F- *mcr*A Δ (*mrr-hsd*RMS-*mcr*BC) φ 80*lac*ZΔ M15 Δ *lac*X74 *rec*A1 *ara*D139 Δ (*ara-leu*) 7697 *gal*U *gal*K *rps*L (StrR) *end*A1 *nup*G

E. coli XL1 blue MRF' chemically supercompetent cells (#200230, Agilent Technologies, Waldbronn, Germany); Genotype: *(mcrA)183 (mcrCB-hsdSMR-mrr)173 endA1 supE44 thi-1 recA1 gyrA96 relA1 lac [F' proAB lacIqZM15 Tn10 (Tetr)]*

Clear Coli® BL21(DE3) electrocompetent cells (#60810-1, Lucigen, Wiscondin, USA); Genotype: *F– ompT hsdSB (rB- mB-) gal dcm lon λ(DE3 [lacI lacUV5-T7 gene 1 ind1 sam7 nin5]) msbA148 ΔgutQ ΔkdsD ΔlpxL ΔlpxM ΔpagP ΔlpxP ΔeptA*

Mammalian cell lines

Cells were obtained from the American Type Culture Collection (ATCC®, Manassas, VA, USA) or the Deutsche Sammlung von Mikroorganismen und Zellkulturen (DSMZ, Braunschweig, Germany), or companies as listed below (**Table 1**).

Table 1: List of mammalian cell lines and reporter cells used for the experiments in the present study.

Cell line	Cell type	Origin
A-431	human epidermoid carcinoma	ATCC® CRL-1555™
A549	human lung carcinoma	ATCC® CCL 185TM
ExpiCHO-S	chinese hamster ovary	Life Technologies, Darmstadt, Germany
Expi293F™	human embryonic kidney	Life Technologies, Darmstadt, Germany (A14527)
EBC-1	human lung carcinoma	JCRB0920 031496
MKN-45	human gastric adenocarcinoma	DSMZ ACC 409
CD40 Nf-κB Luciferase Reporter HEK293	Human embryonic kidney	BPS Bioscience, Cornerstone, San Diego
Recombinant Jurkat cells	Effector cells for ADCC assay	Promega, Mannheim, Germany (G701A)
MDA-MB-468	human breast adenocarcinoma (mammary gland)	ATCC® HTB 132™

HT1080 CD40	Human fibrosarcoma	ATCC® CCL 121TM
Jurkat E6.1	T-lymphocyte	ATCC® TIB 152TM
SK-BR-3	human breast adenocarcinoma (mammary gland)	ATCC® HTB-30™

3.2. Plasmids

Plasmid maps were generated using SeqBuilder v12.3.1 and exemplarily plasmids for different antibody-intein fusion constructs are shown below.

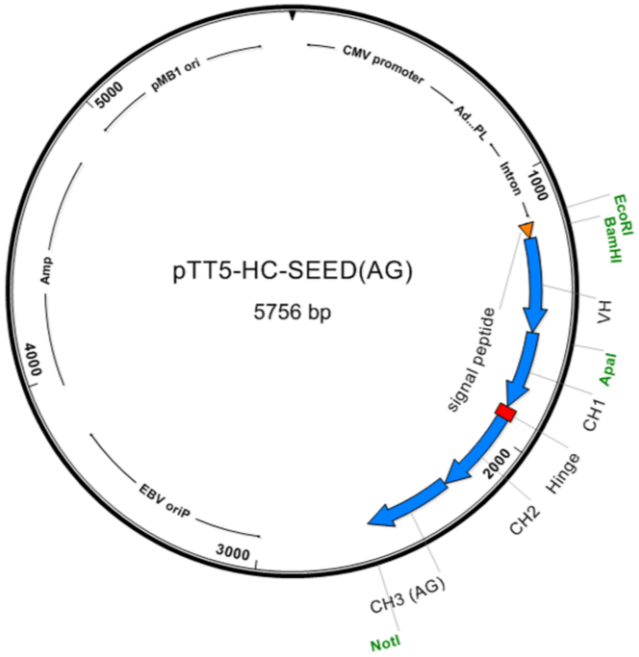

Figure 7: Plasmid map of pTT5-HC-SEED(AG).

The pTT5 vector backbone was obtained from the National Research Council of Canada. The vector was used for mammalian expression systems in CHO or HEK293 cells. The most important features are highlighted and listed as follows: EBV oriP: Origin of replication; Amp: Ampicillin resistance gene (Amp, β-lactamase); pMB1 ori: Bacterial origin of replication; CMV promotor: Cytomegalovirus immediate early promoter used for transient expression and high level yields in mammalian expression systems; Adenovirus TPL: Adenovirus tripartite leader coding region. The rabbit β-globin polyadenylation signal (pA) is located downstream of the antibody sequences. The vector encodes for antibody HC SEED (AG), containing VH-CH1-hinge-CH2-CH3(AG). Restriction enzymes are highlighted in green and used for replacing VH antibody regions via standard cloning.

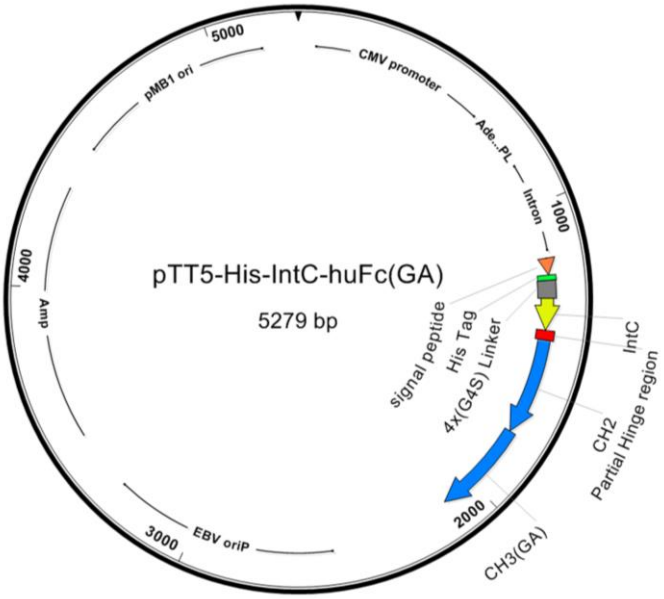

Figure 8: Plasmid map of pTT5-His-IntC-huFc(GA).

The vector encodes for antibody HC SEED (GA), containing His-4x(G4S)-Int^{C}-partial hinge region-CH2-CH3(GA).

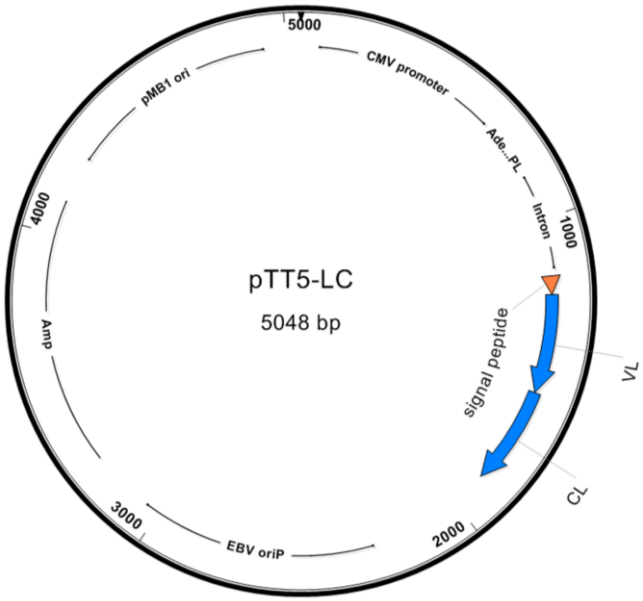

Figure 9: Plasmid map of LC.

The vector encodes for antibody LC, containing VH and CL domain.

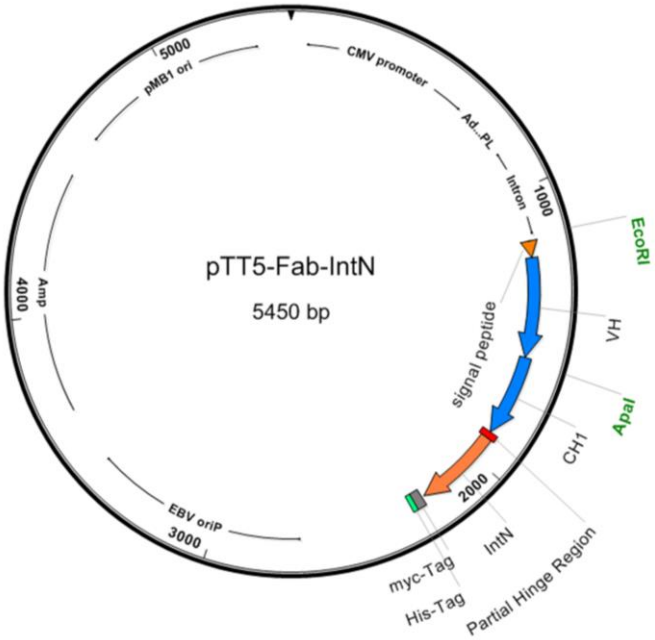

Figure 10: Plasmid map of pTT5-Fab-Int^{N}.

The vector encodes for antibody Fab-Int^{N}, containing VH-CH1-partial hinge-Int^{N}-mycTag-His. Restriction enzymes are highlighted in green and used for replacing VH antibody regions via standard cloning.

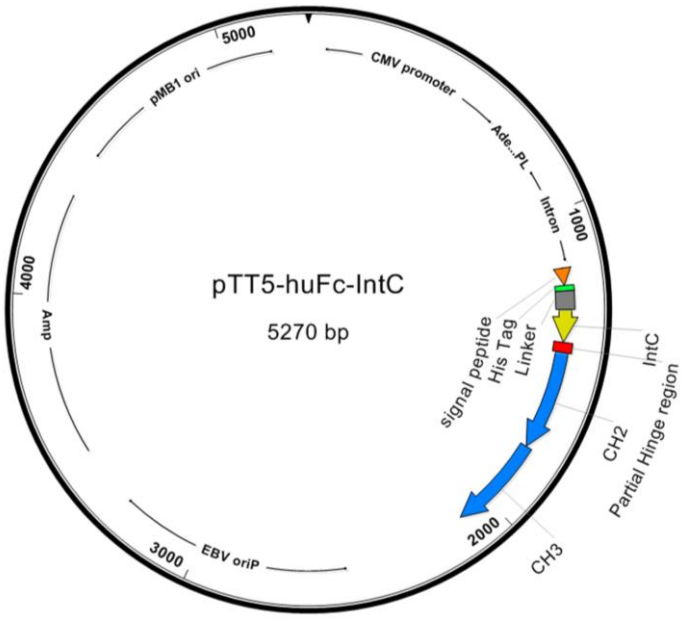

Figure 11: Plasmid map of pTT5-huFc-Int^{C}.

The vector encodes for antibody huFc-Int^{C}, containing His-4x(G4S)-Int^{C}-partial hinge region-CH2-CH3.

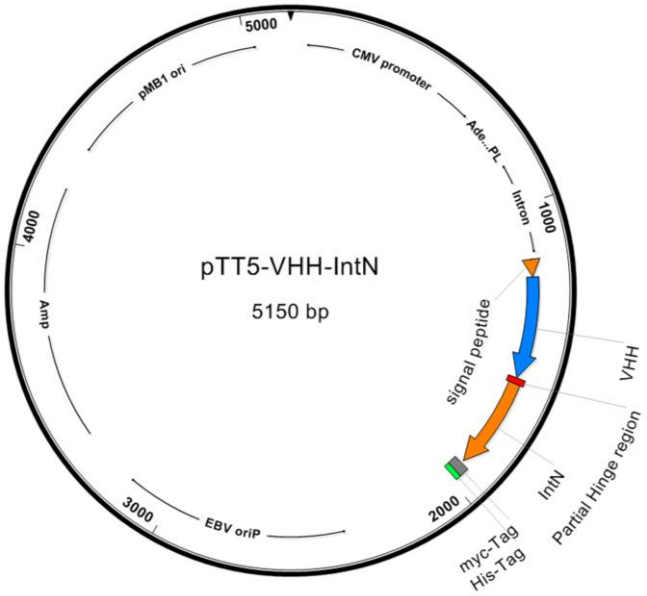

Figure 12: Plasmid map of pTT5-VHH-Int^{N}.

The vector encodes for antibody VHH-Int^{N}, containing VHH-partial hinge region-Int^{N}-mycTag-His.

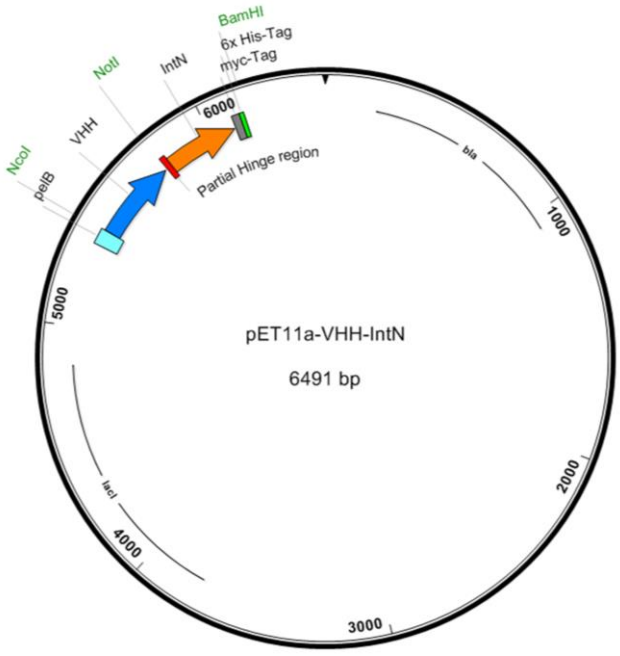

Figure 13: Plasmid map of pET11a-VHH-Int^{N}.

The pET11a vector backbone was obtained from Novagen and the sequence is a convention of the pBR322 plasmid, originally invented by Bolivar and Rodriguez in 1977 (University of San Francisco). The vector was used for bacterial expression in *E. coli*. The most important features are highlighted and listed as follows: LacI: LacI-repressor gene of the lactose operon. Bla: β-lactamase conferring ampicillin resistance. The vector encodes for antibody VHH-IntN, containing VHH-partial hinge region-Int^{N}-mycTag-His. Restriction enzymes are highlighted in green and used for replacing VHH antibody region via standard cloning.

3.3. Enzymes and proteins

Antarctic Phosphatase, calf intestinal (CIP)	New England BioLabs, Ipswich, MA, USA
*Apa*I	New England BioLabs, Ipswich, MA, USA
*Bam*HI-HF®	New England BioLabs, Ipswich, MA, USA
Benzonase	Novagen, Nottingham, GB
Bovine serum albumin (BSA), fraction V	Merck, Darmstadt, Germany
BSA standard solution (2 mg mL^{-1})	Thermo Scientific, Schwerte, Germany
CD40 Avi His	Acro Biosystems, Newark, USA
CD40L-His, Recombinant human (10774H08H50)	Thermo Scientific, Schwerte, Germany
CEACAM5 (35-685) His, Recombinant human	Acro Biosystems, Newark, USA
CEACAM6 (35-320) His, Recombinant human	Acro Biosystems, Newark, USA
EGFR (1-618) His, Recombinant human	Merck, Darmstadt, Germany
*Eco*RI	New England BioLabs, Ipswich, MA, USA
HER2, murine Fc His	Merck, Darmstadt, Germany
HER2 (23-652) His, Recombinant human	Acro Biosystems, Newark, USA
Lysozyme	Roche, Mannheim, Germany
*Nco*I-HF®	New England BioLabs, Ipswich, MA, USA
*Not*I-HF®	New England BioLabs, Ipswich, MA, USA
Immobilized papain (agarose resin)	Thermo Scientific, Schwerte, Germany
Phosphatase inhibitor set II (#P524625)	Merck, Darmstadt, Germany (Calbiochem)
Phusion DNA polymerase	New England BioLabs, Ipswich, MA, USA
Pfu Turbo DNA polymerase	New England BioLabs, Ipswich, MA, USA
Protease inhibitor set III (#P524525)	Merck, Darmstadt, Germany (Calbiochem)
Recombinant human c-MET ECD-strepII-His	Merck, Darmstadt, Germany
Recombinant human c-MET SEMA-PSI-FLAG-His	Merck, Darmstadt, Germany
Recombinant human EGF (236-EG/CF)	R&D Systems, Minneapolis, MN, USA
Recombinant human HGF (294-HGN/CF)	R&D Systems, Minneapolis, MN, USA
Rherbb2 murine Fc	R&D Novoprotein, New Jersey, USA
T4 DNA Ligase	New England BioLabs, Ipswich, MA, USA
Quick Ligase	New England BioLabs, Ipswich, MA, USA

3.3.1. Antibodies

Reference antibodies

Cetuximab (Erbitux®, C225)	Merck, Darmstadt, Germany
anti-hen egg lysozyme (HEL)	Merck, Darmstadt, Germany
APX005M (Apexigen)	Merck, Darmstadt, Germany
C5xC6 bispecific antibody	Merck, Darmstadt, Germany
Trastuzumab (Herceptin®)	Roche, Basel, Switzerland

Reference antibodies were kindly provided by Merck, Darmstadt, Germany.

Primary antibodies for Western Blot

Goat anti-human IgG Antibody, F(ab')2 Fragment specific	Jackson ImmunoResearch, Suffolk, GB
Mouse IgG1 anti-Penta His Antibody (#34660)	Quiagen, Hilden, Germany
Mouse anti-human IgG, F(ab')2 Fragment specific	Jackson ImmunoResearch, Suffolk, GB
Mouse anti-human IgG, Fcg Fragment specific	Jackson ImmunoResearch, Suffolk, GB
Rabbit anti c-MET pAb (M3007-13A)	Biomol, Hamburg, Germany
Rabbit anti EGFR mAb, clone D38B1	Cell Signaling Technologies, Cambridge GB
Rabbit anti phospho-cMET mAb (Y1234/Y1235), clone D26 (#3077)	Cell Signaling Technologies, Cambridge GB
Rabbit anti phospho-EGFR mAb (Y1173), clone E124 (ab32578)	Abcam, Cambridge,GB

Secondary antibodies for Western Blot

Goat anti-mouse IgG (H+L) peroxidase (HRP) conjugate	Jackson ImmunoResearch, Suffolk, GB
Goat anti-mouse IgG (H+L) AP conjugate (#115-055-062)	Jackson ImmunoResearch, Suffolk, GB
Alexa Fluor® 680 goat anti-rabbit IgG (H+L), A21076	Life Technologies, Darmstadt, Germany
Rabbit anti-goat IgG (H+L) x AP conjugate (#305-056-045)	Jackson ImmunoResearch, Suffolk, GB

Detection antibodies for flow cytometry

Alexa Fluor® 488 Pure Fab Goat anti-human IgG (H+L)	Life Technologies, Darmstadt, Germany
Goat Anti-Human IgG (H+L) Fab Fragment, Alexa Fluor® 488 (#109-547-003)	Jackson ImmunoResearch, Suffolk, GB
Goat anti-human IgG, Fc specific, FITC conjugate	Jackson ImmunoResearch, Suffolk, GB

Antibodies for ELISA

Anti-penta-His (POD)	Roche, Mannheim, Germany
Goat anti-mouse IgG (H+L) peroxidase (HRP) conjugate	Jackson ImmunoResearch, Suffolk, GB
Goat anti-human IgG, Fcγ fragment specific peroxidase (HRP) conjugate	Jackson ImmunoResearch, Suffolk, GB

HTRF antibodies and conjugates

pAb anti-human IgG-d2	Cisbio, Bedford, MA, USA
pAb anti-human IgG-XL665	Cisbio, Bedford, MA, USA
pAb anti-human IgG-Tb cryptate	Cisbio, Bedford, MA, USA
Streptavidin-d2	Cisbio, Bedford, MA, USA
Streptavidin-XL665	Cisbio, Bedford, MA, USA
Streptavidin-Tb cryptate	Cisbio, Bedford, MA, USA

3.4. Oligonucleotides

Oligonucleotides were obtained from Eurofins MWG Operon, Ebersberg, Germany.

3.4.1. Primers for site-directed mutagenesis PCR:

IgG1.4 mutations:

PVA_UP	CGTGCCCAGCTCCACCTGTGCCGGACCTTCCGTG
PVA_RP	CACGGAAGGTCCGGCCACAGGTGGAGCTGGGCACG
SS_UP	CAACAAGGCCCTGCCTTCTTCTATCGAGAAAACCATC
SS_RP	GATGGTTTTCTCGATAGAAGAAGGCAGGGCCTTGTTG

IgG1.6 mutations:

PVA_UP	CGTGCCCAGCTCCACCTGTGCCGGACCTTCCGTG
PVA_RP	CACGGAAGGTCCGGCCACAGGTGGAGCTGGGCACG

K322A/P329A_UP

GAGTACAAGTGCGCGGTGTCCAACAAGGCCCTGGCTGCTCCTATCGAG

K322A/P329A_RP

CTCGATAGGAGCAGCCAGGGCCTTGTTGGACACCGCGCACTTGTACTC

3.4.2. Primers for sequencing:

pTT5_UP	CTGCGCTAAGATTGTCAGT
pTT5_RP	CCATATGTCCTTCCGAGTG

3.5. Chemicals

1-StepTM Ultra TMB-ELISA substrate solution	Thermo Scientific, Schwerte, Germany
2-Mercaptoethylamine HCl (2-MEA)	Thermo Scientific, Schwerte, Germany
4-Chloro-1-naphtol	Sigma-Aldrich, Steinheim, Germany
Ammonium sulfate ($(NH_4)_2SO_4$)	Merck, Darmstadt, Germany
Acetic acid	Sigma-Aldrich, Steinheim, Germany
Agar-agar	Merck, Darmstadt, Germany
Agarose	Life Technologies, Darmstadt, Germany
Ampicillin, sodium salt	Life Technologies, Darmstadt, Germany
Acetonitril	Merck, Darmstadt, Germany
BugBusterHT	Merck, Millipore, Germany
CellLytic™ B	Sigma-Aldrich, Steinheim, Germany
Calcium chloride (CaCl2)	Merck, Darmstadt, Germany
Coomassie InstantBlueTM	Expedeon Ltd, San Diego, CA, USA
Coomassie Plus - Bradford Assay™ Reagent	Thermo Scientific, Schwerte, Germany
Cut smart buffer	New England Biolabs, Ipswich, MA, USA
L-Cysteine	Merck, Darmstadt, Germany
L-Dehydroascorbic acid (DHAA)	Sigma-Aldrich, Steinheim, Germany
Desocyribonucleotide triphosphates (dNTPs)	Novagen, Nottingham, GB
Disodium hydrogen phosphate ($Na_2HPO_4*2H_2O$)	Merck, Darmstadt, Germany
Dithiothreitol (DTT)	Thermo Scientific, Schwerte, Germany
EDTA	Sigma-Aldrich, Steinheim, Germany
Ethanol	Merck, Darmstadt, Germany
Eagle Minimal Essential Medium (MEM)	Sigma-Aldrich, Steinheim, Germany
Expi293™ expression medium	Life Technologies, Darmstadt, Germany
Gel filtration standards	Bio-Rad, Munich, Germany
Gel loading dye (6x)	Novagen, Nottingham, GB

GelRed™	VWR International, Darmstadt, Germany
Gibco® Dulbecco's modified eagle medium (DMEM)	Life Technologies, Darmstadt, Germany
Gibco® Dulbecco's PBS (DPBS, w/o $CaCl_2$, $MgCl_2$)	Life Technologies, Darmstadt, Germany
Gibco® Fetal calf serum (FCS)	Life Technologies, Darmstadt, Germany
Gibco® Trypsin-EDTA	Life Technologies, Darmstadt, Germany
Gibco® L-glutamine	Life Technologies, Darmstadt, Germany
Gibco® sodium pyruvate	Life Technologies, Darmstadt, Germany
Gibco® RPMI 1640 medium	Life Technologies, Darmstadt, Germany
Gibco® Opti-MEM	Life Technologies, Darmstadt, Germany
Glucose	Sigma-Aldrich, Steinheim, Germany
Guava instrument cleaning fluid (ICF)	Merck, Darmstadt, Germany
Glycine	Merck, Darmstadt, Germany
Hydrogen chloride (HCl)	Merck, Darmstadt, Germany
Imidazole	Merck, Darmstadt, Germany
Isopropyl-β,D-thiogalactopyranosid (IPTG)	Merck, Darmstadt, Germany (Calbiochem)
Kanamycin sulfate	Merck, Darmstadt, Germany
LPS-EB Ultrapure	InvivoGen, San Diego, California
Methanol	Merck, Darmstadt, Germany
Magnesium chloride hexahydrate ($MgCl_2$*$6H_20$)	Merck, Darmstadt, Germany
Magnesium sulfate heptahydrate ($MgSO_4$*$7H_2O$)	Merck, Darmstadt, Germany
NuPAGE® LDS sample buffer (4x)	Life Technologies, Darmstadt, Germany
NuPAGE® MES SDS running buffer	Life Technologies, Darmstadt, Germany
NuPAGE® sample reducing agent	Life Technologies, Darmstadt, Germany
Nickel(II)sulfate hexahydrate ($NiSO_4$*$6H_2O$)	Merck, Darmstadt, Germany
Nickel phosphate	Merck, Darmstadt, Germany
OptiPRO SFM	Life Technologies, Darmstadt, Germany
Potassium dihydrogen phosphate (KH_2PO_4)	Merck, Darmstadt, Germany
Potassium chloride (KCl)	Merck, Darmstadt, Germany
Peptone	Merck, Darmstadt, Germany
Phusion HF buffer (5x)	New England Biolabs, Ipswich, MA, USA
Perfect DNA™ markers, 0.1 – 12 kbp	Merck, Darmstadt, Germany
Precision Plus ProteinTM standards	Bio-Rad, Munich, Germany
Protein standard HiMark™ pre-stained	Life Technologies, Darmstadt, Germany
RIPA cell lysis buffer (10x, #9806)	Cell Signaling Technologies, Cambridge GB

S.O.C. medium	Life Technologies, Darmstadt, Germany
See Blue® Plus 2 prestained protein standard	Life Technologies, Darmstadt, Germany
Skim milk powder	Merck, Darmstadt, Germany
Sodium azide	Thermo Scientific, Schwerte, Germany
Sodium chloride (NaCl)	Merck, Darmstadt, Germany
Sodium hydroxide (NaOH) 2N	Merck, Darmstadt, Germany
Sodium dihydrogen phosphate (NaH_2PO_4)	Merck, Darmstadt, Germany
Sulfuric acid (H_2SO_4) 1N	Bernd Kraft, Duisburg, Germany
TCEP	Thermo Scientific, Schwerte, Germany
T4 DNA Ligation Buffer (10x)	New England BioLabs, Ipswich, MA, USA
Quick Ligase buffer (2x)	New England Biolabs, Ipswich, MA, USA
TAE buffer	Life Technologies, Darmstadt, Germany
Tris(hydroxymethyl)aminomethane (Tris)	Carl Roth, Karlsruhe, Germany
Tris-hydrochloride (Tris-HCl)	Sigma-Aldrich, Steinheim, Germany
Tween®20	Merck, Darmstadt, Germany
Ultra-low IgG FCS	Life Technologies, Darmstadt, Germany
Yeast extract	Becton Dickinson, Heidelberg, Germany

3.6. Cell culture media

A549, SK-BR-3, A431	DMEM, 10% (v/v) FCS
MDA-MB-468, MKN-45, Jurkat E6-1	RPMI 1640, 10% (v/v) FCS, 2 mM L-glutamine, 1 mM sodium pyruvate
EBC-1, HEK-NFκB-CD40, HT1080 CD40	MEM Eagle, 10% (v/v) FCS, 2 mM L-glutamine
ExpiCHO-S	ExpiCHO™ expression medium
Expi293F™	Expi293™ expression medium
ADCC assay medium	RPMI 1640, 4% (v/v) low IgG FCS (heat inactivated at 56°C for 30 min)

3.7. Solutions, media and buffer

2xTY medium	16 g L^{-1} peptone, 10 g L^{-1} yeast extract, 5 g L^{-1} NaCl, pH 7.0
5xTY medium	10 g L^{-1} peptone, 50 g L^{-1} yeast extract, pH 7.0
Analytical size exclusion chromatography (SEC) mobile phase	PBS, pH 7.4 or 50 mM sodium phosphate (NaH_2PO_4, Na_2HPO_4), 0.4 M sodium perchlorate, pH 6.35
Affinity chromatography for his-tagged proteins (Equilibration buffer)	0.5 M NaCl, 25 mM Na_2HPO_4 x $2H_2O$, 25.2 mM NaH_2PO_4 x H_2O, pH 7.4

Affinity chromatography for his-tagged proteins (Elution buffer)	0.5 M NaCl, 25 mM Na_2HPO_4 x $2H_2O$, 25.2 mM NaH_2PO_4 x H_2O, 500 mM imidazole, pH 7.4
BCIP/NBT reagent, Blue/purple, AP substrate	Merck, Darmstadt, Germany
Blocking solution for Western Blot	2% BSA in PBS-Tween or 5% skim milk powder in PBS-Tween
EDTA solution	0.5 M EDTA, pH 8.0
FACS binding buffer	1% (w/v) BSA in DPBS
Imidazole buffer	2 M imidazole, pH 7.4
Kinetics buffer (KB) for BLI	0.1% (w/v) BSA, 0.05% (v/v) Tween®20 in PBS
	10 g L^{-1} peptone, 5 g L^{-1} yeast extract, 10 g L^{-1} NaCl
LB medium	LB, 0.1 mg L^{-1} ampicillin
LB-A medium	LB-A, 15 g L^{-1} agar-agar
LB-A agar	0.5 M nickel(II)sulfate
Nickel(II)sulfate solution	1.5 M NaCl, 84 mM Na_2HPO_4 x $2H_2O$,
Phosphate buffered saline (10x PBS)	16 mM KH_2PO_4, pH 7.4
	140 mM NaCl, 3 mM KCl,
Phosphate buffered saline (1xPBS)	8 mM Na2HPO4 x 2H2O, 2 mM KH2PO4, pH 7.4
	4 M NaCl, 199.5 mM Na_2HPO_4 x $2H_2O$, 201.5 mM
Phosphate buffer (8x)	NaH_2PO_4 x H_2O, pH 7.4
Protein A chromatography (Equilibration buffer)	PBS, pH 6.8 – pH 7.0 or
	10 mM Na_2HPO_4, 10 mM NaH_2PO_4, 500 mM NaCl, pH 7.0
Protein A chromatography (Elution buffer)	0.1 M sodium citrate, pH 3.0 or
	20 mM acetic acid, pH 3.2
Protein A chromatography (Neutralization buffer)	3 M Tris/HCl, pH 8.5 or 1 M Tris/HCl, pH 9.0
Preparative SEC (mobile phase)	PBS, pH 7.4
Intein splicing buffer	PBS, pH 7.4
Wash solution (PBS-Tween)	0.05% (v/v) Tween® 20 in 1 x PBS pH 7.4

3.8. Kits and laboratory materials

ADCC reporter bioassay kit	Promega, Mannheim, Germany
AirPore™ Tape Sheets, breathable sealing foil	Qiagen, Hilden, Germany
Amicon®Ultra-15 and 0.5 ml centrifugal filter units (10 MWCO)	Merck, Darmstadt, Germany
BCA protein assay kit	Thermo Scientific, Schwerte, Germany

Cell culture flasks T25, T75	Greiner Bio-One, Kremsmuenster, Austria
Cell culture flat and round bottom Nucleon™ delta surface 96 well plates	Thermo Scientific, Schwerte, Germany
Cell culture 24 well plates Costar®	Thermo Scientific, Schwerte, Germany
Cell culture microplate 384 well, white, clear	Greiner Bio-One, Kremsmuenster, Austria
ExpiFectamine™ 293 transfection kit	Life Technologies, Darmstadt, Germany
ExpiFectamine™ CHO transfection kit	Life Technologies, Darmstadt, Germany
Falcon® tubes, 15 ml and 50 ml	VWR International, Darmstadt, Germany
FortéBio tips (AHC, FAB2, ProteinA, HIS2K)	Pall ForteBio LLC, Menlo Park, CA, USA
Gel and PCR clean-up kit NucleoSpin®	Macherey-Nagel, Dueren, Germany
GenElute™ HP Plasmid Midiprep, Maxiprep Kit	Sigma-Aldrich, Steinheim, Germany
HiLoad Superdex 200 pg 26/60 columns	GE Healthcare, Munich, Germany
HiLoad Superdex 200 pg 26/600 columns	GE Healthcare, Munich, Germany
HiLoad Superdex 200 pg 16/600 columns	GE Healthcare, Munich, Germany
HiLoad Superdex 75 pg 16/60 columns	GE Healthcare, Munich, Germany
HiLoad Superdex 200 increase 10/300 GL	GE Healthcare, Munich, Germany
HiTrap MabSelect SuRe columns, 1 mL and 5 mL	GE Healthcare, Munich, Germany
HisTrap HP columns, 1 mL and 5 mL	GE Healthcare, Munich, Germany
His GraviTrap (IMAC)	GE Healthcare, Munich, Germany
His Buffer Kit	GE Healthcare, Munich, Germany
iBind™ Solution Kit (#SLF1020)	Life Technologies, Darmstadt, Germany
iBlot™ Transfer Stack, Nitrocellulose, mini	Life Technologies, Darmstadt, Germany
iBlot™ Transfer Stack, PVDF, mini	Life Technologies, Darmstadt, Germany
iBlot™ Transfer Stack, PVDF, regular	Life Technologies, Darmstadt, Germany
JETSTAR Plasmid Purification Kit (Midi and Maxi column)	Genomed, Loehne, Germany
MaxiSorp™ flat-bottom 96 well microtiter plates	Sigma-Aldrich, Steinheim, Germany
NuPAGE® 4-12% Bis-Tris gels	Life Technologies, Darmstadt, Germany
Nalgene™ Rapid-Flow™ bottle top filter	Thermo Scientific, Schwerte, Germany
Polypropylene microtiter plates 96 and 384 wells, black	Greiner Bio-one, Frickenhausen, Germany
Polypropylene microtiter plates 96 and 384 wells, clear	Greiner Bio-one, Frickenhausen, Germany
Polystyrene round bottom 96 well microtiter plates	Greiner Bio-one, Frickenhausen, Germany

Pur-A-Lyzer™ maxi dialysis kit	Sigma-Aldrich, Steinheim, Germany
Pierce™ Coomassie Plus (Bradford) assay kit	Thermo Scientific, Schwerte, Germany
Pierce™ Fab Preparation Kit	Thermo Scientific, Schwerte, Germany
Qiaprep® Spin Miniprep kit	Qiagen, Hilden, Germany
Quick Ligation Kit	New England BioLabs, Ipswich, MA, USA
QuickChange II site-directed mutagenesis kit	Agilent Technologies, Waldbronn, Germany
SpectraPor® Dialysis membranes (10 kDa MWCO)	Thermo Scientific, Schwerte, Germany
Steriflip® filter device 0.22 µm	Merck, Darmstadt, Germany
Steritop™ bottle top filter 0.22 µm	Merck, Darmstadt, Germany
T-cell activation bioassay (NFAT)	Promega, Mannheim, Germany
Tissue culture 24 well plates	Greiner Bio-one, Frickenhausen, Germany
TMB peroxidase substrate solution	Vector Laboratories, Burlingame, CA, USA
The Blocking Solution	Candor Bioscience, Wangen, Germany
TSKgel SuperSW3000 column	Tosoh Bioscience, Darmstadt, Germany
Ultrafree® Centrifugal filter units	Merck, Darmstadt, Germany
VacuCap 60 PF Filter Unit 0.2 µm Supor Membrane	Pall, Menlo Park, CA, USA
Wizard® SV Gel and PCR Clean-Up System	Promega, Mannheim, Germany
Zeba Spin desalting PD-10 columns	Life Technologies, Darmstadt, Germany
ZymoPURE™ Plasmid miniprep kit	ZymoResearch, Irvine, California, USA
ZymoPURE™ Plasmid midi and maxiprep kit	ZymoResearch, Irvine, California, USA

3.9. Equipment

Analytical balance New Classic MF MS3002S	Mettler Toledo, Giessen, Germany
BiomekFX	Beckman Coulter, California, USA
BioShake XP	Qinstruments, Jena, Germany
Cell counter Vi-CELL® XR	Beckmann Coulter, Brea, CA, USA
Chromatography systems ÄKTAxpress, ÄTKAexplorer 100, ÄKTApure	GE Healthcare, Munich, Germany
Cogent® µScale TFF System	Merck, Darmstadt, Germany
Cytomat 6001 incubator	Thermo Scientific, Schwerte, Germany
Electrophoresis chambers NuPage® Novex ® Gel system	Thermo Scientific, Schwerte, Germany
EnVision 2104 plate reader	Perkin Elmer, Boston, MA, USA
Flow cytometer Guava easyCyte HT 2L	Merck, Darmstadt, Germany
FortéBio Octet RED	Pall ForteBio LLC, Menlo Park, CA, USA

HeraSafe® Clean Bench	Thermo Scientific, Schwerte, Germany
Hot plate magnetic stirrer IKA® RCT basic	Sigma-Aldrich, Steinheim, Germany
HPLC Agilent 1260 Infinity, ChemStation LC 3D	Agilent Technologies, Frankfurt, Germany
iBind™ Western System	Life Technologies, Darmstadt, Germany
iBlot® Dry blotting system	Life Technologies, Darmstadt, Germany
Incubation shaker Minitron	Infros HT, Bottmingen, Switzerland
Incubator Heracell 150	Thermo Scientific, Schwerte, Germany
Megafuge 1.0R, rotor BS4402/A	Thermo Scientific, Schwerte, Germany
Multifuge 3 S-R	Heraeus, Hanau, Germany
Microplate washer, ELx405™	BioTeK, Bad Friedrichshall, Germany
Microtiter plate reader BioTeK Synergy™ 4	BioTeK, Bad Friedrichshall, Germany
Microtiter plate reader SpectraMax® Paradigm®	Molecular Devices, Wals, Austria
MicroLab Starlet liquid handler device	Hamilton, Nevada, USA
Mosquito nanoliter liquid handling system	TTP LabTech, Melbourn, UK
Multidrop microplate dispenser	Thermo Scientific, Schwerte, Germany
Nanodrop ND-1000 Spectrophotometer	Thermo Scientific, Schwerte, Germany
Nanodrop One Spectrophotometer	Thermo Scientific, Schwerte, Germany
pH meter 744	Metrohm, Filderstadt, Germany
Power supply EC 250-90	Thermo Scientific, Schwerte, Germany
PowerPac™ basic power supply	Bio-Rad, Munich, Germany
Prometheus NT.PLEX nanoDSF	NanoTemper Technologies, Munich, Germany
Synapt-G2 mass spectrometer	Waters, Milford, MA, USA
Table centrifuge 5415D	Eppendorf, Hamburg, Germany
Tetrad® 2 Peltier Thermal Cycler (PCR)	Bio-Rad, Munich, Germany
ThermoMixer®	Eppendorf, Hamburg, Germany
Ultracentrifuge Beckmann Optima™ LE-80K, SW41 TI rotor	Global Medical Instrumentation, Ramsey, MN, USA
VSpin microplate centrifuge	Agilent Technologies, FFM, Germany
XCell SureLock™ gel electrophoresis device	Life Technologies, Darmstadt, Germany
Xpeel automated plate sealer	Brooks Life Science, Manchester, UK

Further equipment and laboratory devices, referred as standard laboratory equipment, was used and is not listed or specified above.

3.10. Software

Accelrys Draw 4.2	Biovia, San Diego, CA, USA
ÄKTA UNICORN software ver. 5.31 (Build 407)	GE Healthcare, Munich, Germany
BMKFX 3.3 build 14.0	Beckman Coulter, California, USA
D300e control 3.2.4	Tecan, Männedorf, Switzerland
EnVision 1.12	Perkin Elmer, Boston, MA, USA
FortéBio octet data acquisition ver. 8.0	Pall ForteBio LLC, Menlo Park, CA, USA
FortéBio octet data analysis ver. 8.0	Pall ForteBio LLC, Menlo Park, CA, USA
Gen5™ microplate reader software ver. 1.11.5	BioTeK Instruments, Bad Friedrichshall, Germany
GraphPad Prism v7	GraphPad Software, La Jolla, CA, USA
GuavaSoft v3.1.1	Merck, Darmstadt, Germany
HPLC software ChemStation	Agilent Technologies, FFM, Germany
Image Studio™ software v2.1	LI-COR Biosciences, Bad Homburg, Germany
ImageJ v1.49	Wayne Rasband, National Institute of Health; Maryland, USA
LabChipGX Reviwer v5.2	Perkin Elmer, Massachusetts, USA
Lasergene v12.3.1	DNA Star Inc., Wisconsin, WI, USA
Mendeley Desktop ver. 1.19.4	Elsevier, New York, NY, USA
Microsoft Office 2013	Microsoft Corp., Redmond, WA, USA
Mosquito 3.13.0.0	TTP LabTech, Melbourn, UK
Paradigm™ Software SoftMaxPro v6.3	Molecular Devices, Wals, Austria
Protein Thermal Shift™ software v1.0	Life Technologies, Darmstadt, Germany
PyMOL v1.8.6.0	Schrodinger LLC, San Diego, CA, USA
SAMI Ex 4.0 build 156	Beckman Coulter, California, USA
Vi-CELL® XR v2.04	Beckmann Coulter, Brea, CA, USA
VSpin v4.3.0	Agilent Technologies, FFM, Germany
Venus 3 v4.4 microlab STAR	Hamilton, Nevada, USA
Yasara v17.7.30	YASARA Biosciences, Vienna, Austria

4. Methods

4.1. Molecular biological methods

4.1.1. Plasmid generation

Split intein *Npu* DnaE genes encoding for Int^N and Int^C were subcloned for secretory expression in mammalia suspension cells and bacterial expression in *E. coli* and ordered as gene synthesis from GeneArt Gene Synthesis (Thermo Fisher Scientific®) as codon optimized versions according to their expression hosts.[147] *Npu* DnaE genes were adapted using a multiple cloning site (mcs) to perform standard cloning techniques for subcloning of antibody fragments based on flanking unique restriction sites. Restriction enzymes for subcloning were purchased by New England Biolabs. The vector backbone pTT5 was used to subclone Int^C and Int^N genes via *Bam*HI and *Not*I restriction, serving as a vector template for Fab fragments (pTT5-Int^N). *Eco*RI and *Bam*HI was used to subclone the Int^C gene into pTT5, serving as template for SEED- and Fc-fragments (pTT5-Int^C). Further, the IntN gene was inserted via *Nco*I and *Bam*HI restriction into a pET11 vector backbone, serving as a template for VHH fragments (pET11-Int^N). The vector templates pTT5-Int^N and pET11-Int^N were additionally modified with an N-terminal myc-tag, followed by a hexahistidine tag, located downstream of the Int^N for purification purposes. A hexahistidine tag followed by a 4x (G_3S) linker upstream of the CH2 domain was added for vector template pTT5-Int^C. VH antibody regions encoding for anti-CD40, CD3, CEACAM5, CEACAM6, c-MET, EGFR and Her2 were flanked by restriction sites *Apa*I and *Bam*HI and were subcloned into the pTT5-Int^N template. *Nco*I and *Not*I restriction sites were used to subclone VHH antibody regions into the pET11-Int^N template. The pET11-Int^N template consists of a pelB leader sequence for periplasmic expression in *E. coli*. All constructs were validated and identified by sequencing after cloning. For bacterial expression, the vector pET11-Her2-VHH-Int^N-His_6 was transformed into chemically competent One Shot™ *E. coli* BL21(DE3) (Thermo Fisher Scientific) and into electrocompetent *ClearColi* BL21(DE3) (Lucigen).

4.1.2. Preparation of plasmid DNA

Plasmid DNA was extracted from 5 mL *E. coli* Top10 cultures using a plasmid preparation kit from either GenElute™ HP Plasmid Miniprep Kit or ZymoPURE™ plasmid Miniprep kit, following the instructor's manual. Elution of plasmid DNA was carried out using 40 µL of MilliQ-H_2O. Plasmid DNA for mammalian expression was extracted from 150-200 mL *E. coli* cultures using either GenElute™ HP Plasmid Midi/Maxiprep kit or ZymoPURE™ plasmid Midi/Maxiprep kit. Elution of plasmid DNA was carried out using 1000 – 2500 µL MilliQ-H_2O.

4.1.3. Quantification and quality determination of DNA

Purified DNA concentration diluted in H_2O was measured by UV spectrometry (Nanodrop™ One/ND1000). 1.5 µL of DNA sample was used for UV-visible light absorbance measurement at 260 nm and 280 nm wavelength based on the Beer-Lambert law. DNA concentration was automatically calculated by nanodrop and recorded in ng μL^{-1}. The absorbance ratio between A_{260}/A_{280} was used to assess DNA quality. The DNA is accepted as pure, if the absorbance ratio is around ~1.8. A ratio below 1.8 typically indicates contamination with protein, phenol

or other contaminants absorbing strongly in that range. DNA with a ratio below 1.8 was not used for further treatment.

4.1.4. DNA sequencing

All isolated DNA samples (15 µL, 50-100 ng µL^{-1}) were sent to Eurofins MWG Operon (Ebersberg, Germany) for sequencing using primers listed in **Chapter 3.4.2**

4.1.5. Standard Cloning (Subcloning) Restriction and ligation

Restriction endonuclease enzymes were used for standard cloning into vector backbones pTT5 or pET11a. These enzymes were used to assess DNA fragmentation at defined recognition sequences. For each construct, 1 µg DNA was digested using two different restriction enzymes and the corresponding restriction buffer. Preparative digestion was carried out for at least 2 h at the temperature optimum of the respective enzymes using a final volume of 30 µL. Restriction enzymes were heat inactivated at 80°C for 20 min, to stop the digestion. Vector backbone DNA was further treated with 1 µL calf intestinal Antarctic phosphatase (CIP) for 45 min at 37°C, to catalyze dephosphorylation at the 5'- end of DNA strands. Dephosphorylation prevents the vector backbone from re-ligation. Insert DNA was not treated with CIP to ensure proper insertion into vector backbone. CIP was heat inactivated by 65°C for 10 min. To ensure successful ligation of pTT5 vector backbone and Fab-Int^{N}, oaSEED-Int^{C} or Fc-Int^{C} or pET11a vector backbone and VHH- Int^{N}, a 1:3 molar ratio of backbone DNA to insert DNA was used. The following equation (Equation 1) was used to calculate the appropriate amount of insert DNA used for ligation. Typically, 100 ng of dephosphorylated vector backbone DNA was used as starting material.

$$\text{Insert [ng]} = \frac{\text{Insert bp}}{\text{Vector bp}} * \text{Vector [ng]} \qquad \text{Eq. 1}$$

Sizes of vector backbones pTT5 and pET11a as well as for the inserts are listed in **Chapter 3.2**. 1 µL QuickLigation was supplemented with the respective Ligation buffer and mixed with dephosphorylated vector backbone DNA and Insert DNA up to a final volume of 20 µL. Compounds were mixed properly, and the reaction was performed for 5 min at 25°C. A negative control was used by replacing the insert DNA with MilliQ-H_2O. An empty pTT5 or pET11a vector was serving as a positive control for transformation in Top10 cells and plating on LB agar plates (**Chapter 4.2.1**). The ligation mix (1 µL) was transformed into *E. coli* BL21 (DE) and colony PCR was performed to verify the correct insertion of the inserts.

4.1.6. Two-step polymerase chain reaction for site-directed mutagenesis (QuickChange)

For introduction, deletion or changes of nucleotides, site-directed mutagenesis was performed using a QuikChangeII site-directed mutagenesis kit. Aside from the manufacturers protocol, a second PCR protocol was developed to avoid primer dimer formation and improved mutagenesis rate. Briefly a master mix (5 µL reaction buffer, 1 µL PfuUltra HF DNA polymerase (2.5 U/µL), ddH_2O to a final volume of 50 µL) for two-step PCR

was prepared in 0.2 µL PCR tubes on ice. All non-enzyme components were thawed at room temperature. Master mix components were mixed by pipetting. The master mix was split into 2x48 µL and to each part 0.1 µM of either forward or reverse primer was added. Individual first step amplifications were allowed by an initial denaturation step at 98°C for 30s, followed by 5 cycles of amplification using a denaturation step at 98°C for 10s, annealing at 55°C for 30 s and extension at 68°C for 5 min depending on the plasmid size (1 min / 1 kb of plasmid). The annealing temperature was adjusted according to the melting temperatures of the used primers. Both PCR mixtures including either forward or reverse primers, were mixed and subsequently evenly distributed again to 50 µL. A second amplification step was performed using the same conditions as amplification step 1 for 14 cycles including an additional final extension step at 68°C for 3 min. PCR mix was incubated on ice for 2 min and treated with 1 µL *Dpn*I restriction enzyme for 1-1.5 h at 37°C, to digest parental methylated DNA. 1-2 µL of the digested PCR mix was transferred to supercompetent XL1-Blue *E. coli* cells for transformation.

4.1.7. Colony PCR

The correct ligation of pTT5 vector backbone and Fab-Int^N, oaSEED-Int^C or Fc-Int^C or pET11a vector backbone and VHH- Int^N was determined by colony PCR. Bacterial colony material (half of a colony) from agar plates was picked in 0.2 mL PCR tubes with 50 µL REDTaq® solution containing reaction buffer with $MgCl_2$, 0.4 nM dNTP mix and 0.06 units μL^{-1}. Components were mixed properly by pipetting and placed in a PCR cycler. The insert amplification started with an initial denaturation step at 94°C for 3 min, denaturation at 94°C for 30 s, annealing at 55°C for 30 s, extension at 72°C for 1 min and a final extension step at 72°C for 6-10 min. Colony PCR products were analyzed via gel electrophoresis according to **Chapter 4.1.9**. Gel bands were expected at the size of the insert for correct ligation. A negative control sample was used by replacing primer pairs by MilliQ-H_2O.

4.1.8. DNA purification

DNA fragments derived from Gel extraction or PCR amplification were purified using a gel extraction / clean up kit (QIAquick Gel Extraction Kit) according to the manufacturers protocol. DNA was eluted with pre-warmed H_2O (60°C) in a final volume of 10-20 µL. The DNA concentration was determined by UV spectrometry (Nanodrop™ One/ND1000).

4.1.9. Gel electrophoresis and gel extraction

The migration velocity of DNA fragments depends on molecular weight, conformation, agarose gel concentration and strength of the electrical field. Charged molecules migrate with different velocities through the gel depending on their molecule sizes. Linear DNA fragments of the vector backbone pTT5 or pET11a were separated using a 0.8% agarose gel, while Insert DNA fragments were separated using a 1.5 – 1.8% agarose gel. Agarose gels were prepared in TAE buffer and supplemented with GelRed™ solution (1:10 000). DNA samples were treated with 6x loading dye and subsequently loaded (6 µL) on agarose gels. A standard Perfect DNA™ marker (0.1 – 12 kbp) served as a ladder for size determination. Electrophoresis was performed at constant 110 V

for 30 to 35 min. The DNA bands were visualized under UV light using the gel imaging system GBX. The bands corresponding to the correct size of the linearized vector backbone and insert were excised of the gel using a clean scalpel. Gel fragments were transferred to an Eppendorf tube and further prepared for DNA extraction following the manufacturers protocol from QIAquick Gel Extraction Kit.

4.2. Microbiological methods

4.2.1. Transformation in *E. coli* and plasmid preparation

50-100 ng of plasmid DNA was added to 50 µL of chemically competent Top10 *E. coli* cells for heat shock transformation. Cells were thawed on ice for 10 min and afterwards supplemented with plasmid DNA followed by an incubation on ice for 30 min. Cells were undergoing a thermal shock at 42°C for 45 s followed by another incubation step on ice for 2 min. Cells were allowed to recover after addition of 500 µL super optimal broth with carbolite repression (SOC) medium at 37°C for 1.5 h. 150 µL transformed cells were plated on LB agar plates with selection marker ampicillin. Plates were cultivated over night for at least 18 h at 37°C until further treatment or stored at 4°C for at most 4 weeks. Glycerol stocks were prepared in 17% glycerol after cultivation of liquid pre-cultures in LB medium (**Chapter 4.2.4**) for long term storage and kept at -80°C.

4.2.2. *ClearColi* transformation

ClearColi® BL21 (DE3) electrocompetent cells were thawed on ice for 10-20 min and afterwards 25 µL were transferred into a chilled microcentrifuge tube on ice and supplemented with 1 µL plasmid DNA. The cell/DNA mix is transferred into a chilled electroporation cuvette avoiding bubbles. Electroporation was performed according to the manufacturers protocol (10 µF, 600 Ohm, 1800 V). Cells were supplemented with 975 µL expression recovery medium and incubated at 37°C for 1.5 h under shaking conditions (200-250 rpm). 100 µL of transformed cells were plated on LB agar plates with selection marker ampicillin. Plates were cultivated for 32 - 40 h at 37°C until further treatment or stored at 4°C for at most one week. Glycerol stocks were prepared in 17% glycerol after cultivation of liquid pre-cultures in LB medium (**Chapter 4.2.4**) for long term storage and kept at -80°C.

4.2.3. Culture medium

All liquid and solid culture medium were autoclaved for 20 min at 121°C and 200 kPa. For selective production of bacterial strains, Kanamycin (Kan) or Ampicillin (Amp) with a concentration of 50 µg mL^{-1} or 100 µg mL^{-1} respectively was added to the culture medium after sterilization. Ampicillin was sterilized separately by using filter sterilization 0.2 µm (Whatman™, Sigma-Aldrich) and added under sterile conditions to the autoclaved culture medium at a temperature < 60°C.

4.2.4. Cultivation of liquid pre-cultures in 200 mL scale

Freshly transformed *E. coli* BL21(DE3) and *ClearColi* BL21(DE3) containing pET11-Her2-VHH-*Npu*DnaE^{N}-His_6 were grown on selective LB-agar plates with ampicillin resistance. One colony was picked and transferred into LB medium containing 2% glucose and incubated 16 h over night at 28°C and 160 rpm (50 mm throw).

Cryostocks were prepared by adding 17% glycerol to the cells exhibiting an OD_{600} between 5 and 8 and a pH range between 6.2 and 7.2. Cells were stored at -80°C until usage. Cells were thawed at room temperature and pre-culture was inoculated with an OD_{600} of 0.00005 using LB medium supplemented with 2% glucose. Pre-culture was incubated at 28°C at 160 rpm (50 mm throw) for 16 h overnight. Cells were transferred into Superbroth medium (20 g L^{-1} tryptone, 5 g L^{-1} yeast extract, 2.4 g L^{-1} $MgSO_4$, 0.5 g L^{-1} NaCl, 0.186 g L^{-1} KCl and 20 mM glucose) with a cell density of OD_{600} 0.3 and grown until mid-log phase 0.6 - 0.8 at 30°C and 160 rpm (50 mm throw). Cells were induced with 400 µM IPTG and incubated at 35°C for 3 h at 160 rpm (50 mm throw). Cells were harvested and prepared for purification.

4.2.5. Cultivation of liquid pre-cultures in MTP´s

ClearColi BL21(DE3) and *E. coli* BL21(DE3) cryostocks containing pET11-Her2-VHH- *Npu*DnaE^N-His_6 were thawed at room temperature and pre-culture was set up in microtiterplates (Greiner) using either SOC medium for *E. coli* BL21(DE3) or Inhouse prepared minimal medium for *ClearColi* BL21(DE3). 10 µL from cryostocks (OD_{600}: 6.4) were transferred into 190 µL expression medium per well and incubated at 37°C and 700 rpm overnight. *ClearColi* pre-cultures were incubated for 48 h. Cells were transferred into Superbroth medium (20 g L^{-1} tryptone, 5 g L^{-1} yeast extract, 2.4 g L^{-1} $MgSO_4$, 0.5 g L^{-1} NaCl, 0.186 g L^{-1} KCl and 20 mM glucose) with a cell density of OD_{600} 0.3 and grown until mid-log phase 0.6 - 0.8 at 37°C and 700 rpm (25 mm throw). Cells were induced with 60 µM, 100 µM and 400 µM IPTG and incubated at 34°C for 3-24 h at 700 rpm (25 mm throw). Cells were harvested and prepared for analysis and purification.

4.3. Biochemical methods

4.3.1. Determination of Protein concentration

The concentrations of purified recombinant proteins were determined by either Bradford assay, absorbance measurement or Novagen® BCA protein assay kit. For BCA assay, a stock solution of 2 mg mL^{-1} BSA dissolved in 50 mM Tris-HCl buffer pH 7.5 or PBS pH 7.4 was prepared and diluted to various BSA concentrations as a standard. Sample concentration of the target proteins was determined using the equation achieved from regression curve corresponding to the standard. Therefore 25 µL of each sample was mixed with 200 µL of the BCA solution, and incubated for 30 min at 37°C. The BCA assay is based on the Biuret reaction. Amino acids from the target protein form a permanent bond with Cu^{2+} ions, resulting in a dark violet colored complex. This complex is stable enough to avoid precipitation of copper ions in alkaline environment. The color shift is detectable at a wavelength of 562 nm with a detection limit of 20 – 2000 µg mL^{-1} according to the manufacturers protocol. After cooldown at RT the absorbance of the samples was measured and analyzed via standard curve equation. Determination of protein concentration via Bradford assay using the Pierce™ Coomassie Plus assay kit, was performed according to the manufacturers protocol. In brief, a standard calibration curve was generated by serial dilutions of 0.1 – 1 mg mL^{-1} BSA. Samples were diluted to fit the range of the BSA concentrations and 5 µL of each sample and BSA dilution for standard curve generation was added in duplicates or triplicates into a 96 well microtiter plate. Additionally, 150 µL Bradford reagent was added to the samples and mixed by pipetting followed by incubation for 30 min protected from light. Absorbance was measured at 595 nm and

protein concentrations were calculated via standard curve equation. Protein concentration of purified samples was measured by absorbance at 280 nm using the Nanodrop ND-1000 or Nanodrop One based on the law of Lambert-Beer. 1.5 – 2 µL of purified sample was added to the Nanodrop pedestal and protein concentration was calculated by addition of molecular weight (kDa) and molar extinction coefficient (M^{-1} cm^{-1}) parameters of the sample.

4.3.2. Antibody purification via MabSelect columns

Cell free Expi293F supernatant including antibody fragments fused to Int^C were loaded with 2.5 mL min^{-1} onto a 5 mL HiTrap MabSelect SuRe column (GE Healthcare) after equilibration with 10 CV PBS (pH 7.4) using an ÄKTA Pure system. After sample loading and wash out with PBS, elution was carried out isocratically with 20 mM acetic acid at pH 3.2. Elution fractions were collected as 1 mL fractions and pH was adjusted to pH 6.8 by using neutralization buffer containing 1 M Tris at pH 8. The fractions containing the protein of interest were pooled and concentrated with Amicons (Merck Millipore) for additional purification steps. Purity was analyzed by SDS-Gel PAGE and SE-HPLC before further treatment. Concentrated antibody solution was loaded onto a HiLoad Superdex 200 pg column (GE Healthcare) for final polishing. Elution was carried out in PBS (pH 6.8) and collected as 1 mL fractions in a 96 deep well plate. Fractions containing the protein of interest were pooled and filter sterilized (0.2 µm Whatman™) before storage. Purity was monitored by precast SDS-PAGE (Thermo Fisher Scientifics) using standard protocols and SE-HPLC, while identity was confirmed by mass spectrometry analysis. Purified antibody fragments were stored either at 4°C or treated with liquid nitrogen for storage at -80°C.

4.3.3. Antibody purification via MabSelect beads

25 mL cell free supernatant, containing POI, was treated with 400 µL MabSelect SuRe beads (GE Healthcare) with a binding capacity of 35 mg human IgG mL^{-1} and incubated for 1 h at room temperature under shaking conditions. Solution was resting for 30 min, until beads sedimented at the bottom. Supernatant was carefully discarded, and beads were resuspended in 5 mL Expi293F Expression medium. Beads were transferred into a 24 well filter plate (Sigma-Aldrich) or bottle top filter (0.22 µm, Nalgene Rapid-Flow Bottle Top Filter, Thermo Fisher Scientific) for larger volumes > 50 mL. Beads were washed 4 times with 1 mL high salt buffer (25 mM Sodium phosphate buffer, 0.5 mM NaCl, pH 7.0) by applying vacuum and subsequently washed 4 times with 1 mL low salt buffer (20 mM Sodium phosphate buffer, 0.15 mM NaCl, pH 7.0. Antibodies were eluted with 4 x 500 µL elution buffer (20 mM acetic acid, pH 3.2) and pH was adjusted with 200 µL neutralization buffer (0.5 M sodium phosphate buffer pH 8.0) directly after elution. Solution was concentrated via Amicons (Merck Millipore) and filter sterilized for storage at 4°C.

4.3.4. Antibody purification via Ni-NTA columns

Cell free Expi293F supernatant including antibody fragments fused to Int^N or antibody fragments derived from cell free *E. coli* supernatant after cell lysis (**Chapter 4.3.5**) were diafiltrated using either the Cogent® µScale Tangential Flow Filtration (TFF) System with three Pellicon® 3 88 cm^2 cassettes (10K Da MWCO) or dialysis

membranes (SpectraPor®, 10K Da MWCO) and samples were dialyzed against PBS pH 7.4 over night at 4°C, followed by ion metal affinity chromatography (IMAC). IMAC is capable to capture proteins compromising a hexahistidine tag by high affinity towards Ni^{2+}. Samples were loaded with 1 mL min^{-1} onto a 1 mL or 5 mL HisTrap™ HP column (GE Healthcare) under native conditions after equilibration with 10 CV buffer A (50 mM Na-P, 500 mM NaCl, 20 mM imidazole pH 7.4) using an ÄKTA Pure system. The column matrix consists of agarose functionalized with nitrilotriacetic acid (NTA). Additionally, Ni^{2+} ions are immobilized on the column matrix interacting with histidine residues from recombinant proteins and facilitates the affinity binding of these proteins. Column bound proteins are displaced by metal binding ligands such as imidazole in relatively high concentrations. Supernatant from *E. coli* cell lysis was treated additionally with 5 mM $MgCl_2$, 25 U/ml Benzonase, Protease Inhibitor CocktailSET III 1:1000. Reducing agent was left out in buffer A, to avoid unspecific C-terminal cleavage of the fused intein. After sample loading and wash out with buffer A, elution was performed by increasing the imidazole concentration stepwise from 20 mM, 50 mM, 100 mM, 150 mM, 250 mM to 500 mM. Fractions containing proteins were collected in 1 mL deep well plates and pooled afterwards according to the chromatogram. Each pooled fraction was analyzed by precast SDS-PAGE to estimate the fractions containing the protein of interest, followed by concentration using Amicons (Merck Millipore) and an additional purification step via size exclusion for final polishing. Concentrated antibody solution was loaded onto a HiLoad Superdex 200 column (GE Healthcare). Elution was carried out in PBS (pH 6.8 or 7.4) and collected as 1 mL fractions in a 96 deep well plate. Fractions containing the protein of interest were pooled and filter sterilized (0.2 µm Whatman™) before storage. Purity was monitored by precast SDS-PAGE (Thermo Fisher Scientific) using standard protocols and SE-HPLC, while identity was confirmed by mass spectrometry analysis. Purified antibody fragments were stored either at 4°C or treated with liquid nitrogen for storage at -80°C.

4.3.5. *E. coli* cell lysis for Ni-NTA purification

After cell harvest, cells were treated with lysis buffer containing 16 mL Celllytic B per g cell pellet 50 mM Tris-HCl, 0.5 M NaCl, 10 mM imidazole and 1U benzonase. Lysis was performed for 30 min at 220 rpm (25 mm throw incubator) at RT. Cell debris was centrifuged afterwards at 20.000 rpm for 30 min at 4°C (Multifuge 3SR, Heraeus). A 1 mL HisTrap™ HP column (GE Healthcare) was equilibrated with 15 CV binding buffer (50 mM Tris-HCl, 0.5 M NaCl, 10 mM imidazole). Sample was loaded onto the column and wash out was performed with 15 CV binding buffer. Elution was carried out by increasing the imidazole concentration stepwise from 20 mM, 50 mM, 100 mM, 150 mM, 250 mM to 500 mM (**Chapter 4.3.4**). Fractions containing proteins were collected in 1.5 mL Eppendorf tubes and pooled after SDS-PAGE analysis and concentrated using Amicons (Merck Millipore). Protein of interest was determined by western blot analysis and fractions were dialyzed over night against PBS pH 7.4 (Pur-A-Lyzer, Sigma-Aldrich) and stored at 4°C for additional experiments.

4.3.6. Size exclusion chromatography (SEC)

Size exclusion chromatography (SEC) is a chromatography method to distribute proteins in solution by their size or molecular weight depending on the length and pore sizes of the column. SEC is mostly the last step

within a purification process and therefore known as protein polishing. SEC allows to efficiently separate the protein of interest from aggregates or higher and smaller molecular size impurities. This method can be distinguished into preparative and analytical SEC.

4.3.7. Preparative SEC

Preparative SEC was applied to obtain monomeric antibodies and antibody fragments in high purity. Reference antibodies and oaSEED fragments were transported in an aqueous solution (PBS pH 7.4) through a HiLoad Superdex 26/60 200 pg, Hi Load Superdex 26/600 200 pg or HiLoad Superdex 16/600 200 pg depending on the sample volume. Fab fragments were purified using a HiLoad Superdex 16/60 75 pg column. Small sample volumes < 500 µL were purified using a HiLoad Superdex 200 increase 10/300 GL column. In brief, all columns were equilibrated with 2 CV PBS buffer (pH 7.4) and a flow rate of 1 mL min^{-1} followed by sample addition via sample loop injection. Fractions were collected in a 96 deep well plate in a final volume of 200 – 800 µL depending on the used column. Fractions including the protein of interest were pooled and concentrated with Amicon® Ultra-15 centrifugal filters (10K Da MWCO). Protein concentration was determined by Nanodrop measurement as described in **Chapter 4.1.3**. Purity was determined by SDS analysis (**Chapter 4.3.12**) and analytical SEC (SE-HPLC).

4.3.8. Analytical SEC

Antibody purity and molecular size after purification was determined by analytical size exclusion high performance liquid chromatography (SE-HPLC). Samples were transported in aqueous solution (mobile phase) through a TSK Super SW3000 column using an HPLC Agilent 1260 (ChemStation LC 3D) device. The column was equilibrated with mobile phase buffer at a flow rate of 0.35 mL min^{-1} for at least 45 min, resulting in a stable baseline measured by UV detection. 5 molecular weight markers (Gel filtration standard, BioRad) were used for correct molecular size determination. Antibody samples were diluted in PBS buffer, if necessary, to a final concentration of 1 mg mL^{-1}. A minimum of 10 µg per sample was injected to the system. The UV signal was detected at 214 nm and 280 nm followed by peak integration for purity determination (ChemStation software). Molecular size was calculated based on obtained retention times of the desired proteins and the gel filtration standard.

4.3.9. Split intein mediated antibody reconstitution and purification (molar ratios)

Fab/VHH- and SEED-fragments fused to Int^N and Int^C split intein segments were mixed in an equimolar ratio (1:1) in splicing buffer (PBS: 10 mM $PO4^{3-}$, 2.7 mM KCl 150 mM NaCl, pH 7.4) for PTS mediated bsAb reconstitution. Fab- and Fc- fragments offering 2 ligation sites were mixed in a molar ratio of 1:2, to generate bivalent antibodies. TCEP was added to the antibody fragments in a final concentration of 0.5 mM, to activate PTS, followed by incubation for 2 h at 37°C or 4 h at RT. After reconstitution, the antibody mixture was treated with 30 µL pre-washed HisPure Ni-NTA resin (Thermo Fisher Scientific), offering a total binding capacity of 1.8 mg, to remove non-reconstituted antibody fragments. Additionally, 10 mM imidazole was added to avoid unspecific binding of reconstituted antibodies to the Ni-NTA resin. The mixture was incubated at RT for 1 h

under shaking conditions (Thermomixer) at 900 rpm to capture non-reconstituted antibody fragments. The supernatant was separated from the Ni-NTA resin and supplemented with a 20-molar excess of dehydroascorbic acid (DHAA) over TCEP and incubated at 37°C for 1-2 h or at RT overnight to quench PTS and complete re-oxidation of the reconstituted antibody. To monitor successful PTS and formation of reconstituted antibodies, Samples were taken every 10 to 20 min and supplemented with 4x lithium dodecyl sulfate (LDS) buffer (Invitrogen) including 0.1% H_2O_2 for complete oxidation of TCEP. Samples were boiled at 70°C for 10 min and samples were analyzed by SDS-PAGE (4-12% Bis-Tris gels, Novex, Invitrogen) followed by Coomassie Instant blue protein staining (Expedeon) according to **Chapter 4.3.12** and **4.3.13**.

4.3.10. HT protein analysis

High throughput protein analysis of reconstituted antibodies was performed by LabChipGXII (PerkinElmer). The LabChip and reagents were equilibrated for 30 min at RT. Dye solution was thawed completely and vortexed for 20 s at 9300 rcf. 520 µL of Protein express gel matrix was transferred to the provided spin filter. 20 µL of protein dye solution was added to the gel matrix in the spin filter and mixed gently by inverting. When solution is homogeneously mixed, it was spun down at 9300 rcf for 5 min. 250 µL of protein express gel matrix was transferred into another spin filter, serving as a destain solution. The solution was centrifuged at 9300 rcf for 5 min. Prepared solutions were prevented from light exposure and stored in the dark until ready to use. Each wells of the lab chip were aspirated, using an empty pipette tip and applied vacuum to remove storage liquid. All wells were rinsed 2 times with distilled water. Each active chip well (1, 2, 3, 4, 7, 8, 9 and 10) was filled either with gel dye solution (3, 7, 8 and 10) or destain solution (well 2 and 9). 120 µL of marker solution was transferred to chip well 4. Samples for LabChip analysis were prepared in a 96 well PCR plate (Eppendorf). 5 µL of protein sample was transferred into the 96 well plate for high sensitivity analysis. 35 µL of Milli-Q® water was added to each sample and mixed well by pipetting. Protein express ladder was vortexed for 10 s and centrifuged briefly to ensure no precipitation in the solution. 12 µL protein express ladder was transferred into a microcentrifuge tube. Samples and protein express ladder were incubated at 70°C for 10 min for denaturation. Samples were spun down after boiling at 1200 rcf for 2 min. 120 µL Milli-Q® water was added to the protein express ladder, while 750 µL of protein express wash buffer was transferred to the provided buffer tube. Samples, LabChip, protein express ladder and protein express wash buffer was placed into the LabChip GXII touch device. High throughput analysis was executed and monitored online using the LabChip GX v5.2 software. Electropherograms and virtual gels of reconstituted antibody samples were evaluated and analyzed with LabChip GX Reviewer v5.2.

4.3.11. Enzyme-linked immunosorbent assay (ELISA)

ELISA was conducted to confirm binding to recombinant target protein huCD40-avi-his (Merck KGaA). The wells of a Nunc 96 well MaxiSorb flat bottom plates (Thermo Fisher Scientific) were coated with 100 ng to 1 µg well^{-1} target protein diluted in 100 µL PBS (pH 7.4) and incubated either for 1 h at room temperature or at 4°C over night. A microplate washer ELx405 (BioTek) washed the coated plate with 3 x 300 µL PBS (pH 7.4 + 0.05% Tween). Subsequently the wells were blocked with 300 µL blocking solution (PBS, pH 7.4 + 2% BSA per

well) and incubated for 1 h at RT, to saturate unspecific binding sites. After incubation the wells were washed again with 3 x 300 µL PBS (pH 7.4 + 0.05% Tween) and supplemented afterwards with 10 to 100 ng well^{-1} reconstituted CD40 antibodies. Reconstituted antibodies were diluted in blocking buffer in a final volume of 100 µL and incubated for 1 h at RT. A repeated washing step with 3 x 300 µL PBS (pH 7.4 + 0.05% Tween) was conducted followed by addition of detection antibody goat-anti-human conjugated to POD (g-a-h POD), diluted 1:5000, and incubation for 1 h at RT. The wells were washed again with 3 x 300 µL PBS (pH 7.4 + 0.05% Tween). 100 µL of 1-step Ultra TMB ELISA solution (Thermo Fisher Scientific) was added to each well and incubated for 1 to maximum 10 min, until a blue color shift was observed. 100 µL of 1 M H_2SO_4 solution was added to each well, resulting in another color shift from blue to yellow. Reference antibodies were used as a positive control. Fc-Int^C and Fab-Int^N single fragments and combined without the addition of TCEP were used as a negative control. Wells treated with PBS buffer instead of reconstituted antibodies, served as negative controls and to visualize potential background effects of g-a-h POD detection antibody. To confirm positive ELISA signaling, the coated target proteins on the plate surface were incubated with anti-penta his (1:1000) and goat-anti-mouse POD (1:5000), serving as a coating control. Absorbance after color change was measured at 450 nm using a Paradigm™ plate reader (BeckmanCoulter). Analysis was performed using a multimode analysis software. Binding to other recombinant target proteins confirmed by ELISA, was conducted similar to the above described protocol.

4.3.12. SDS-PAGE

Protein determination and purity was analyzed by sodium dodecyl sulfate polyacrylamide gel electrophoresis (SDS-PAGE). Proteins are migrating to a NuPAGE® Bis-Tris gel (4-12%) and forced to distribute by molecular weight in an electric field. Protein samples for electrophoresis were loaded onto the wells after mixing with 4x LDS sample buffer and heated up to 70°C for 10 min for denaturation. A protein standard SeeBlue® Plus 2 prestained protein marker indicating different protein sizes was added as a marker in one of the wells. The chamber was filled with MES(2-(N-morpholino) ethanesulfonic acid) running buffer. The proteins were separated using a fixed voltage of 200 V for 38 min. Gels were removed from the cast and stained by using Coomassie staining solution (**Chapter 4.3.13**) or further treated for western blot analysis (**Chapter 4.3.14**).

4.3.13. Coomassie staining

Bis-Tris gels were transferred after electrophoresis into Coomassie staining solution (InstantBlue™). Gels were slowly agitated at RT for 45 min. The staining solution was replaced by H_2O and incubated under shaking conditions for 60 min to visualize the protein bands.

4.3.14. Western Blotting

Specific protein detection and visualization was performed by western blot analysis. After SDS-PAGE under denaturing conditions, gels were transferred to a polyvinylidene difluoride (PVDF) membrane and proteins were blotted on the membrane using the iBlot system (program 3, 7 min and 20 V). The membrane was rinsed in iBind solution and prepared for specific antibody detection using the iBind system according to the

manufacturers protocol. The membrane was treated with a primary antibody, which recognizes and binds to a specific target. A second antibody, conjugated to horse reddish peroxidase (HRP) or alkaline phosphatase (AP), which recognizes and binds the primary antibody, was used for visualization of the target protein in the sample. After antibody treatment the membrane was rinsed with H_2O and transferred to a BCIP/NBT detection solution. The colorimetric detection mediated by HRP or AP and the corresponding substrate in the detection solution resulting in a stained membrane indicating the specific target protein. Blot development was stopped by replacement of detection solution and a quick rinse in H_2O.

4.3.15. Homogeneous Time Resolved Fluorescence (HTRF)

HTRF is a combination of a classical Förster resonance energy transfer (FRET) with a time resolved detection of fluorescence. The FRET system is based on the energy transfer of two fluorophores in close proximity. One fluorophore is acting as a donor, the other one as acceptor. In combination with time resolved measurement, this technology allows for elimination of non-specific short-lived background fluorescence caused by sample components like buffers, proteins or cell lysates. In brief, HTFR reagents were reconstituted according to the manufacturers protocol. Streptavidin-d2 was mixed with 0.3% Tween-20 in terbium buffer in a final concentration of 0.1 mg mL^{-1}. pAb anti-human IgG-Tb cryptate was diluted with 0.3% Tween-20 and terbium buffer in a final concentration of 0.01 mg mL^{-1}. Each sample was diluted in PBS pH 7.4 and 0.3% Tween-20 to a final concentration of 0.1 µM. All samples and HTRF reagents were dispensed automatically (Tecan D300e liquid dispenser) in a 1536 well plate. Terbium buffer was used for normalization with 0.3% Tween-20 diluted in PBS pH7.4. 0.075 µL of Streptavidin-d2 solution (0.1 mg mL^{-1}) and IgG-Tb solution (0.01 mg mL^{-1}) was added to 0.05 µL sample solution (0.1 µM). The final volume in each well contained 5 µL. The plate was sealed with a sealing foil to avoid evaporation of the samples. Samples were incubated 4 h at RT followed by fluorescence measurement at 337 nm and 665nm/615nm ratio (EnVision 2104 plate reader). To calculate the ratio for data reduction for each well, following equations were used:

$$\text{ratio} = 10^4 * \frac{\text{Emission}_{620\text{nm}}}{\text{Emission}_{665\text{nm}}} \qquad \text{Eq.2}$$

The ratio calculation was used to minimize well to well variations because the background noise of the donor is normalized for each well.

Minimization of plate to plate variations were calculated by the equation below (Eq.3) normalizing the measurement for each well.

$$\Delta F = \frac{\text{ratio}_{\text{sample}} - \text{ratio}_{\text{negative control}}}{\text{ratio}_{\text{negative control}}} \qquad \text{Eq.3}$$

To cross validate the HTRF measurements, HPLC analysis was performed.

4.4. Cell biological methods

4.4.1. Thawing mammalian cell lines and suspension cultures

Adherent or suspension cell lines were provided in cryovials at -180°C. Cells were thawed in a water bath at 37°C under slight swirling of the cryovial. Cells were immediately treated with 10 mL pre-warmed medium after thawing and transferred into a 50 mL falcon tube. Cells were centrifuged at 250 x g for 10 min at RT to remove DMSO and serum components, contained in the cryopreservation medium. The supernatant was carefully removed, and cells were resuspended in fresh pre-warmed medium (10 mL). Adherent cells were seeded in a T-25 or T-75 flask depending on the cell density and incubated for 3 to 4 days at 37°C, 5% CO_2 in a humidified atmosphere. Suspension cells were seeded in a 50 mL shaking flask (Corning) for 3 to 4 days at 37°C, 5% CO_2 and 90 rpm (50 mm throw). Adherent cells were split after reaching a confluency of >80% with a viability of >90%, while suspension cells were split after reaching >95% viability with a certain cell density according to the manufacturers protocol.

4.4.2. Transient antibody expression in Expi293F

Plasmids were prepared using GenElute™ HP Plasmid Maxiprep Kit (Sigma-Aldrich) following manufacturer's instructions and sequence was verified by sequencing. Expi293F cells (source) were seeded with 1.3 x 10^6 vc mL^{-1} 2 days post transfection. Cells should have reached a cell density of >3.0 x 10^6 vc mL^{-1} and a viability of >96% at the day of transfection. Cells were diluted to 2.9 x 10^6 vc mL^{-1} prior to transfection using pre-warmed Expi293F expression medium. Cell counting was determined using Vi-Cell® XR (BeckmanCoulter). The DNA was diluted in OptiMEM serum free medium to a final concentration of 1 mg L^{-1} and gently mixed. The chain ratio for heavy and light chains was 1:1 for Fab fragments and 1:1:1 for SEED-molecules. 2.7 µL ExpiFectamine™ 293 Reagent per µg DNA was diluted in OptiMEM serum free medium and gently mixed. ExpiFectamine™ 293 Reagent was transferred to diluted DNA and incubated at room temperature for 20 min for complexation. The DNA/Fectamine complex was added dropwise to the cells under shaking conditions. Cells were incubated at 37°C and 5% CO_2 at 80 rpm (50 mm throw). Cells were supplemented with 5 µL mL^{-1} ExpiFectamine™ 293 Transfection Enhancer 1 and 50 µL mL^{-1} ExpiFectamine™ 293 Transfection Enhancer 2, 20 h post transfection. Culture was harvested either after 6 days post transfection, or when cell viability dropped below 80%. Cells were centrifuged at 4000 x g for 20 min at 4°C and supernatant was filter sterilized (0.22 µm, Nalgene Rapid-Flow Bottle Top Filter, Thermo Fisher Scientific) before following purification or analysis.

4.4.3. Cell culture

HT1080 hCD40 (human fibrosarcoma), SK-BR-3 and A549 cells were cultured in DMEM high glucose medium supplemented with 10% FCS, 2 mM L-glutamine and 1 mM sodium pyruvate.

MDA-MBA-468 (human adenocarcinoma), MKN-45 (human gastric adenocarcinoma), Jurkat E6.1 cells were cultured in RPMI 1640 medium supplemented with 10% FCS, 2 mM L-glutamine and 1 mM sodium pyruvate.

CD40 HEK293 stable cell line and EBC-1 cells were cultured in MEM medium with earl salts, 10% FCS, 2 mM L-glutamine and 1 mM sodium pyruvate and 1 mM non-essential amino acids.

All cell lines were cultured at 37°C in a humidified 5% CO_2 atmosphere. Cells were sub-cultured in cell culture adherent T75 flasks (Greiner) at 90% confluence and >90% viability monitored by microscopy (Leitz LABOVERT, Wetzlar, Germany) and ViCell XR (BeckmanCoulter) analysis. To split cells, conditional medium was removed from the flask and cells were washed with pre-warmed PBS. To loosen adherent cells from surface attachment, 1 mL of pre-warmed 0.05% trypsin/EDTA was added and incubated for 5 min at 37°C. Trypsinization was stopped by adding fresh culture medium, including FCS. Cell density was determined by ViCell XR (BeckmanCoulter) analysis and cells were seeded with an appropriate cell density (1:5 or 1:10 depending on the cell doubling time) to a new T75 flask.

4.4.4. Flow cytometry

Guava easyCyte HT cytometer was used to perform flow cytometric analysis. Adherent cells were detached from the well surface by addition of 1 mL pre-warmed 0.05% trypsin/EDTA, when cells reached a confluency of 80-90%, followed by incubation for 5 min at 37°C. Fresh culture medium, containing FCS, was added to stop trypsinization, followed by cell counting via Vi-CELL XR. 1 x 10^5 cells per cavity of a 96 well plate (Greiner) were used to investigate cellular binding. Cells were washed in 200 µL FACs binding buffer (PBS pH 7.4, 1% BSA) and subsequently distributed to each cavity of the 96 well plate in a final volume of 100 µL. After washing, cells were treated with reconstituted antibodies using a final concentration of 10 µg mL^{-1} and further incubated for 1 h on ice. Cells were centrifuged at 250 x g for 10 min at 4°C and washed twice with 200 µL binding buffer. Secondary fluorescently labeled detection antibody (Alexa Fluor® 488-conjugated AffiniPure Goat Anti-Human IgG) was incubated together with cells for 30 min to maximum 1 h at 4°C, protected from light to prevent fluorescent activation, to determine cell binding. Finally, cells were washed twice again and resuspended in binding buffer, prior to FACS analysis. Software Guava ExpressPro was used for analysis.

4.4.5. Cellular binding of CEACAM bsAb on MKN-45 and HEK293 Nf-κB reporter cell line cells

Flow cytometric analysis was performed using the Guava easyCyte HT cytometer (**Chapter 4.4.4**). Cellular binding of reconstituted and parental CEACAM bsAbs were performed with 1 x 10^5 cells per cavity in a 96 well plate (Greiner). Binding was confirmed by using MKN-45 cells as a positive cell line for CEACAM and HEK293 Nf-κB reporter cells as a negative cell line. On the day of flow cytometry analysis, cells were detached and distributed to 96 well plates according to **Chapter 4.4.3** To detach adherent cells from the well surface, 1 mL of pre-warmed 0.05% trypsin/EDTA was added and incubated for 5 min at 37°C at a confluency of 80-90%. Trypsinization was stopped by adding fresh culture medium, including FCS and cells were counted by Vi-CELL XR. Cells were washed afterwards in FACS binding buffer (PBS pH 7.4, 1% BSA) and distributed to the 96 well cavities in a final volume of 100 µL. Cells were treated with 10 µg mL^{-1} reconstituted and parental CEACAM5 and CEACAM6 bsAb and incubated for 1 h on ice. Cells were centrifuged at 250 x g for 10 min at 4°C and washed twice with binding buffer. All washing steps were carried out in a final volume of 200 µL. Cells were treated with secondary fluorescently labeled detection antibody (Alexa Fluor® 488-conjugated AffiniPure Goat Anti-Human IgG) to determine positive or negative cell binding. Secondary antibody was incubated for

30 min up to 1 h at 4°C covered from light to prevent fluorescent activation. Cells were washed again in binding buffer twice and resuspended before performing FACS analysis. Software Guava ExpressPro was serving as a determination tool for cell binding.

Analogous experiments with flow cytometry were performed for bivalent CD40 agonists binding to HT1080 CD40 and MDA-MB-486 cells and cellular binding of c-METxEGFR bsAbs on EBC-1 and A546 cells. Cellular binding of a bispecific T-cell engager OKT3xHer2 was conducted by FACS on SK-BR-3 and Jurkat E6.1 cells following the above mentioned protocol.

4.4.6. Antibody dependent cell mediated cytotoxicity (ADCC) assay

Antibody dependent cell mediated cytotoxicity (ADCC) assays were performed by using ADCC Reporter Bioassay Core Kit (Promega) according to the manufacturers protocol. Target cells (HT1080 or MKN-45) were seeded with 1.25 x 10^4 viable cells per cavity in an opaque white 96 well plate suitable for cell culture treatment (Perkin&Elmer). The inner 60 wells were used for ADCC activity determination, while the outer wells were filled with 75 µL ADCC buffer (low IgG FBS heat inactivated (Gibco) diluted in RPMI to avoid edge effects during the assay. Cells were incubated for 1 day over night at 37°C, 5% CO_2 at humidified atmosphere, to allow attachment. Medium was removed carefully and replaced by 25 µL ADCC buffer. Cells were treated with 50 nM to 1 µM antibodies diluted in ADCC buffer. Modified Jurkat effector cells were thawed in water bath at 37°C and diluted with ADCC buffer. The E:T ratio was set at 6:1 and 25 µL of effector cells (75 000 per well cavity) was added to the cells, followed by an incubation step at 37°C, 5% CO_2 for 6 h in a humidified atmosphere. BioGlo Luciferase substrate was resolved at RT prior to assay and covered from light until usage. After 6h incubation time, cells were equilibrated to RT for 15 min, followed by the addition of 75 µL per well BioGlo Luciferase substrate. Another incubation step was performed for 5-30 min at RT covered from light. Luminescence signal was measured with the Synergy4 (BioTek) at 0.5 s per well using a sensitivity of 170. The Gen5 software was used as a tool for ADCC determination. Background luminescence occurring from ADCC buffer was subtracted from sample wells and the relative luminescence units were plotted against the logarithmic scaled antibody concentration. Dose response curves were fitted using sigmoidal 4PL model by GraphPad Prism 7.

4.4.7. CD40 activation assay (CD40 reporter cell line)

A BPS Bioscience CD40 HEK293 Stable Cell Line (BPS Bioscience) was used to conduct CD40 activation. Therefore, CD40 expressing HEK293 cells were detached and seeded afterwards with 2.5 x 10^4 cells per cavity of a 96 well plate suitable for cell culture treatment (Perkin&Elmer). Only the 60 inner wells were used for CD40 activation. The outer wells were filled with 75 µL culture medium, to avoid edge effects. After seeding, cells were incubated for 1 day at 37°C, 5% CO_2 at a humidified atmosphere. After attachment, cells were treated with reconstituted antibodies, diluted in assay buffer, using a concentration range between 200 nM and 2 pM. Cells were incubated at 37°C, 5% CO_2 for 6 h at humidified atmosphere. BioGlo Luciferase substrate was reconstituted and adjusted to RT prior to cell treatment and protected from light until usage. Cells were equilibrated to RT for 15 min after antibody treatment, followed by addition of 75 µL BioGlo Luciferase

substrate per well. Further incubation at RT for 5-30 min was performed and protected from light exposure. Luminescence signals were measured at 0.5 s per well and a sensitivity of 170 using the Synergy4 (BioTek). Luminescence readout was analyzed with the Gen5 software. Luminescence background noise caused by the assay buffer was subtracted from sample wells. The relative luminescence units were plotted against the logarithmic scaled antibody concentration and dose response curves were generated and fitted by using a 4PL model in GraphPad Prism 7.

4.4.8. T-cell Activation Bioassay (NFAT)

T-cell activation assays were performed by using a T-cell Activation Bioassay (NFAT) Kit (Promega) according to the manufacturers protocol. Therefore, cells were detached and seeded afterwards with 4.0 x 10^4 cells per cavity of a 96 well plate suitable for cell culture treatment (Perkin&Elmer). Only the inner 60 wells were used for T-cell activation. The outer wells were filled with 75 µL assay buffer (low IgG FBS heat inactivated (Gibco) diluted in RPMI medium, to avoid edge effects. After seeding, cells were incubated for 1 day at 37°C, 5% CO_2 at humidified atmosphere. After attachment of the cells the medium was carefully removed and replaced by 25 µL assay buffer. Cells were treated with 25 µL reconstituted antibodies, using a concentration range between 0.01 nM and 100 nM to induce T-cell activation. Jurkat effector cells bearing a modified NFAT-re-luc2 pathway, were thawed quickly in a water bath at 37°C and diluted with assay buffer according to the manufacturers protocol (Promega). Cells were treated with 25 µL effector cells (1 x 10^5 cells per well cavity) and incubated at 37°C, 5% CO_2 at humidified atmosphere for 6 h. BioGlo Luciferase substrate was reconstituted and adjusted to RT prior to cell treatment and protected from light until usage. Cells were equilibrated to RT for 15 min after antibody treatment, followed by addition of 75 µL BioGlo Luciferase substrate per well. Further incubation at RT for 5-30 min was performed and protected from light exposure. Luminescence signals were measured at 0.5 s per well and a sensitivity of 170 using the Synergy4 (BioTek). Luminescence readout was analyzed with the Gen5 software. Luminescence background noise caused by the assay buffer was subtracted from sample wells. The relative luminescence units were plotted against the logarithmic scaled antibody concentration and dose response curves were generated and fitted by using a 4PL model in GraphPad Prism 7.

4.4.9. c-MET and EGFR phosphorylation assay

The phosphorylation of c-MET and EGFR was determined by western blot analysis using detection antibodies specifically directed against phosphorylated c-MET and EGFR. c-MET and EGFR expressing cancer cells (A549, EBC-1) were seeded with 1x10^5 vc per well in a 24 well tissue plate (Thermo Fisher) and incubated for 1 day at 37°C, 5% CO_2 at humidified atmosphere. The medium was replaced by a serum-starvation medium, lacking FCS, after a confluency of 80 – 95% was reached. Cells were incubated for another day at 37°C, 5% CO_2 at humidified atmosphere. Cells were treated with 300 nM reconstituted bispecific F06xhu225H and B10v5xhu225H antibodies and incubated for 3 h at 37°C, 5% CO_2. Cell stimulation was performed by addition of 100 ng/mL HGF and EGFR (R&D Systems) followed by incubation for 10 min at 37°C. Cells without HGF and EGF stimulation served as a negative control. Cells were treated subsequently with ice cold RIPA buffer containing protease inhibitor set III, phosphatase inhibitor set II (Calbiochem) and Benzonase (1:1000, Novagen)

under shaking conditions for 1 h at 4°C for cell lysis. Cell lysate samples were supplemented with 4x LDS sample buffer and boiled for 10 min at 70°C for SDS-PAGE analysis. The resulting gel was blotted on a PVDF membrane (**Chapter 4.3.14**) and treated afterwards with specific anti-phospho-c-MET (Cell Signaling Technologies) and anti-phospho-EGFR antibodies (R&D Systems) for phosphorylation detection. Expression levels of c-MET and EGFR were detected after blotting by using specific anti-cMET (Biomol) and anti-EGFR antibodies (Cell Signaling Technologies). Western blot analysis was performed according to **Chapter 4.3.14**.

4.5. Biophysical methods

4.5.1. Biolayer interferometry (BLI)

Binding kinetics of purified IgG antibodies and reconstituted IgG antibodies were determined by using the Octet RED96 system (ForteBio, Pall Life Science) at 30°C and 1000 rpm agitation speed in a final volume of 200 µL in black 96-well microplates. 3-5 µg mL^{-1} of reconstituted antibodies, diluted in PBS buffer (pH 7.4), were captured with anti-human IgG Fc (AHC) biosensor tips after equilibration in Dulbecco´s PBS (Life Technologies) for 60 s (baseline). Capturing of reconstituted antibodies was performed for 180 s followed by an incubation step for 45 s in kinetics buffer (PBS, 0.1% Tween-20 and 1% bovine serum albumin, (BSA). The biosensor tips were then transferred into wells containing the appropriate target recombinant antigen, diluted in kinetics buffer using a concentration range varying from 200 nM to 3.13 nM. The association step was conducted for either 400 s or until the highest concentration showed saturation. Dissociation was performed in kinetics buffer for 800 s to determine k_{on} and k_{off} values. A replacement of the antigen by kinetics buffer was serving as a negative control (reference measurement). A non-binding isotype control anti-hen egg lysozyme (anti-HEL) and an unrelated antigen were used in each experiment to observe potential unspecific binding. The reference measurement was subtracted from sample measurements (antibodies) for data fitting. Kinetic parameters were determined by using using a 1:1 Langmuir binding model after Savitzky-Golay filtering (ForteBio data analysis software 9.1).

4.5.2. Thermal shift assay

The Prometheus NT.Plex nano DSF (Nano Temper) was used to determine the thermal stability of antibodies. The intrinsic fluorescence of tryptophan and tyrosine residues under native conditions are detected and measured at 330 and 350 nm. 10 µL antibody sample was used to ensure complete filling of each capillary (Standard, Catalog no. PR-AC002, Nano Temper). An initial discovery scan can be performed to ensure fluorescence signal detection and excitation power adjustment. Melting temperatures (T_m) were monitored online starting from 20°C to 95°C using a temperature slope of 1°C min^{-1} for 1 h and 15 min. Data was analyzed with the PR.ThermControl v2.1 software (Nano Temper).

4.5.3. Automation (Hamilton & BiomekFX)

The Hamilton MicroLab starlet liquid handler (Hamilton) was used for semi-automated reconstitutions in a 96 well format. Antibody precursor fragments fused to Int^C or Int^N, TCEP, Ni^{2+} beads and DHAA were prepared and diluted in PBS pH 7.4 and supplied in reservoir tanks. Ni^{2+}beads were washed at least 3 times manually to

remove the ethanol. Antibody precursor fragments were mixed in an appropriate molar ratio, depending on the fragments, in final volume of 200 µL by the liquid handler, resulting in 58 µg total protein per well. 25 µL TCEP was added using a final concentration of 0.5 mM. The plate was removed manually and incubated for 2 h at 37°C after sealing. Addition of 25 µL diluted Ni^{2+} magnetic beads (Invitrogen) was performed by the liquid handling system. The beads are capable to bind 40 µg tagged protein per 25 µL beads according to Invitrogen. Therefore, beads were diluted in PBS pH 7.4 to offer a binding capacity of 5 µg his tagged protein per well, which was hypnotized to be enough to remove all non-reconstituted antibody fragments. The plate was sealed and transferred manually again to an incubator at RT for 1 h under shaking conditions at 700 rpm (25 mm throw, Infors HT). After incubation the plate was centrifuged at 4000 x g for 2 min (Multifuge X3R, Thermo Scientific) and transferred back to the Hamilton stack holder, which carried a strong magnet plate to capture magnetic beads at the well bottom. 200 µL of the reconstitution mixture was transferred into a fresh 96 well plate by the liquid handler. The liquid handler was taught to not touch the well bottom to ensure no bead transfer into the new plate. Subsequently DHAA was added in a 10-fold molar excess over TCEP by the liquid handler system and incubated after sealing for 1-2 h at 37°C or overnight at 4°C (Infors HT) respectively. Reconstitution efficiency was analyzed by SDS-PAGE (**Chapter 4.3.12**) and ELISA (**Chapter 4.3.11**).

The BiomekFX (Beckman) was used as a fully automated system for antibody reconstitutions in a 384 well format. Antibody precursor fragments fused to Int^C or Int^N, TCEP, Ni^{2+} beads and DHAA were prepared and diluted in PBS pH 7.4 and supplied in 50 mL falcon tubes. Ni^{2+}beads were washed at least 3 times manually to remove the ethanol. Antibody precursor fragments were mixed by 2 multidrop systems (Thermo Fisher Scientific) in an appropriate molar ratio, depending on the fragments, in final volume of 40 µL by the liquid handler, resulting in 14 µg total protein per well. The plate was delivered by a robot arm. 7 µL TCEP was added by multidrop dispenser using a final concentration of 0.5 mM. The plates were sealed by a plate sealer for 8 s at 150°C and mixed afterwards with a Bioshaker at 2200 rpm for 30 s. Plates were transferred into a plate carousel and incubated for 2 h at 37°C. After de-sealing 14 µL diluted Ni^{2+} magnetic beads (Invitrogen) were added by multidrop dispenser. The beads offered the same binding capacity as mentioned above. The plates were sealed again for 8 s at 150°C and mixed afterwards with a Bioshaker at 2200 rpm for 30 s, followed by incubation for 15 min at 37°C. Mixing and incubation was repeated 4 times every 15 min to ensure no sedimentation of the beads. Plates were centrifuged after capturing non-reconstituted antibodies at 100 rpm for 2 min using a Vspin centrifuge. After de-sealing 35 µL of each well were transferred stepwise by the BiomekFX liquid handler to fresh 384 well plates. The plate stack holder was adjusted with a strong magnet to ensure immobilization of the beads to the well bottom. 17.5 µL were transferred as a first step into the fresh plate and centrifuged afterwards to ensure no bead transfer by the liquid handler. Finally, another 17.5 µL was transferred to the fresh 384 well plate. 11 µL DHAA was added by multidrop dispenser in a 10-fold molar excess over TCEP to each well, containing the reconstituted antibodies. The plates were sealed and mixed with the Bioshaker at 2300 rpm for 30 s and transferred afterwards to the plate carousel for incubation at 37°C for 1-2 h or at 4°C overnight.

For normal distribution calculation, the following equation was used to display f(x):

$$f(x) = \frac{1}{\sigma\sqrt{2\pi}} e^{-\frac{1}{2}\left(\frac{x-\mu}{\sigma}\right)^2}$$ Eq. 4

4.5.4. Mass spectrometry (MS)

ESI-MS (Electrospray ionization mass spectrometry) was performed by a Dionex U3000 HPLC system coupled to a Synapt-G2 mass spectrometer, using a Proteomix RP-1000 4.6 mm x 100 mm (Sepax) column. 0.5 µg of protein solution was applied in mobile phase H_2O and 0.1% formic acid 0.5 mL min^{-1}. A linear gradient of acetonitrile (ACN) and 0.1% formic acid was used. Detection of protein fragments was achieved at 214 nm measurement and identification was achieved by the online coupled mass spectrometer.

5. Results

5.1. Design and generation of antibody intein fusions

In order to investigate post translational reconstitution of antibody fragments by PTS via split intein *Npu* DnaE, antibody Fab fragments, oaSEED or Fc fragments were fused to split intein parts flanked by their natural exteins. Therefore, the flexible hinge region was split in half and intein parts Int^C and Int^N were fused to the partial hinge according to **Figure 14**. A glycine serine linker $(4xGS)_4$ was inserted upstream of Int^C, allowing additional flexibility for the following hexahistidine tag for impurity removal of non-reconstituted antibody fragments.

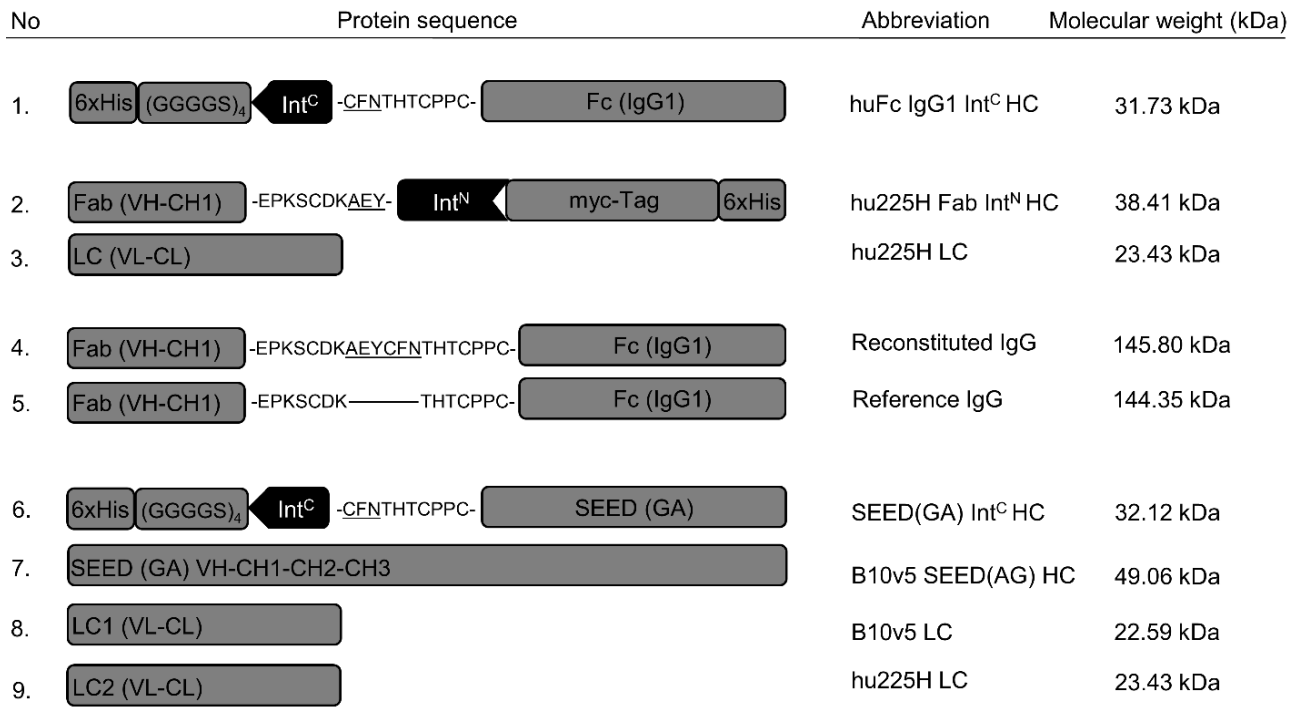

Figure 14: Schematic illustration of protein sequences for antibody fragments HC and LC fused to split intein parts Int^C and Int^N.

Schematic HC and LC sequences of huFc IgG, Fab or oaSEED fragments are illustrated fused to Int^C or Int^N and their corresponding exteins within the hinge region. N- and C- terminal exteins are depicted as amino acid sequence (underlined) attached to the partial hinge region. Additionally, a glycine-serine linker and a hexahistidine tag is attached upstream to Int^C of huFc or oaSEED fragments, while a hexahistidine tag is attached downstream of the Int^N sequence. (1) HC of huFc IntC fragments. (2)(3) hu225H Fab Int^N HC with corresponding LC. (4)(5) Reconstituted IgG HC with altered hinge region compared to naturally reference IgG HC. Hinge region of both variants are aligned to focus on the amino acid modification based on the respective exteins. (6-9) B10v5 oa SEED Int^C HC with corresponding HC and LC. Detailed sequence information is listed in the materials section.

Intein sequences were derived from Stevens *et al.*,[147] fused to the corresponding antibody fragments and ordered as gene synthesis in a pTT5 vector backbone at GeneArt® (Thermo Fisher Scientific). The antibody VH regions were flanked by unique restriction sites *Bam*HI and *Apa*I, to easily exchange the target specificity by standard cloning. VHH coding regions were exchanged by using unique restriction sites *Nco*I and *Not*I. Antibody Fab fragments fused to Int^N and oaSEED or Fc fragments fused to Int^C were expressed in mid-scale by transient expression of Expi293F cells. Purification of Int^C-fusions was performed by Protein A affinity chromatography,

while Int^N-fusions were purified via IMAC. Analysis of purified antibody fragments was monitored by SDS-PAGE (**Figure S1, Figure S2**) and SE-HPLC (**Figure S3**). Expression yields of several Fab fragments ranged from 16.0 to 137.5 mg L^{-1} after final polishing by SEC. Trastuzumab Fab Int^N showed an 8-fold higher yield compared to the high affinity variant hu225H Fab Int^N and a 3-fold higher yield compared to the low affinity variant hu225L Fab Int^N. Anti-CD40 Fab Int^N as well as C6 Fab Int^N showed similar yields within the 90 mg L^{-1} range. Highest yield of 137.5 mg L^{-1} was observed for Trastuzumab Fab Int^N, while the lowest yield was detected for hu225H Fab Int^N with 16.0 mg L^{-1}. Protein purity of the entirety of the Fab fragments was higher than 96% monomeric content and all antibodies showed acceptable expression rates. High molecular weight impurities like protein aggregates would have an impact on antibody reconstitution and might result in false positive or negative results in cellular based functional assays, therefore it is of importance to start with good quality precursor material for antibody reconstitution. Expression yields of oaSEED fragments were in the same range between 82.0 and 104.8 mg L^{-1} after purification, except oaF06 Int^C showing an expected decreased yield of 33.0 mg L^{-1}. Fc fragments showed highest obtained yield in the range of 254 to 403 mg mL^{-1} with a monomeric content of 100% after purification.

Table 2: Expression yields of antibody fragments fused to split intein parts including purity parameters after purification.

Antibody fragments fused to either the C-terminal (Int^C) part or N-terminal (Int^N) part of the split intein *Npu* DnaE were generated by transient transfection of Expi293F cells. Purification was performed by ProteinA affinity chromatography for oaSEED-Int^C and Fc-Int^C fragments, while IMAC was performed for Fab-Int^N fragments. Protein yields were calculated as mg L^{-1} and total yield for 200 mL culture volume (mg/200 mL). Protein purity was determined by SE-HPLC analysis after preparative SEC to specify the percentage of purified monomer. oa = one-armed

Antibody fragment	Yield [mg/200 mL]	Yield [mg L^{-1}]	Monomer after SEC [%]
C6 Fab Int^N	18.2	91.0	96.2
CD40 Fab Int^N	17.6	88.0	96.4
Trastuzumab Fab Int^N	27.5	137.5	98.0
hu225H Fab Int^N	3.2	16	98.8
hu225L Fab Int^N	9.5	47.5	96.2

Antibody fragment	Yield [mg/200 mL]	Yield [mg L^{-1}]	Monomer after SEC [%]
oaTrastuzumab Int^C	16.4	82.0	96.5
oaC5 Int^C	21.0	104.8	94.6
oaB10v5 Int^C	20.2	101.0	99.0
oaF06 Int^C	6.6	33.0	98.0
oaOKT3 Int^C	19.2	96.0	99.5
IgG1 Fc Int^C	80.1	400.5	100.0
IgG2 Fc Int^C	66.5	332.5	100.0
IgG1.4 Fc Int^C	80.6	403.0	100.0
IgG1.6 Fc Int^C	50.8	254.0	100.0

Antibody fragments for bsAb reconstitution and functional characterization are listed in **Table 2**. Protein yields and purity of all antibody fragments were suitable for antibody reconstitution and further characterization of reconstitution efficiency and functionality determination.

5.2. Evaluation of reconstitution efficiency for mono- and bispecific antibodies

In terms of generating several mono- and bispecific antibodies by split intein mediated antibody reconstitution, it was tested if the modified hinge region by flanking extein and intein sequences fused to a hexahistidine tag were still able to perform PTS. As a proof of concept, several formats were tested under optimized conditions for successful antibody reconstitution. All reconstitution reactions were performed at 37°C for 2 hours after activation with 0.5 mM TCEP considered as optimal conditions for antibody reconstitution. Monospecific antibody anti-CD40 was reconstituted by mixing anti-CD40 Fab fragment and IgG1 Fc fragment in a ratio of 2:1. PTS was activated immediately after TCEP addition and monitored by SDS-PAGE analysis, as shown in **Figure 15 A**. Samples were taken every 10 min to evaluate reconstitution efficiency. A new band occurred already after 10 min at ~50 kDa, indicating the PTS product of both HC antibody fragments through ligation. The newly reconstituted HC only occurs after TCEP addition, while no band was observed at 0 min serving as a negative control. The gel band at ~40 kDa represents the HC of anti-CD40 Fab fragment fused to Int^N, while the ~25 kDa gel band represents the HC of IgG1 Fc Int^C fragment under reducing conditions. Both bands got depleted over time and the reconstituted product increased. A gel band at ~14 kDa occurred, showing the spliced Int^N part after reconstitution of both HCs derived from antibody fragments. Reconstitution of full length anti-CD40 antibody was completed after 120 min. The SDS-PAGE analysis showed almost complete conversion of precursor antibody fragments (**Figure 15 A**).

Bispecific antibody reconstitution efficiency was evaluated by mixing Trastuzumab oaSEED Int^C fragment with a hu425 Fab Int^N fragment in an equimolar ratio (1:1) (**Figure 15 B**). Again, a new gel band at ~50 kDa occurred after TCEP activation and increased over time until antibody fragment depletion based on successful reconstitution. Spliced Int^N and Int^C fragments were increasing over time and indicated at ~12 kDa and ~4 kDa respectively.

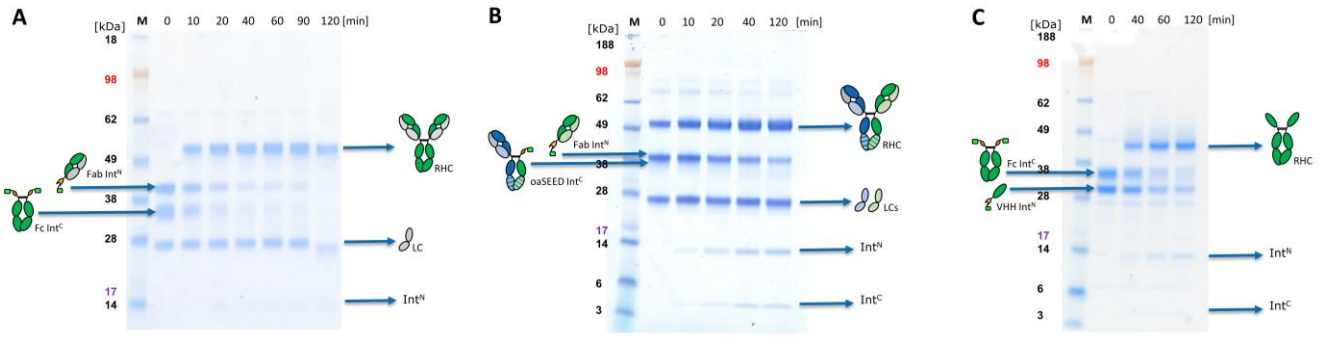

Figure 15: Evaluation of reconstitution efficiency for mono- and bispecific antibodies.

Different antibody fragments were mixed in an equimolar ratio for bsAbs and in a 2:1 ratio for mAbs and activated with 0.5 mM TCEP after PTS optimization and incubated at 37°C. **A:** Reconstitution of CD40 Fab fragments with an IgG1 Fc fragment via PTS over time. The newly occurring gel band at ~50 kDa after 10 min incubation, indicated the splicing product of Fab heavy and Fc heavy chain (RHC: Reconstituted HC). B: Reconstitution of a Her2 oaSEED fragment with hu425 Fab. C: Reconstitution of Her2 VHH fragments with an IgG1 Fc fragment. Splicing efficiency for all tested formats was fast and mostly completed after 1h with a yield of >90%.

In order to proof that antibody reconstitution is not format dependent and does not cause any sterically hindrance, purified Her2 VHH Int^N derived from an *E. coli* expression and IgG1 Fc Int^C derived from mammalia expression were mixed in a molar ratio of 2:1 and successfully reconstituted over time (**Figure 15 C**). As assumed, a new gel band occurred at ~40 kDa indicating the reconstituted HC of both antibody fragments, while Int^N and Int^C were spliced and appeared at ~14 kDa and ~4 kDa. The reconstitution efficiency is comparable to monospecific full-length (**Figure 15A**) and bispecific antibody reconstitution (**Figure 15B**) and was not limited to the antibody format. However, a reconstitution of 100% was not achieved after 120 min while generating bsAbs and VHH-Fc antibodies through PTS (**Figure 15B, C**). Although, it is possible to generate precursor antibody fragments in different host cells like *E. coli* or mammalia, without inhibiting the PTS activity.

The general reconstitution efficiency over time was calculated by integration of peak areas, determined by pixel analysis using ImageJ (**Figure S4**). SDS-Gel analysis depicted in **Figure 15A** was used for pixel analysis and peak area generation. Integration of the peak areas at different time points were used to generate an extrapolated Michaelis Menten kinetic (GraphPad Prism v7). Time point at 0 h exhibited the highest peak value for antibody fragments (substrate) and is considered as 100% (**Figure 16**). Over time depletion of the antibody fragments was observed, forming the final reconstituted full-length IgG antibody. Antibody reconstitution was mostly completed, yielding ~90% reconstituted mAb after 120 min at 37°C (**Figure 16**).

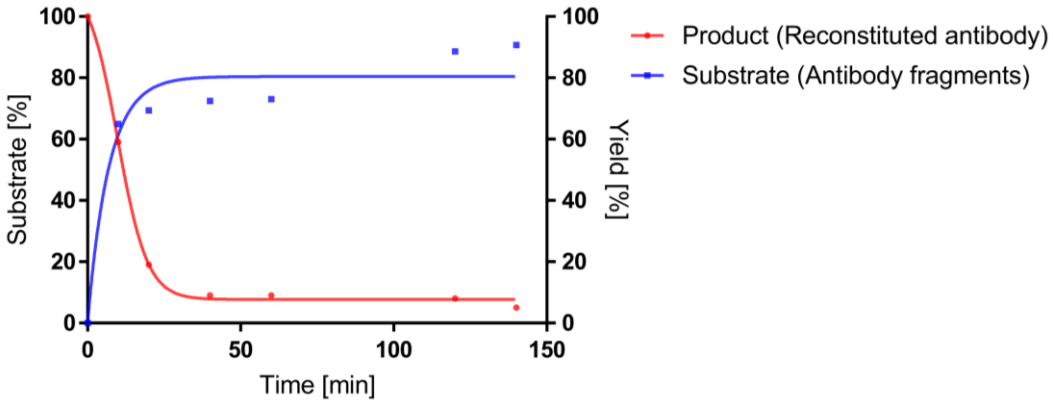

Figure 16: Antibody reconstitution efficiency by PTS over time.

Reconstitution of CD40 IgG1 antibody starts immediately after PTS activation through TCEP addition. Antibody fragments depleted over time, while the reconstituted full-length antibody is generated by PTS. Left y-axis indicates antibody fragments as substrates for antibody reconstitution through PTS. X-axis shows PTS efficiency over time, while second y-axis depicts the reconstituted antibody conversion. Values for substrate and reconstituted antibody was calculated from the peak area after pixel analysis of each sample point and extrapolated using GraphPad Prism 7 software. The complete data set is located in the supplemental section (**Figure S4**).

The illustrated example for antibody reconstitution efficiency by calculation was conferrable to upcoming reconstitution experiments. It was observed that a format independent overall reconstitution yield of around 90% can be expected under optimized conditions after 2 h.

Of note, protein impurities or aggregation often lead to false positive results in functional cellular assays. Therefore, the specific design of the antibody fragments offers a purification tag after each intein sequence for non-reconstituted antibody removal. Furthermore, TCEP is necessary for antibody reconstitution and the disulfide bonds between HC-HC and HC-LC are present in a reduced form. Investigations for a one-pot

purification strategy, which is not dependent on extensive elution steps and the re-oxidation of disulfide bonds for correctly assembled antibody chains is presented in the subsequent **Chapter 5.2.1**.

5.2.1. One-Pot purification and identification of reconstituted antibodies

To demonstrate the purification strategy and setup for non-reconstituted antibody fragments, anti-CD40 Fab Int^N fragment was mixed with a surplus ratio of 3:1 with IgG1 Fc Int^C to ensure non-complete antibody reconstitution. PTS was stopped after 120 min due to depletion of IgG1 Fc Int^C substrate (**Figure 17A**; Lane 3). After addition of Ni^{2+} beads and incubation under shaking conditions for 1 h, supernatant was separated from the beads, containing reconstituted full-length anti-CD40 IgG without any non-reconstitution impurities in form of antibody fragments as shown in **Figure 17A** (Lane 4). Beads were further eluted with imidazole and non-reconstituted antibody fragments were present in the gel fraction after SDS-PAGE analysis, serving as a proof of concept for the purification setup and no unspecific binding of reconstituted mAb to Ni^{2+} beads. (**Figure 17A** Lane 5). The hexahistidine tag downstream and upstream of the respective split intein sequence is still accessible for affinity purification and furthermore did not disturb the splicing reaction itself. PTS successfully removed the hexahistidine tag, as well as the corresponding split intein part from the ligated reconstituted tag-less mAb, which is now masked against IMAC purification via Ni^{2+} beads. After re-oxidation with a 10-fold surplus of DHAA over TCEP, a reconstituted anti-CD40 mAb with intact disulfide bonds was achieved without any non-reconstituted antibody fragment impurities, monitored by SDS-PAGE analysis (**Figure 17A**; Lane 6).

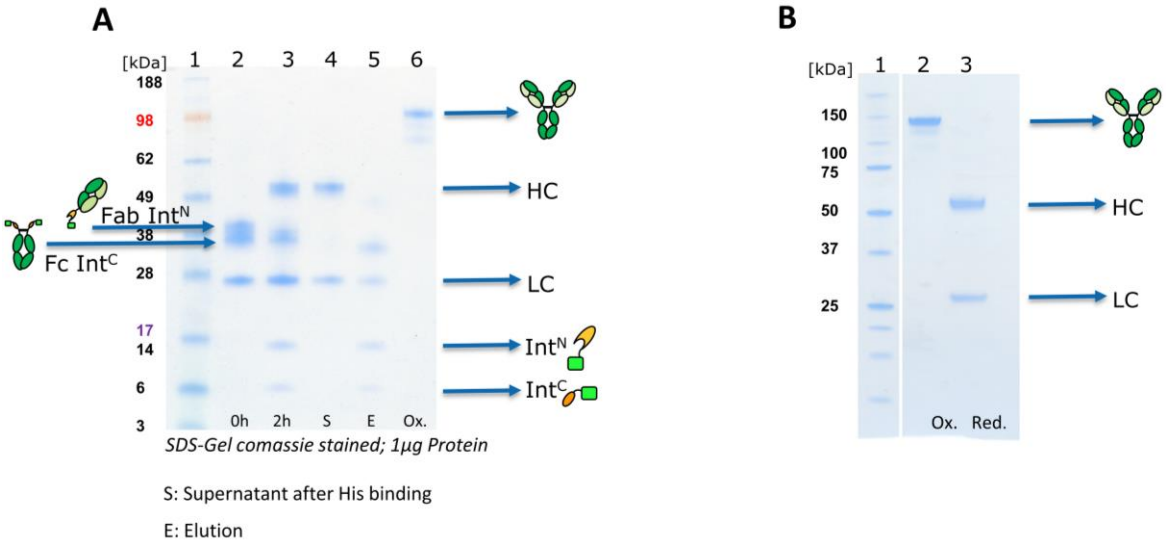

Figure 17: One-pot purification for reconstituted antibodies.

Non reconstituted antibody fragments and spliced split intein parts compromising a hexahistidine tag were removed after Ni^{2+} bead addition. **A:** Antibody reconstitution with a surplus of Fab fragment followed by one-pot purification using Ni^{2+} beads. Lane 1: Marker; Lane 2: Fab Int^N and huFc IgG1 Int^C mixed with TCEP at 0 h. Lane 3: Fab Int^N and huFc IgG1 Int^C mixed with TCEP after 2 h reconstitution. Lane 4: Reconstituted HC and LC after Ni^{2+} treatment and non-reconstituted antibody removal. Lane 5: Elution fraction using 500 mM imidazole. Lane 6: Re-oxidation of reconstituted mAb (Lane 4) treated with a 10-fold molar excess of DHAA over TCEP. (S) Supernatant; (E) Elution; (Ox.) Re-oxidated mAb fraction **B:** SDS-Gel analysis of reconstituted monospecific anti-CD40 antibody under oxidized and reduced conditions to verify successful antibody reconstitution. Full-length antibody occured at ~144 kDa under oxidizing conditions (Lane 2), while two bands occured at ~50 kDa for the HC and ~25 kDa for the LC under reducing conditions (Lane 3). Lane 1: Marker.

Finally, reconstituted anti-CD40 antibody was concentrated and further analyzed by SDS-PAGE analysis under oxidizing and reducing conditions (**Figure 17B**). A gel band at ~50 kDa and ~25 kDa for HC and LC under reducing conditions was observed, while a gel band at ~144 kDa was observed under oxidizing conditions. The SDS-PAGE analysis gave a first indication of successfully produced reconstituted antibodies by PTS, showing all expected antibody chains.

Further evaluation of the reconstitution efficiency, with respect to reconstituted antibody purity and purification, was performed by generating a c-METxEGFR bsAb mediated by PTS and analyzed with SE-HPLC at specific time points (**Figure 18**). Samples were quenched with H_2O_2, oxidizing the reducing agent TCEP, antibody fragments and reconstituted bsAb for quantitative analysis. Antibody reconstitution was initiated immediately after TCEP addition, indicating and confirming the fast kinetics of the *Npu* DnaE split intein. Incubation after 10 min at 37°C already yielded in 39% of the reconstituted bsAb, while antibody precursor fragments were decreasing over time. Antibody reconstitution was stopped after 1.5 h, resulting in 12% non-reconstituted antibody precursor fragments. Finally, the non-reconstituted antibody fragments were purified with Ni^{2+} beads, increasing reconstituted bsAb purity up to 94% (**Figure 18**). Reconstitution efficiency and splicing kinetics were comparable to the previously executed SDS-PAGE analysis experiments (**Figure 16/17A**).

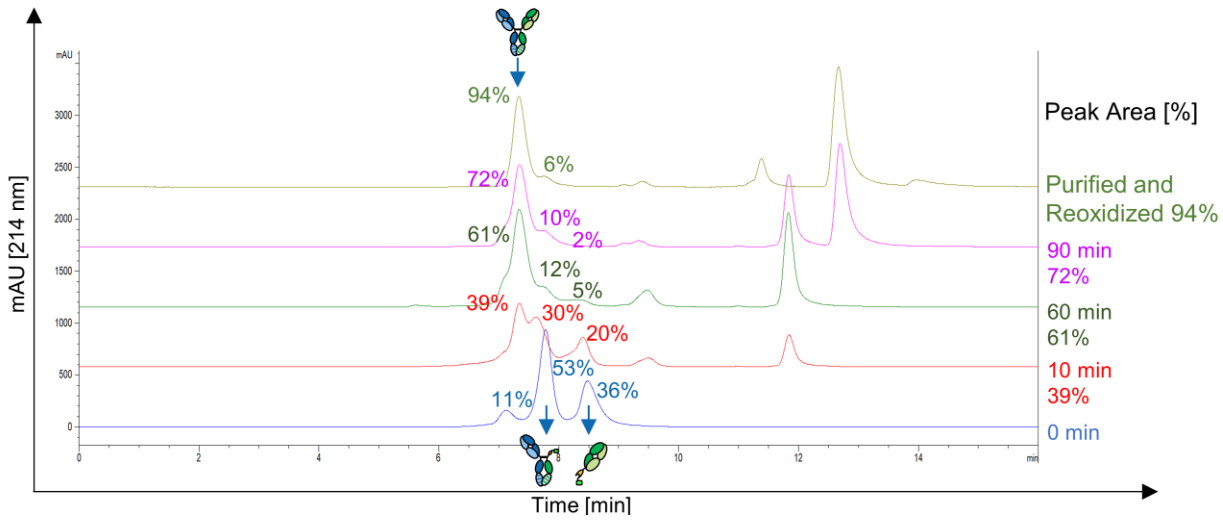

Figure 18: Determination of the reconstitution efficiency and purification of a bsAb via HPLC analysis.

Antibody precursor fragments B10v5 oaSEED Int^C and hu225H Fab Int^N were mixed in an equimolar ratio and incubated for 2 h at 37°C after addition of 0.5 mM reducing agent TCEP. Samples were taken at specific time points and reconstitution reaction was quenched by the addition of H_2O_2, inactivating TCEP through oxidation. The mixture was treated with Ni^{2+} beads to remove non-reconstituted antibody fragments. Reconstitution efficiency and antibody purity was determined by analytical SE-HPLC analysis.

As SDS-PAGE is not as precise as SE-HPLC or mass spectrometry, further investigations to verify correctly assembled HC was demanding. A reconstituted anti-CD40 antibody was analyzed by MS under reducing conditions. **Figure 19A** shows the MS spectrum of the HC and LC as already proofed by SDS-PAGE analysis (**Figure 17B**). The most important fragments of the reconstituted antibodies are the HC parts of the Fab and Fc fragment. In case of successful reconstitution, the HC of the Fab fragment is ligated to the HC of the Fc

portion and gives valuable information about the correct formed molecule. The spectrum showed clearly a mass of 51.9 kDa, indicating the correctly assembled HC after PTS. A higher molecular mass was detected compared to the theoretical mass. A N-glycosylation by N-glycan type G0F with a mass of 1445 Da was detected as well as an O-glycosylation with a mass of 948 Da and a missing pyroglutamate (pGlu) with 17 Da. The newly formed HC exhibited several glycosylation modifications as expected for heavy chains and was matching with the theoretical calculated mass (**Figure 19B**). The LC was detected without any modifications and was matching with the expected theoretical mass.

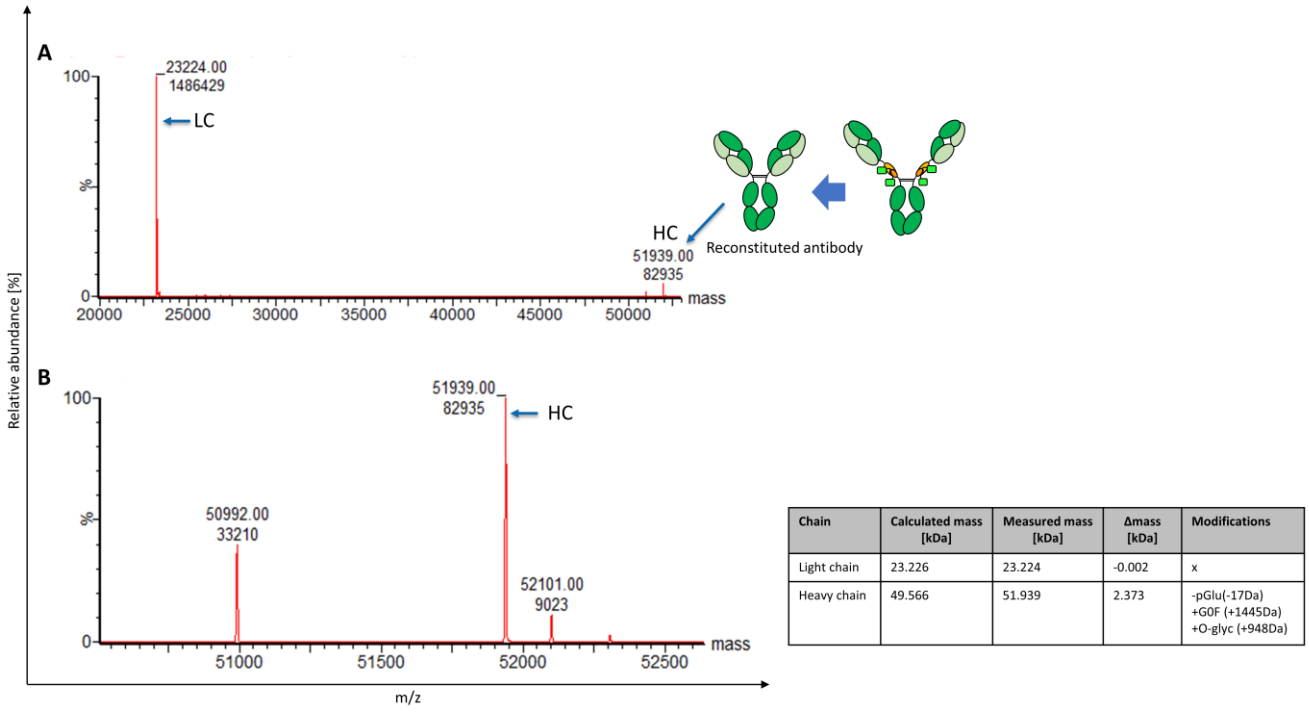

Chain	Calculated mass [kDa]	Measured mass [kDa]	Δmass [kDa]	Modifications
Light chain	23.226	23.224	-0.002	x
Heavy chain	49.566	51.939	2.373	-pGlu(-17Da) +G0F (+1445Da) +O-glyc (+948Da)

Figure 19: Identification of correctly reconstituted heavy chains by mass spectrometry.

MS spectra of reconstituted anti-CD40 after PTS reaction and one-pot purification. Analysis was performed by ESI-MS. **(A)** MS spectrum of HC and LC after reconstitution reaction under reducing conditions. **(B)** MS spectrum of HC including modifications. Calculated mass is correlating with the measured mass and indicates successful antibody reconstitution by PTS.

MS data confirmed the results obtained from SDS-PAGE analysis for successfully reconstituted anti-CD40 antibody. Non-reconstituted antibody impurities or false assembled heavy chains were not detected in the MS spectrum. Anti-CD40 IgG was used as a proof of concept model for antibody reconstitution based on the less complicated format compared to bsAbs. Split intein mediated antibody reconstitution is not format biased as already investigated in **Chapter 5.2**. However, the bispecific format comprises two different heavy- and light chains. The addition of TCEP, which resulted in reduced disulfide bonds, followed by re-oxidation with DHAA gave reasons to believe that it could be a potentially mismatched chain assembly. Therefore, experiments were performed to evaluate correct HC and LC assembly after reconstitution and re-oxidation in a bispecific format.

5.2.2. Correct assembly of HC and LC after bispecific antibody reconstitution

In order to investigate correct assembly of HC and LC after antibody reconstitution, antibody fragments with wrong LCs were produced. A Trastuzumab oaSEED Int^C fragment paired with a hu225 LC, was reconstituted

with a hu225 Fab Int^{N} fragment, paired to a Trastuzumab LC. **Figure 20A** shows the different versions, which can potentially occur after antibody reconstitution based on the mild reducing environment caused by TCEP. This would result in LC shuffling after re-oxidation. Reconstitution of the Her2xEGFR bsAb with wrong LCs (Her2xEGFR^{FC}) was completed after 2 h. Antibody fragments Trastuzumab oaSEED Int^{C} and hu225 Fab Int^{N} bearing the wrong LC were completely depleted and re-oxidation with DHAA overnight showed a band at ~147 kDa after SDS-PAGE analysis, indicating a full-length bsAb antibody (**Figure 20B**).

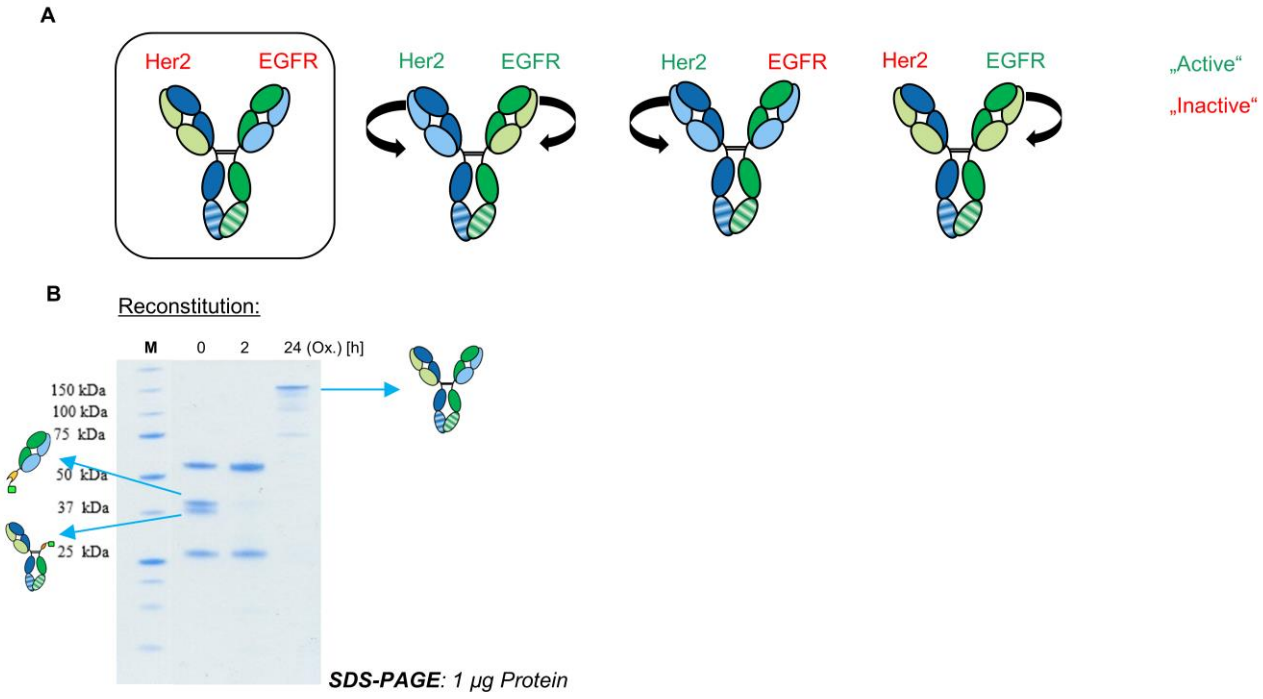

Figure 20: Investigation of potential LC shuffling under mild reconstitution conditions.

(A) bsAb variants after reconstitution and re-oxidation with potential chain shuffling. In terms of LC inversion one or both binding moieties should bind their respective antigen. **(B)** Trastuzumab oaSEED Int^{C} was produced with a hu225 LC. Hu225 Fab Int^{N} was produced with a Trastuzumab LC and both fragments were reconstituted via PTS.

BLI analysis was performed and monovalent Trastuzumab oaSEED Int^{C} paired to the hu225 LC showed no binding to recombinant Her2 as expected because of the wrong LC (**Figure 21C**). Monovalent Trastuzumab oaSEED paired to the correct Trastuzumab LC was binding with high affinity to recombinant Her2 and served as a positive control. Hu225 Fab Int^{N} paired to Trastuzumab LC was neither binding to recombinant Her2 or EGFR as shown in **Figure 21A** and **21B**. It was hypothesized, if LC shuffling occurred during antibody reconstitution, Her2xEGFR^{FC} should bind either to recombinant Her2 or EGFR or both, according to the shuffling variants depicted in **Figure 20A**. Her2xEGFR^{FC} was neither binding to recombinant Her2 nor to EGFR, revealing that no LC shuffling occurred during the reconstitution reaction (**Figure 21A, B**). Her2xEGFR^{FC} is referred to a reconstituted Her2xEGFR bsAb with false LC paring.

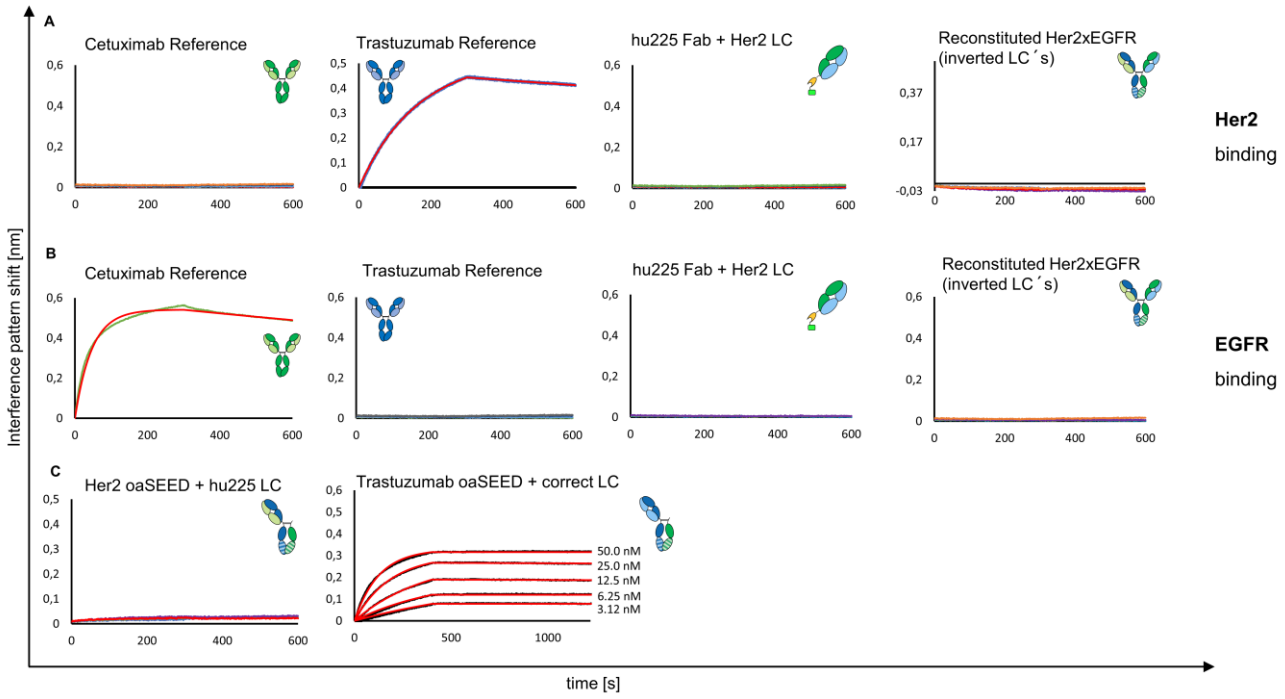

Figure 21: BLI analysis of reconstituted Her2xEGFR^{FC} bsAb paired to wrong LCs.

(A) Panel A shows binding to recombinant Her2. Cetuximab served as a negative control and showed no binding to recombinant Her2, while Trastuzumab served as a positive control binding recombinant Her2 with high affinity. Hu225 Fab Int^{N} pairing to Trastuzumab LC as well as Her2xEGFR^{FC} showed no binding to recombinant Her2. **(B)** Panel B shows binding to recombinant EGFR. In this panel Cetuximab served as a positive control binding with high affinity to recombinant EGFR, while Trastuzumab is not binding and served as a negative control. Hu225 Fab Int^{N} pairing to Trastuzumab LC as well as Her2xEGFR^{FC} showed no binding to recombinant EGFR. **(C)** Monovalent Trastuzumab oaSEED Int^{C} paired to hu225 LC showed no binding to recombinant Her2, while monovalent Trastuzumab oaSEED paired with the correct Trastuzumab LC was binding with high affinity to recombinant Her2. Her2xEGFR^{FC}: FC = False chains

Reference antibody Cetuximab showed binding with high affinity to recombinant EGFR, but no binding to Her2. Reference antibody Trastuzumab showed binding with high affinity to recombinant Her2, but no binding to EGFR. The BLI analysis of reconstituted Her2xEGFR^{FC} gave a first hint of correctly assembled LCs during antibody reconstitution using a bispecific format. In addition, further investigations for potential LC shuffling was verified by ESI-MS analysis. For this, 1 mg of reconstituted F06xhu225L bsAb (c-METxEGFR) was digested with immobilized papain for 3 h at 37°C to cleave within the hinge region and separating the Fab fragments from the Fc portion. Fab fragments were analyzed by ESI-MS under non reducing conditions to evaluate correct assembly of HC and LC. The released Fab with the c-MET (F06) binding moiety exhibited a mass of 47.3 kDa and matched with the theoretical calculated mass for pairing the correct F06 LC. The released Fab with the EGFR (hu225L) binding moiety exhibited a mass of 47.5 kDa matching the theoretical mass of correctly paired hu225L LC (**Figure 22**). The theoretical masses for a potential LC shuffling during reconstitution are illustrated in **Figure 22** with a mass of 46.9 kDa for hu225L HC paired with F06 LC and a mass of 48.0 kDa for F06 HC paired with hu225L LC. The LC chain mispairing variants were under the level of detection according to mass spectrometry analysis and evidence that LC shuffling did not occur during

reconstitution. Fab digestion with papain was repeated using reconstituted B10v5xhu225H bsAb to further validate correctness of the compiled data (**Figure S5**). No LC shuffling was observed.

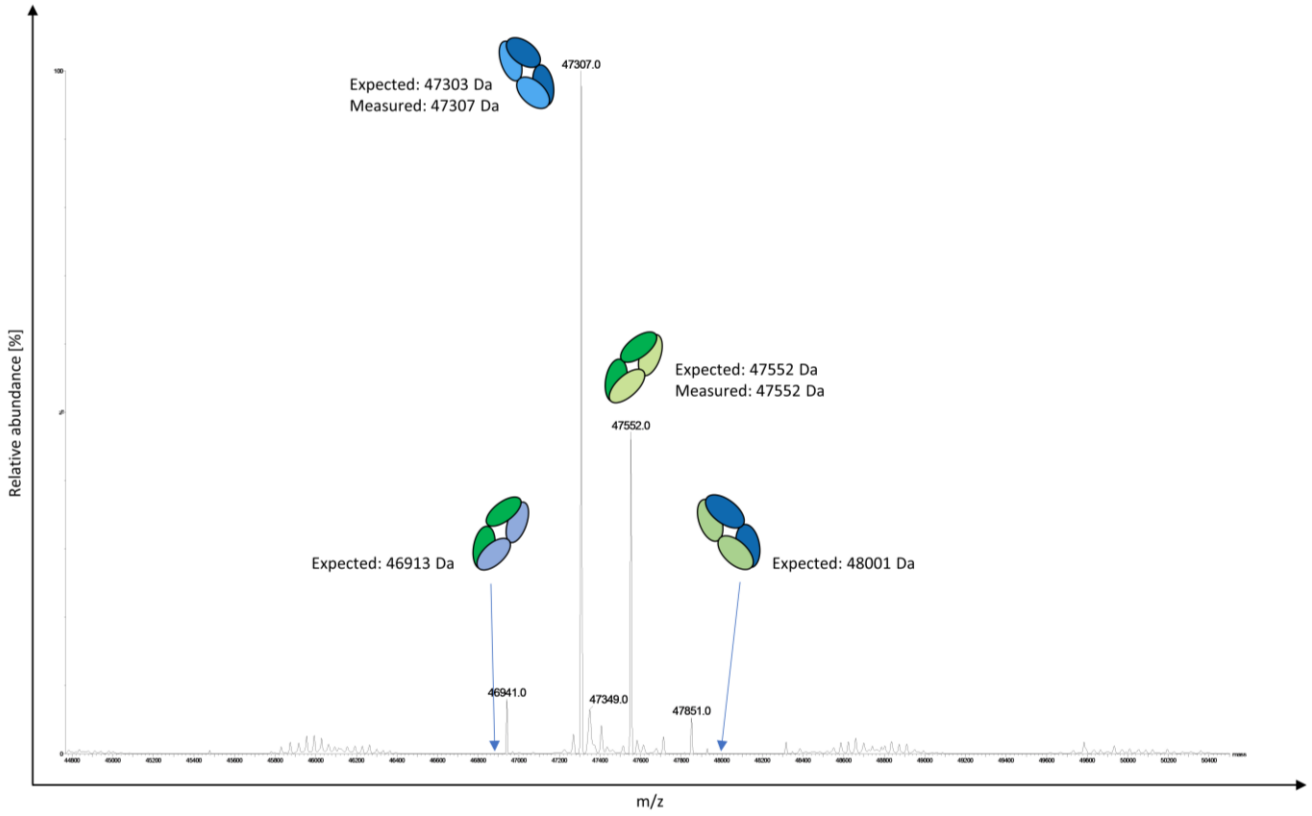

Figure 22: Papain digestion of reconstituted c-METxEGFR bsAb for Fab release and LC shuffling investigation by MS analysis.

Reconstituted bsAb F06xhu225L was treated with Papain and incubated for 3 h at 37°C under shaking conditions for Fab release. Fabs were further analyzed by ESI-MS. The expected mass of F06 (c-MET) Fab as well as hu225L (EGFR) Fab correlates with the measured mass. The expected masses for both Fabs with an LC switch was depicted in the spectrum but was not detected.

BLI analysis and mass spectrometry experiments specified in this chapter were a proof that the mild reducing conditions needed for activation of PTS and bsAb reconstitution did not favor chain mispairing and LC shuffling. With this information, a set of various mAbs and bsAbs were reconstituted with respect to investigate reproducibility, biophysical and functional characterization.

5.2.3. Split intein mediated generation of various antibody formats

After verification of correctly assembled HCs and LCs of reconstituted antibodies, several antibody formats were produced for further investigation of biophysical properties. Four different reconstituted anti-CD40 antibodies were generated with different Fc effector portions, to showcase an easy switch of the effector function (**Table 3**). Protein purity after antibody reconstitution ranged from 88.5% to 95.8%. Highest monomeric content after antibody reconstitution was achieved with bsAbs ranging from 94.0% to 99.4%.

Table 3: Antibody reconstitution rates after PTS and purification.

Antibody fragments were mixed in an equimolar ratio for bsAbs and a molar ratio of 2:1 for mAbs and PTS was activated by addition of TCEP. Reconstituted antibodies were re-oxidized with DHAA and impurities removed by one-step IMAC through Ni^{2+} beads and dialyzed against PBS pH 7.4 for further biophysical and functional characterization. The purity of reconstituted antibodies was analyzed by SE-HPLC and SDS-PGAE and depicted as monomeric content in percent. Correct assembly of HC and LC was confirmed by MS.

Reconstituted antibody	Format	Monomer after SEC [%]
Anti-CD40 IgG1	monospecific	89.4
Anti-CD40 IgG2	monospecific	95.8
Anti-CD40 IgG1.4	monospecific	88.5
Anti-CD40 IgG1.6	monospecific	93.8
C5xC6 (CEACAM5xCEACAM6)	bispecifc	96.5
B10v5xhu225L (c-METxEGFR)	bispecifc	99.2
B10v5xhu225H (c-METxEGFR)	bispecifc	94.0
F06xhu225L (c-METxEGFR)	bispecifc	99.4
F06xhu225H (c-METxEGFR)	bispecifc	n.D.
OKT3xHer2 (CD3xHer2)	bispecifc	n.D.

Table 3 shows reconstitution reproducibility and purity content of several formats and targets amenable for further biophysical and biochemical characterization. SE-HPLC analysis for reconstituted antibodies can be reviewed in **Figure S6**. In addition, mass spectrometry was conducted to determine intact molecules after PTS reaction (**Figure S7-S10; Table S1**).

5.3. Characterization of reconstituted antibodies

5.3.1. Biophysical characterization of reconstituted antibodies via BLI analysis

Potential differences in biophysical properties and antibody functionality after PTS caused by the hinge region modification, compared to natural reference antibodies, were investigated by characterization via biolayer interferometry (BLI) and thermo shift analysis. Parameters were compared to reference antibodies and antibody fragments. Reconstituted bsAb C5xC6 resulted in a K_D of 0.42 nM binding recombinant CEACAM6 and a K_D of 0.26 nM binding recombinant CEACAM5. Respectively the reference C5xC6 bsAb presented a K_D value of 0.46 nM binding recombinant CEACAM6 and a K_D of 0.43 nM binding recombinant CEACAM5 (**Table 4, Figure 23A, B**). The monovalent C5 oaSEED variant obtained a K_D of 0.73 nM while the K_D of the single C6 Fab fragment was determined with 0.15 nM. Kinetic parameters for reconstituted C5xC6 and reference antibody were in the same nanomolar range, signifying that PTS is not compromising the molecular interactions to recombinant cognate antigen. Furthermore, no affinity loss was observed after reconstitution of bsAb C5xC6 compared to the monovalent and bispecific references.

The binding affinity for reconstituted anti-CD40 was determined with 6.8 nM and compared against reference anti-CD40 with a K_D value of 5.9 nM (**Table 4; Figure S11**). Thermostability analysis revealed, that reconstituted anti-CD40, exhibited a T_m of 69.3°C and did not differ from the reference anti-CD40 antibody with

a T_m of 69.7°C (**Table 4; Figure S12**). However, a slight difference in thermostability was observed measuring T_m of reconstituted C5xC6 with 66.1°C and C5xC6 reference with a T_m of 68.0°C (**Table 4; Figure S12**). To proof conformity, several reconstituted bsAbs and mAbs were compared to their naturally reference antibodies and precursor antibody fragments as listed in Table 4. Obtained kinetic parameters and thermostability of reconstituted antibodies showed in general similar binding affinities in the nanomolar range to recombinant antigens and similar thermostabilities compared to their reference antibodies.

Table 4: Kinetic parameters of reconstituted bsAb compared to parental monovalent oaSEEDbodies, Fab fragments, monospecific and bispecific references.

Reconstituted bsAb were compared to their parental monovalent antibodies, monospecific or bispecific references. Antibodies were captured by anti-human Fc biosensor tips and subjected to respective antigen binding. Melting temperatures were analyzed by thermal shift assays. (ND: Not defined.)

Antibody	Analyte	K_D	K_D error	k_a	k_a error	k_d	k_d error	T_m
		[M]	[M]	[M^{-1} s^{-1}]	[M^{-1} s^{-1}]	[s^{-1}]	[s^{-1}]	[°C]
C5xC6 Reference	Ceacam6	4.6E -10	4.7E -12	2.1E +05	1.8E +03	9.5E -05	4.6E -06	68.0
C5xC6 Reconstituted	Ceacam6	4.2E -10	8.4E -12	4.2E +05	2.9E +03	1.8E -04	3.3E -06	66.1
C5xC6 Reference	Ceacam5	4.3E -10	4.5E -12	5.9E +05	2.8E +03	2.6E -05	2.4E -06	68.0
C5xC6 Reconstituted	Ceacam5	2.6E -10	4.2E -12	5.2E +05	2.9E +03	1.6E -04	2.3E -06	66.1
oa C5	Ceacam5	7.3E -10	6.3E -12	2.7E +05	1.2E +03	1.9E -04	1.5E -06	ND
C6 Fab	Ceacam6	1.5E -10	1.6E -10	3.8E +04	6.0E +02	3.4E -04	2.4E -06	ND
CD40 Reference	CD40	5.9E -09	5.3E -11	4.9E +05	4.2E +03	2.9E -03	8.4E -06	69.7
CD40 Reconstituted	CD40	6.8E -09	4.5E -11	5.2E +05	3.2E +03	3.6E -03	7.1E -06	69.3
B10v5xhu225L	c-MET	8.9E -10	1.1E -11	1.5E +05	6.4E +02	1.3E -04	1.6E -06	63.8
B10v5xhu225H	c-MET	8.6E -10	9.6E -12	1.8E +05	7.8E +02	1.5E -04	1.6E -06	63.5
F06xhu225H	c-MET	5.4E -08	3.4E -11	1.5E +06	5.4E +04	8.3E -02	9.9E -04	65.3
oa F06	c-MET	1.1E -08	1.0E -12	4.6E +06	5.4E +04	4.9E -02	2.2E -04	65.1
oa B10v5	c-MET	0.4E -10	3.4E -12	3.5E +05	1.1E +03	1.6E -04	1.1E -06	63.3
B10v5xhu225L	EGFR	2.2E -07	2.9E -10	6.1E +05	1.1E +04	1.2E -01	2.8E -03	63.8
B10v5xhu225H	EGFR	1.9E -10	3.9E -12	3.8E +05	1.9E +03	7.2E -05	1.4E -06	63.5
Trastuzumab Reference	Her2	1.5E -10	8-5E -12	8.7E +04	2.8E +02	1.3E -05	7.4E -07	ND
Trastuzumab Reconst.	Her2	2.5E -10	6.5E -12	9.3E +04	2.4E +02	2.4E -05	6.1E -07	ND

In order to evaluate bispecificity for reconstituted antibodies, simultaneous binding of two recombinant antigens was performed. A stepwise association of both respective antigens was performed. Reconstituted C5xC6 was able to bind both CEACAM5 and CEACAM6 simultaneously as shown in **Figure 23C**. Recombinant EGFR was used as a negative control in a high concentration of 100 nM, to test unspecific binding. No binding to recombinant EGFR was observed with C5xC6 antibodies. Reconstituted bsAbs retained their physiological properties after PTS and were not inhibited by sterically obstruction during simultaneous binding of two distinct antigens.

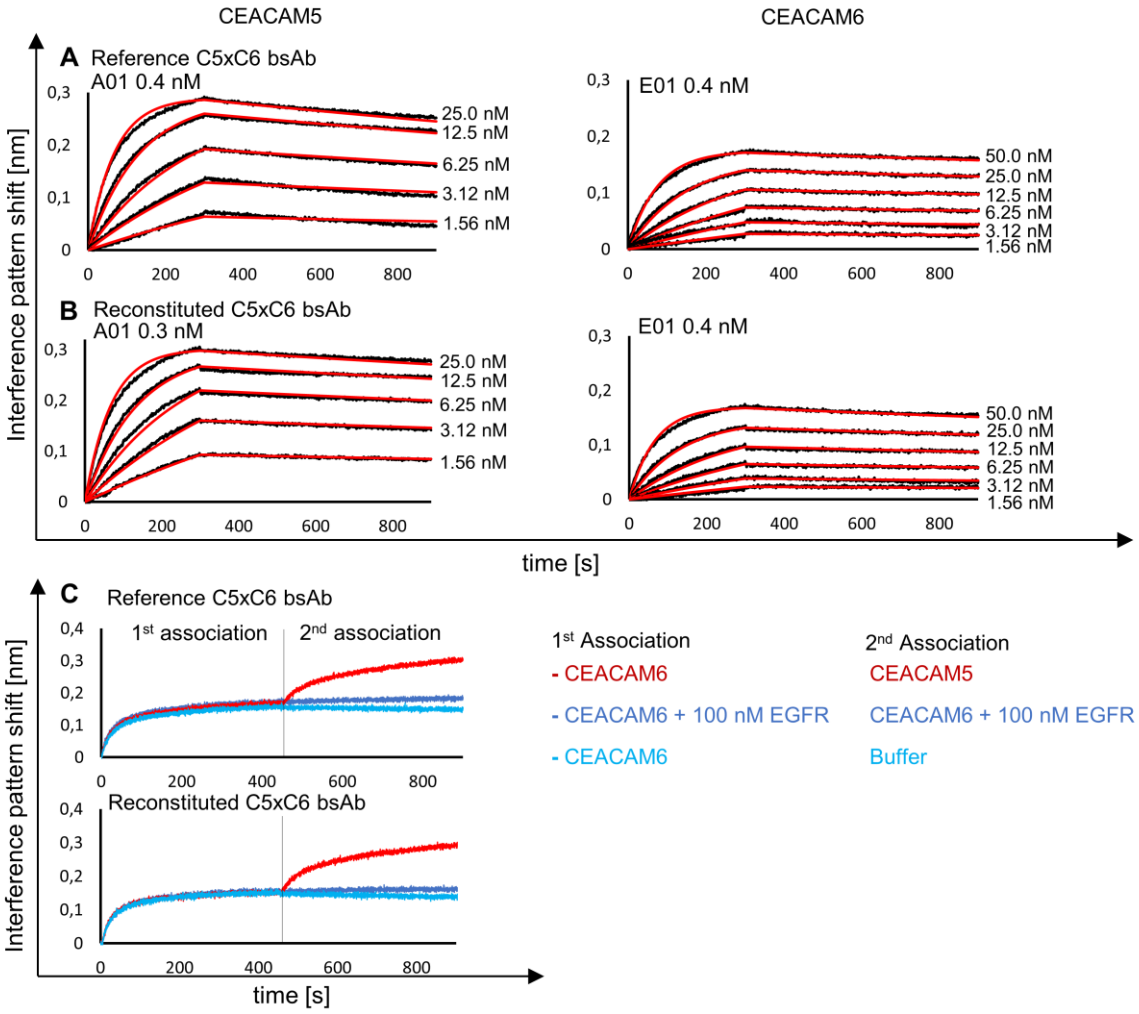

Figure 23: Affinity comparison between reconstituted C5xC6 and reference C5xC6 bsAb binding to soluble CEACAM5 and CEACAM6 using BLI analysis.

BsAbs were analyzed with ProteinA biosensor tips. K_D was determined after 400 s association and 1200 s dissociation of the respective antigens and monitored with varying concentration of analyte over time, resulting in an interference pattern shift (nm). (**A**) Similar kinetic parameters were detected for reference C5xC6 compared to reconstituted C5xC6 illustrated in (**B**). (**C**) Simultaneous binding of soluble recombinant CEACAM5 and CEACAM6 by reconstituted bsAb C5xC6. Both antigens CEACAM5 and CEACAM6 are associated stepwise. Reference antigen recombinant EGFR was used as a negative control in high concentration of 100 nM, to test unspecific binding. No binding to recombinant EGFR was observed by C5xC6.

It was successfully demonstrated that reconstituted antibodies were able to bind to their soluble recombinant antigens. Recombinant antigen binding of reconstituted antibodies was the first step to investigate, if the reconstitution method has an impact on antibody binding or affinity. Of course, antibodies need to perform on the cellular level and need to show antigen binding on the cell surface of certain cancer cell lines to finally fulfill their expected biological function and mode of action. To confirm specific cellular target binding, flow cytometry (FACS) analysis was conducted and described in the next chapter.

5.3.2. Cellular antigen binding of reconstituted antibodies

Cellular binding to target expressing tumor cells was investigated using several reconstituted antibodies. Flow cytometry analysis was conducted to examine cellular binding properties after antibody reconstitution with respect to hinge region modifications. Tumor cells MKN-45 with high cell surface receptor levels of CEACAM5

and CEACAM6 were used to determine target binding. A high fluorescence signal was monitored for reconstituted C5xC6 bsAb, indicating strong binding to related antigens. To compare potential effects on cellular binding behavior based on the altered hinge region after reconstitution, a C5xC6 bispecific reference antibody was used containing a natural IgG1 hinge region. The histograms of reconstituted C5xC6 and reference antibody are illustrated as overlays in **Figure 24**, showing similar fluorescence signals and therefore similar cellular binding to CEACAM5 and CEACAM6. Additionally, the monovalent antibody fragments C5 oaSEED and C6 Fab were used as control antibodies, resulting in slightly lower fluorescence signals compared to the bsAbs (**Figure 24**). Isotype control anti-HEL was used as a negative control and showed no binding to MKN-45 cells. Fluorescent signal was not detected after treatment of HEK293 Nf-κB cells with reconstituted C5xC6 and reference C5xC6, since HEK293 cells were not expressing CEACAM5 or CEACAM6 (**Figure 24**).

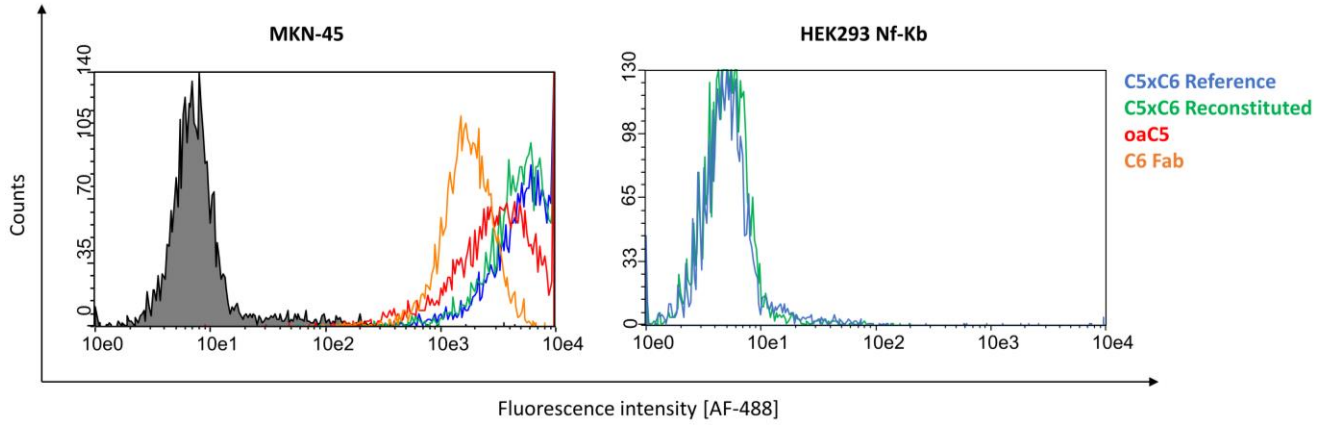

Figure 24: Cellular binding of reconstituted C5xC6 bsAb and non-reconstituted antibody fragments to cancer cell line MKN-45.

MKN-45 cells were seeded with 1x10^5 vc/well and incubated with 10 µg mL^{-1} antibodies for 1 h. Antibodies were detected with Alexa Fluor 488-conjugated anti-human IgG (H+L) Fab via FACS analysis. Binding was detected with reconstituted C5xC6 bsAb and its corresponding monovalent antibody fragments C5 oaSEED and C6 Fab. The fluorescence signal for reconstituted C5xC6 was similar to the C5xC6 reference, while no signal was detected for both bsAbs on negative cell line HEK293 Nf-κb. Analysis was conducted using the green fluorescent channel with adjusted forward and side scatter (Guava easyCyte HT cytometer). Green: Reconstituted C5xC6; Blue: C5xC6 Reference; Red: oaC5-SEED-Int^C; orange: C6-Fab-Int^N; Black: Non-related isotype control (anti-HEL).

In addition to FACS analysis of C5xC6 bsAbs, several c-METxEGFR bsAbs were investigated. Binding was detected with reconstituted B10v5xhu225H, B10v5xhu225L and F06xhu225H and the corresponding monovalent antibody fragments B10v5 oaSEED and hu225H Fab on c-MET/EGFR expressing cancer cell lines A549, EBC-1 and SK-BR-3. A549 cells present a medium cell surface receptor level of human c-MET (18.0 ± 0.6 x 10^3) and human EGFR (39.6 ± 0.6 x 10^3), while EBC-1 cells exhibit high levels for human c-MET (261.6 ± 1.1 x 10^3) and medium levels for human EGFR (62.2 ± 1.1 x 10^3). Weaker binding was observed with the monovalent antibody controls indicating that reconstituted antibodies are able to bind simultaneously to c-MET and EGFR (**Figure 25**). Reconstituted B10v5xhu225L showed low detection signals compared to B10v5xhu225H on A549 cells as presented in **Figure 25**, based on the weak affinity profile of the hu225L binding moiety, determined by BLI analysis (**Figure S13**). This pattern was observed and confirmed as well for binding to SK-BR-3 cells. Furthermore, a lower fluorescence signal was detected with F06xhu225H compared

to B10v5xhu225H consisting of different c-MET binding moieties F06 and B10v5 (**Figure 25**). The observation of lower detection levels of F06xhu225H was confirmed by BLI analysis (**Figure S13**).

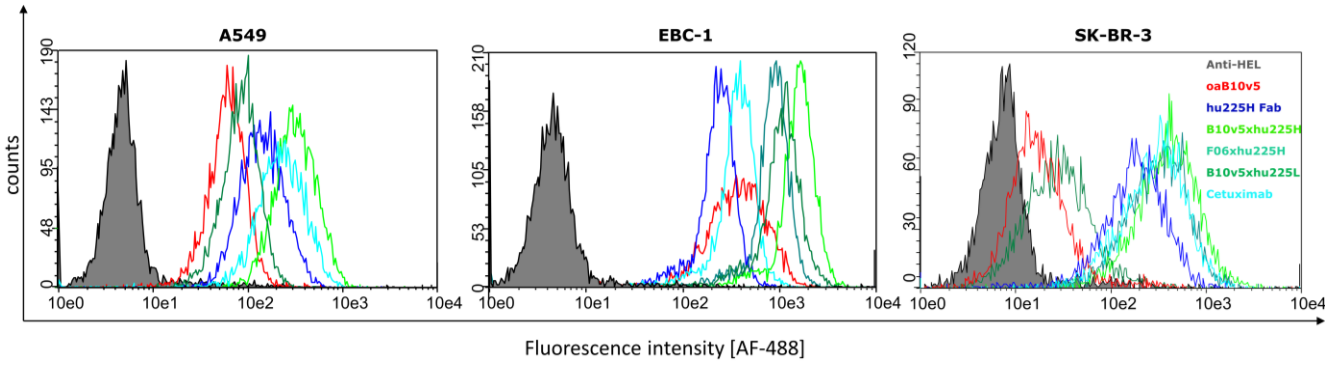

Figure 25: Cellular binding of reconstituted c-METxEGFR bsAbs and non-reconstituted antibody fragments to several cancer cell lines.

Cells were seeded with 1x10^5 vc/well and incubated with 10 µg mL^{-1} antibodies for 1 h. Antibodies were detected with Alexa Fluor 488-conjugated anti-human IgG (H+L) Fab via FACS analysis. Binding was detected with reconstituted c-METxEGFR bsAbs B10v5xhu225H, B10v5xhu225L and F06xhu225H and the corresponding monovalent antibody fragments B10v5 oaSEED and hu225H Fab on c-MET/EGFR expressing cancer cell lines A549, EBC-1 and SK-BR-3. Cetuximab served as an additional positive control and anti-HEL was used as an isotype negative control. Light green: B10v5xhu225H; Dark turquois: F06xhu225H; Dark green: B10v5xhu225L; Turquois: Cetuximab (positive control); Red: B10v5 oaSEED; Blue: hu225H Fab; Black line: Non-related isotype control (anti-HEL).

In congruence, cellular binding of reconstituted anti-CD40 mAbs bearing different Fc portions were compared to reference anti-CD40 mAb on CD40 expressing HT1080 cancer cells, obtaining overlapping histograms and therefore similar detection levels after FACS analysis (**Figure S14**). As expected, no binding was observed by incubating anti-CD40 mAbs with CD40 negative MDA-MB-468 cells.

The altered hinge region of reconstituted mAbs and bsAbs did not compromise binding to cellular targets and was comparable to reference antibodies. It has been proved that reconstituted antibodies bind similar to their specific recombinant and cellular antigens compared to their references. The final and most important question leads to the preservation of biological functionality after antibody reconstitution, addressing a specific mode of action.

5.3.3. Biological functionality of reconstituted antibodies

Biological functionality of reconstituted antibodies was evaluated in several functional cellular assays, like CD40 surface receptor agonism, T-cell activation or c-MET and EGFR receptor phosphorylation. Reconstituted anti-CD40 mAbs consisting of different IgG Fc backbones were compared against the published CD40 agonistic antibody APX005M (Apexigen). APX005M was reproduced as bivalent IgG1. An IgG1, IgG1.4, IgG1.6 and an IgG2 Fc backbone was used for reconstitution with anti-CD40 Fab to simulate easy effector function switch using split inteins. The reconstituted anti-CD40 mAbs showed similar dose response curves compared to the reference APX005M, resulting in an IC50 value range of 2 – 7 nM (**Figure 26**). A slightly higher IC50 value was observed using anti-CD40 IgG 1.4 with 7.3 nM compared to all other tested mAbs (**Figure 26**). However, the maximum signal asymptote for reconstituted mAbs was not as high compared to APX005M, likely through varying cell levels per well, responsible for luminescence signals. Furthermore, saturation of dose response

curves for all variants was not clearly reached. Antibody concentrations must be adjusted to reach signal saturation for a better IC50 value statement (**Figure 26**). Differences in signal detection could also potentially be evidence for the modified hinge region after PTS.

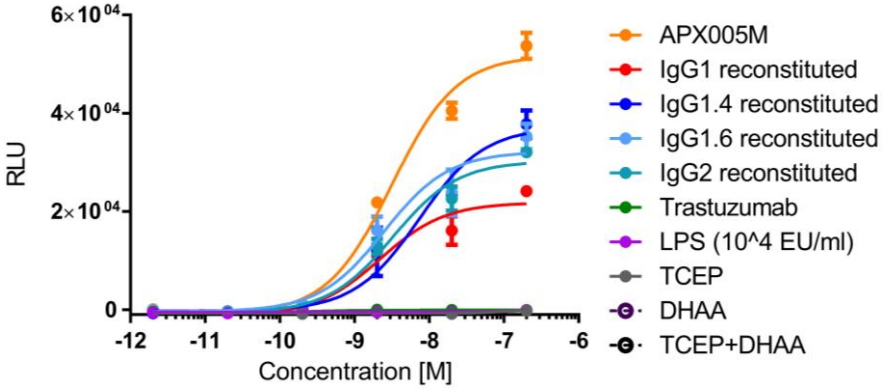

Figure 26: CD40 activation by reconstituted anti-CD40 agonist antibodies.

CD40 expressing HEK293 cells containing a modified Nf-κb pathway triggering luciferase production were seeded with 2.5x10⁴ vc/well and treated with reconstituted anti-CD40 antibodies in different concentrations ranging from 0.002 nM to 200 nM. BioGlo Luciferase substrate was added for luminescence readout. Luminescence signal was monitored and relative luminescence units (RLU) are representing normalized luminescence to untreated cells. Tested reconstituted anti-CD40 antibodies showed similar luminescence signals for CD40 activation. Reference antibody APX005M showed slightly higher detection signal and was used as a positive control while Trastuzumab was used as a negative control. LPS is known to influence certain cell assays and was added up to a concentration of 500 nM as an assay control, showing no signal detection. TCEP and DHAA were added to see potential luminescent signal interference. Number of measurements: Triplicates for each concentration.

Lipopolysaccharide (LPS) was added in different concentrations from 0.005 nM to 500 nM to observe potential luminescence signaling based on the assumption that LPS is known to interfere with several cellular assays (**Figure 26**). In addition, TCEP and DHAA was added in dose concentrations to eliminate false positive signaling. LPS, TCEP and DHAA or their mix did not lead to luminescence signal elucidation and therefore not influencing the cell assay readout.

BsAbs CD3xHer2 either bearing a Her2 Fab binding arm or a Her2 VHH binding moiety were reconstituted and used to evaluate the ability of reconstituted bsAbs to trigger an often-desired mode of action. T-cell activation was assessed by effector cell engagement to Her2 overexpressing cancer cells SK-BR-3 after incubation with reconstituted bsAbs. Jurkat effector cells with a modified NFAT pathway initiated a luciferase reporter readout. Specific cellular binding to human T-lymphocyte expressing CD3 Jurkat E6.1 cells and Her2 expressing SK-BR-3 cells by reconstituted CD3xHer2(Fab) was preliminary proved by flow cytometry (**Figure S15**). Reconstituted CD3xHer2(Fab) and CD3xHer2(VHH) T-cell engagers performed with similar potencies after T-cell activation within an EC50 range between 0.3 nM and 0.5 nM (**Figure 27**). Treatment with monospecific CD3 oaSEED alone with effector and cancer cells was not elucidating strong signal increase, although a slight increase at a concentration of 100 nM was observed, likely through clustering of CD3 oaSEED (**Figure 27**). Cetuximab was used as a negative control and was not triggering luminescence signaling, as expected based on the lacking CD3 paratope. The influence of TCEP and DHAA was not altering the assay signal readout (**Figure 27**).

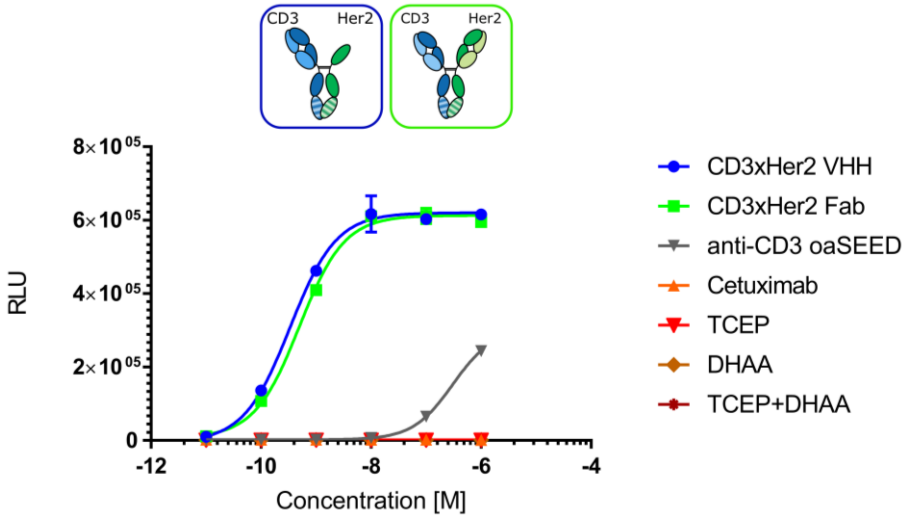

Figure 27: T-cell activation through reconstituted CD3xHer2 bsAbs.

SK-BR-3 cancer cells exhibiting high levels of surface receptor Her2 were used as antigen presenting cells and were incubated with reconstituted CD3xHer2 Fab (blue) and CD3xHer2 VHH (green) in different concentrations ranging from 0.01 nM to 100 nM. Cancer cells and reconstituted antibodies were treated with TCR/CD3 (NFAT) effector cells (Jurkat) and incubated for 6 h. CD3xHer2 bsAbs are able to bind Her2 on SK-BR-3 and CD3 on modified Jurkat cells, stimulating NFAT luciferase activity. BioGlo Luciferase substrate was added for luminescence readout. Luminescence signal was monitored and relative luminescence units (RLU) are representing normalized luminescence to untreated cells. TCEP (red), DHAA (dark orange) and their mix (dark red) was added in dose concentrations to evaluate potential signal increase and assay interference. Cetuximab (orange) was used as a negative control not comprising a CD3 binding moiety. Monospecific anti-CD3 oaSEED (grey) was used as negative control for potential elucidation of luminescence signaling.

Further evidences for reconstituted bsAb functionality was achieved and demonstrated by inhibition of c-MET and EGFR phosphorylation. A549 cancer cells, offering moderate c-MET and EGFR expression levels, were treated with c-METxEGFR bsAbs B10v5xhu225H and F06xhu225H and stimulated with or without HGF and EGF. Retained phosphorylation inhibition of c-MET (p-c-MET) and EGFR (p-EGFR) was observed by B10v5xhu225H and F06xhu225H without treatment of EGF and HGF, as already described in literature,[84] indicating functionality of c-METxEGFR bsAbs after reconstitution (**Figure 28**).

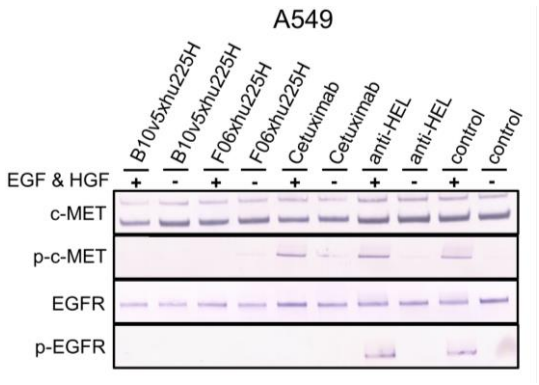

Figure 28: Inhibition of c-MET and EGFR phosphorylation by reconstituted c-METxEGFR bsAbs.

A549 cells with moderate c-MET and EGFR expression levels were used to verify c-METxEGFR bsAb functionality by inhibiting receptor phosphorylation. Cells were incubated with 300 nM bsAbs B10v5xhu225H, F06xhu225H, Cetuximab and isotype control anti-HEL after starvation (medium without FCS) of the cells and stimulation with or without recombinant EGF (50 ng/well) and HGF (30 ng/well). Cells were treated with RIPA buffer for 1 h and cell lysates were prepared for SDS-PAGE and Western Blot analysis. Phosphorylated c-MET and EGFR was detected by specific AP-labeled phospho-c-MET or phospho-EGFR secondary antibodies. B10v5xhu225H and F06xhu225H showed successfully inhibition of c-MET and EGFR simultaneously. Cetuximab showed only phosphorylation inhibition of EGFR but no inhibition for c-MET, while isotype control anti-HEL showed no inhibition for both. Control: No antibody treatment.

Cetuximab was used as a positive control for p-EGFR inhibition, while no inhibition of p-c-MET was observed (**Figure 28**). Anti-HEL was used as an isotype negative control showing no inhibition of either p-c-MET or p-EGFR.

In summary, biological functionality of reconstituted mAbs and bsAbs was successfully demonstrated using several different cellular assays and antibody combinations. The reconstitution method can produce functional antibodies without restrictions in activity but downscaling for the implementation into an HTS platform must be ensured. Before an automated method can be set up, it must be ensured that transferring the reconstitution method to a plate format does not affect the antibody properties.

5.4. Downscaling of antibody reconstitution to 96 well format and automation suitability

Antibody reconstitution of mAbs and bsAbs was transferred and miniaturized into a 96 well plate format to make the technology amenable for HTS. In order to investigate if antibody reconstitution still works in small volumes, a manual pipetting approach was conducted and compared against a semi-automated experiment using the Hamilton MicroLab Starlet liquid handler system. Furthermore, the reconstitution efficiency was investigated between both approaches. As a proof of concept, a surplus of anti-CD40 Fab Int^N fragments were mixed with an IgG1 Fc Int^C portion by manual pipetting, resulting in reconstituted anti-CD40 mAb, using a final volume of 200 µL. All wells were analyzed for reproducibility. **Figure 29** shows a subset out of n = 80 replicants after antibody reconstitution. The whole 96 well plate analysis is shown in **Figure S16**.

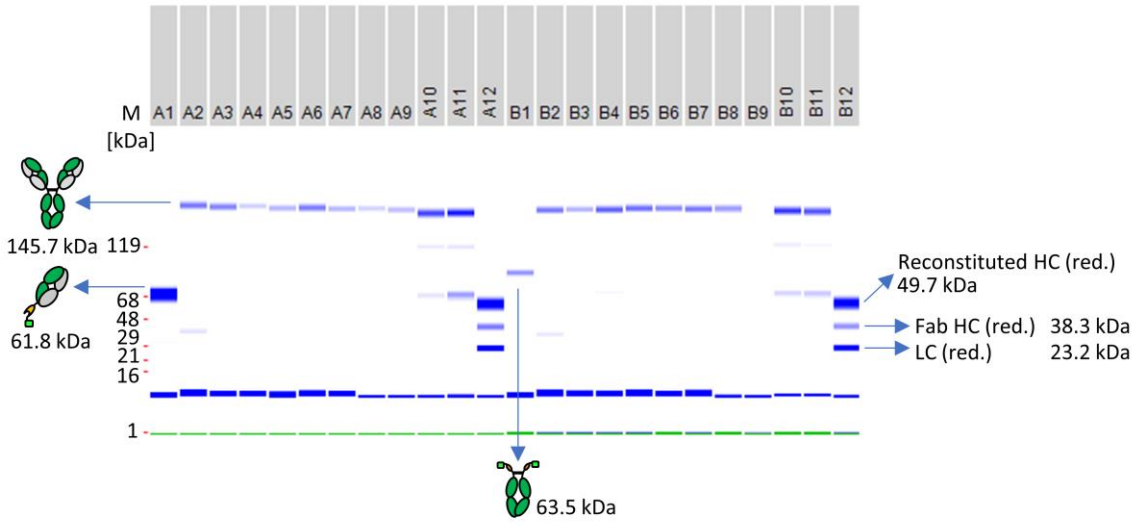

Figure 29: Electronical SDS-PAGE analysis of antibody reconstitution used to demonstrate downscaling and reproducibility in a 96 well format.

A subset of the whole 96 well plate is illustrated and a surplus of anti-CD40 Fab Int^N was used in a ratio 3:1 over huFc Int^C. A1: Single anti-CD40 Fab Int^N (61.5 kDa). B1: single huFc Int^C (63.5 kDa). A2 to A9: Antibody fragments anti-CD40 Int^N and huFc Int^C were mixed in a ratio 3:1 and 0.5 mM TCEP was added for PTS activation. Reconstituted antibodies were separated from non-reconstituted antibodies anti-CD40 Fab Int^N and huFc Int^C by addition of 25 µL Ni^{2+} beads with a binding capacity of 40 µg 25 $µL^{-1}$ and further treated with a 10-fold molar excess of DHAA over TCEP for re-oxidation. Gel bands for reconstituted anti-CD40 antibodies were observed at 145.7 kDa under non-reduced conditions. A10-A11: Not treated with Ni^{2+} beads after reconstitution reaction, resulting in reconstituted anti-CD40 antibody as well as antibody fragments anti-CD40 Int^N and huFc Int^C. A12: Antibody fragments anti-CD40 Int^N and huFc Int^C after TCEP treatment without the addition of Ni^{2+} beads and DHAA (control). Gel band at 1 kDa (green): Lower Marker (LM). Blue band below 16 kDa: System Peak. The whole gel panel of the 96 well plate analysis is shown in **Figure S16**.

Wells A12 and B12 were not treated with Ni^{2+} beads and DHAA after PTS reaction, serving as a negative control (**Figure 29**). Wells A2-A11 and B2-B11 contained full-length reconstituted anti-CD40 mAb, indicated by a gel band at 145.7 kDa and monitored by SDS-PAGE analysis. However, the band sizes of the final product in the gel were not uniform, likely through manual pipetting and resulting volume variations in each well upon normalization of the reconstituted antibody concentration. Non-reconstituted antibody Fab Int^N fragments (61.8 kDa) were still present in wells not treated with Ni^{2+} beads and captured successfully in wells treated with Ni^{2+} beads, indicating the importance of the purification strategy (**Figure 29**, wells A10-11, B10-11).

Binding of reconstituted anti-CD40 mAbs to recombinant human CD40 was conducted and confirmed by ELISA (**Figure 30**). The absorbance signal at 450 nm was slightly varying and non-uniform throughout the whole 96 well plate, as already observed by SDS-PAGE analysis for manual antibody reconstitution (**Figure 29, Figure 30B**). For negative controls and wells without TCEP treatment or lacking the monovalent Fab Int^N and Fc Int^C counterparts, no signals were observed (**Figure 30A/B**).

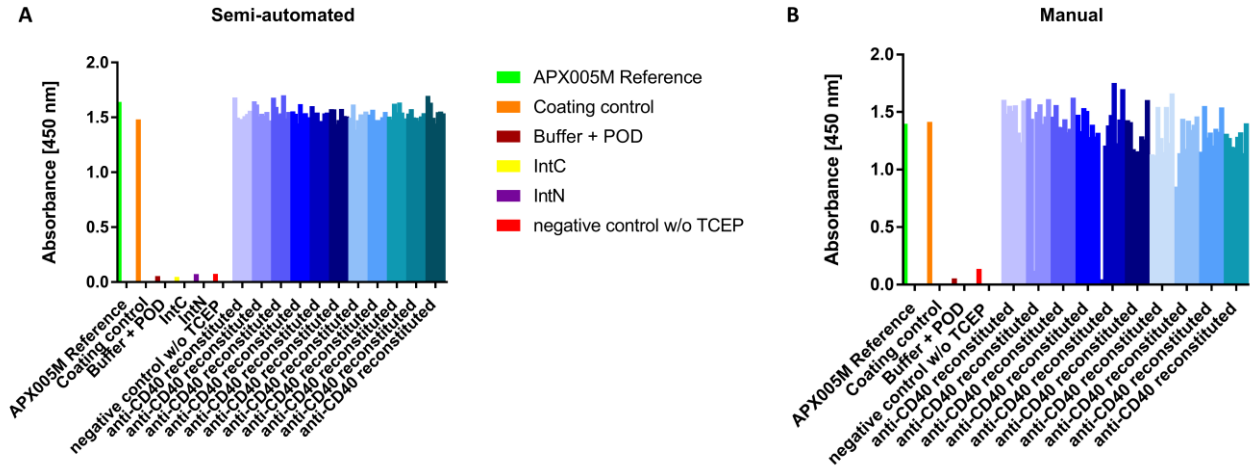

Figure 30: ELISA readout of reconstituted anti-CD40 mAbs in 96 well format semi-automated by Hamilton MicroLab Starlet liquid handler compared to manual pipetting.

Antibody reconstitution was performed in 96 wells, mixing anti-CD40 Fab Int^N with huFc Int^C in a 3:1 molar ratio with 0.5 mM TCEP in a final volume of 200 µL resulting in a total protein amount of 58 µg. Non-reconstituted antibody fragments anti-CD40 Fab Int^N and huFc Int^C were removed by 25 µL Ni^{2+} beads with a binding capacity of 40 µg/25 µL supported by a strong magnet (semi-automated **(A)**) and reconstituted anti-CD40 mAbs were supplemented with a 10 fold molar excess DHAA over TCEP for re-oxidation. ELISA was performed after binding recombinant human CD40 with reconstituted mAbs and detected with a Fc specific goat-anti-human IgG conjugated to peroxidase at absorbance 450 nm. (**A**) Overall absorbance signal of semi-automated antibody reconstitution in 96 well plate format after ELISA. (**B**) Overall absorbance signal of manual generated antibody reconstitution in 96 well plate format after ELISA. Negative controls anti-CD40 Fab Int^N, huFc Int^C and both fragments combined without TCEP treatment showed no absorbance signal.

The semi-automated reconstitution was compared against the manual reconstitution, to avoid errors and variations observed as slightly uniformity throughout the 96 well plate after SDS-PAGE and ELISA analysis. A normal distribution was generated from the ELISA readout with n = 80 replicates (**Figure 31**). The reconstitution efficiency was improved up to 15% using the semi-automated system by calculating the mean variation of the overall signal absorbance of each experiment, estimated by ELISA (**Figure 31**). The overall signal absorbance of the semi-automated reconstitution showed a more precise uniformity after ELISA readout, compared to the manual reconstitution, indicating the importance and demand of an automated system.

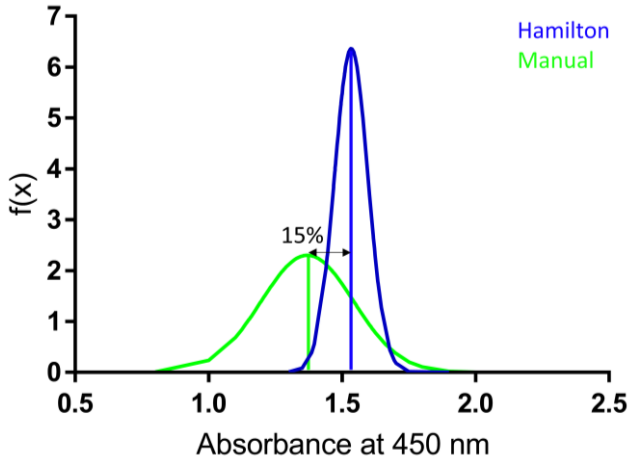

Figure 31: Comparison of reconstitution reproducibility between semi-automated and manually generated mAbs in 96 well format.

ELISA was conducted manually and semi-automated via Hamilton liquid handler after reconstitution of anti-CD40 Fab Int^N and huFc Int^C fragments in 96 well plate format. A normal distribution of both experiments with n = 80 antibody reconstitutions was generated via GraphPad Prism v7. The calculated mean variation of each conducted experiment was compared with each other giving a 15% improvement of reconstitution reproducibility by semi-automation. The amplitude displays the density function f(x) calculated with **equation 4 (Chapter 4.5.3)**.

It was successfully demonstrated that neither antibody reconstitution is compromised by downscaling into a 96 well plate format, nor the purification strategy to remove non-reconstituted antibody fragments. An automated system improves the reconstitution efficiency and therefore improves the accuracy of generating bsAbs for HTS. HTS platforms serve as massively cost and time saving applications and therefore an even smaller plate format of 384 wells and a fully automated system is desired. A fully automated system further benefits the operating expense. The next chapter describes a fully automated reconstitution approach and the investigation to further miniaturize the reconstitution method into a 384 well plate format without the limitations of a semi-automated approach.

5.5. Fully automated production of reconstituted antibodies designed for HTS in a 384 well format

Based on the investigations described in **Chapter 5.4**, antibody reconstitution was transferred into a 384 well plate format and generated fully automated, using the BiomekFX HT platform. To compare the reconstitution results of **Chapter 5.4**, anti-CD40 mAbs were used again as a proof of concept. Each well was supplied with anti-CD40 Fab Int^N fragments and IgG1 Fc Int^C portion for antibody reconstitution and tested for reproducibility. ELISA was used as a readout for reconstituted anti-CD40 mAbs after binding to recombinant human CD40. Similar overall absorption signals were observed for the 384 well plate reconstitution compared to the semi-automated reconstitution in 96 well plates (**Figure 32A**). A slight non uniform absorbance signal was observed and is depicted in **Figure 32A** as a heat map, illustrating each single well of the whole plate. The automated pipetting for antibody reconstitution molecules and reagents was conducted row by row and might lead to concentration variations in each well. Furthermore, reconstituted antibody concentration was

normalized and could account for absorption signals inconsistencies, although the signal range variation is negligible small.

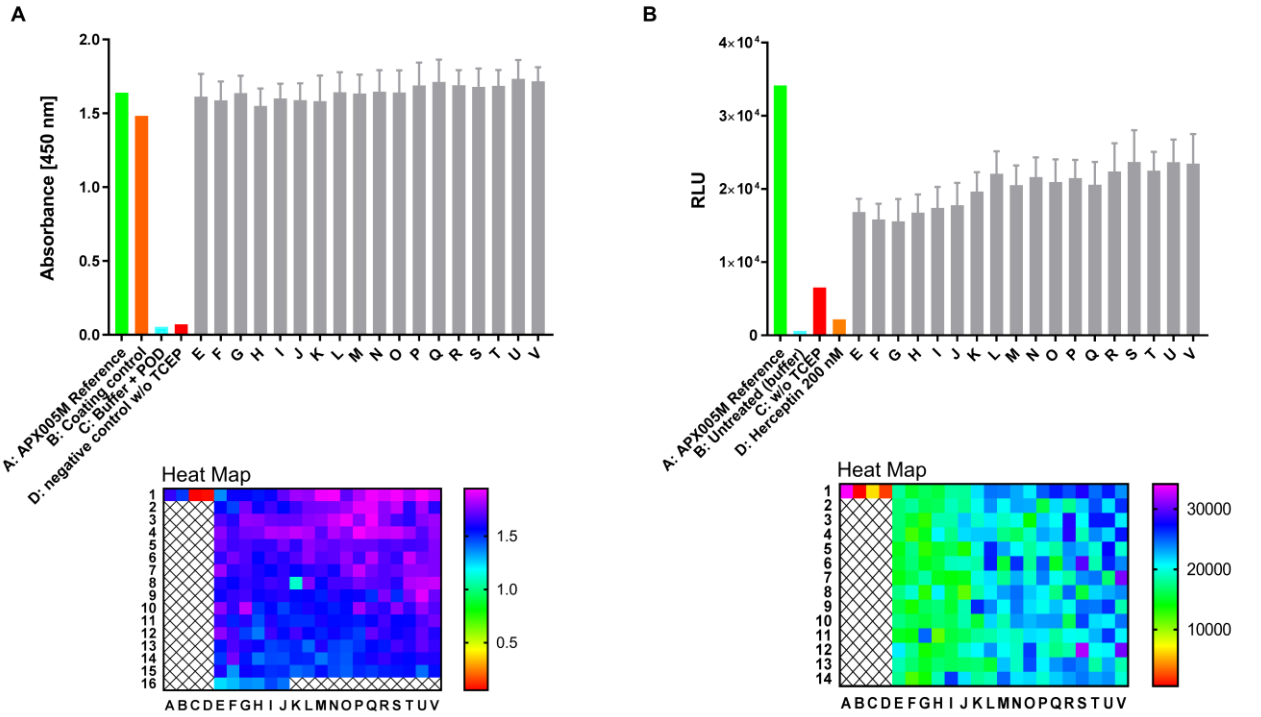

Figure 32: Fully automated anti-CD40 mAb reconstitution and functionality determination in 384 well using the BiomekFX HT platform.

Antibody reconstitution was performed in 384 wells, mixing anti-CD40 Fab Int^N with huFc Int^C in a 2:1 molar ratio with 0.5 mM TCEP in a final volume of 40 µL resulting in a total protein amount of 14 µg. Non-reconstituted antibody fragments anti-CD40 Fab Int^N and huFc Int^C were removed by 14 µL magnetic Ni^{2+} beads with a binding capacity of 40 µg/25 µL supported by a strong magnet and reconstituted anti-CD40 mAbs were supplemented with a 10 fold molar excess DHAA over TCEP for re-oxidation. ELISA was performed after binding recombinant human CD40 with reconstituted mAbs and detected with a Fc specific goat-anti-human IgG conjugated to peroxidase at absorbance 450 nm. **(A)** Overall absorption signal of fully automated antibody reconstitution (E-V) in 384 well pate format after ELISA. Each column starting from E to V represents a cluster of 16 wells including the mean with standard deviation for each cluster. The heat map shows signal detection at 450 nm after performed ELISA for each well in the 384 well plate. **(B)** Antibody functionality of automated reconstituted anti-CD40 mAbs was determined by CD40 activation assay. Human CD40 expressing HEK293 cells were treated with 4 nM reconstituted antibodies (E-V), 200 nM APX005M (positive control) and 200 nM Trastuzumab (negative control) for 6 h activating an engineered Nf-κB pathway for luciferase transcription. Luminescence signal was recorded and relative luminescence units (RLU) are representing normalized luminescence to untreated cells. The heat map illustrates CD40 activation for each single well on the plate. Error bar: Mean with standard deviation (SD).

Pharmaceutical antibody development highly demands broad functional screening capacity and therefore, reconstituted anti-CD40 mAbs, generated from fully automated 384 well reconstitution, were used without further treatment to perform a feasibility study in a functional CD40 activation cell assay (**Figure 32B**). Parental CD40 agonist APX005M and Trastuzumab were used in a concentration of 200 nM as references showing expected activation signal or no signal respectively. All reconstituted anti-CD40 mAbs were inducing CD40 activation at a concentration of 4 nM, as already investigated previously (**Figure 26**). The overall luminescence signal after CD40 activation seemed to show well dependency, as indicated by the heat map depicted in **Figure 32B**, likely through varying cell levels per well by manual pipetting. However, antibody reconstitution was successfully miniaturized to 384 well plate format and furthermore improved by a fully automated platform amenable for HTS and enlarged screening capacities, including biological functionality of the tested reconstituted antibodies.

5.6. Quantification for HT antibody reconstitution by HTRF analysis suitable for 1536 well format

HT reconstitution of antibodies offers a full spectrum of molecules in different formats being produced and screened. Therefore, a critical look into the products and byproducts and also the amounts of undesired products remaining following reconstitution have to be considered. One way to prove efficient and reproducible reconstitution rates is the determination by Homogenous Time Resolved Fluorescence (HTRF) quantification suitable for 1536 well plate format. Biotin labeled Fab Int^N fragments were reconstituted with oaSEED Int^C fragments and quenched at specific time points to track the reconstitution rate (**Figure 33A**). Antibody reconstitution was not compromised by Fab Int^N fragments labeled with biotin, as detected by SE-HPLC analysis used for cross validation of reconstituted bsAb (**Figure 33B**). Antibody reconstitution was stopped after 3 h yielding >90% non-purified bsAb, determined by SE-HPLC. A similar pattern was observed after HTRF analysis and fluorescence signal reached its maximum after 3 h (**Figure 33C**). No fluorescence signal was detected using negative controls single oaSEED Int^C and single biotinylated Fab Int^N after treatment with anti-human IgG-Tb and Strepdavidin-d2. Fluorescence signal will only be detected, when both antibody fragments are present.

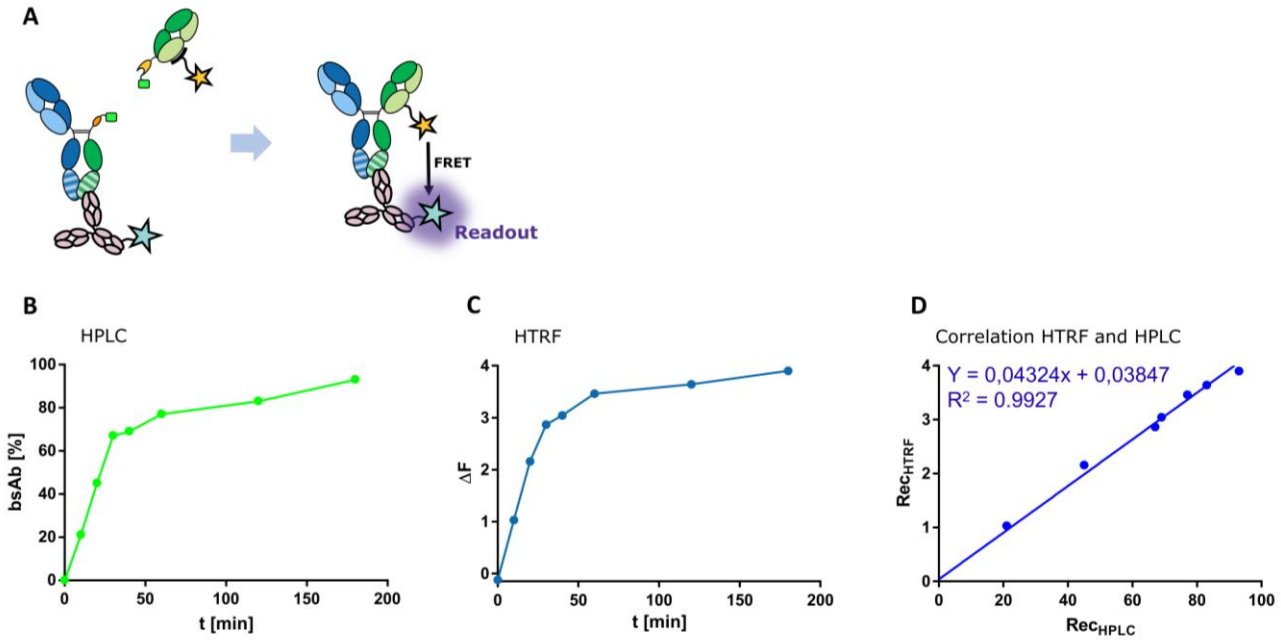

Figure 33: Quantification of HT antibody reconstitution efficiency determined by cross validation of SE-HPLC and HTRF analysis in 1536 well format.

Antibody fragment Fab Int^N with a molar concentration of 0.1 mM was biotinylated with a molar excess (1:10) of NHS-PEG4-Biotin and incubated at RT for 0.5 h. Residual non-reacted NHS-PEG4-Biotin was removed by Zeba Spin desalting columns. Biotinylated Fab Int^N fragment was reconstituted with an oaSEED Int^C fragment in an equimolar ratio and quenched at different time points with H_2O_2 to stop PTS. HTRF was performed by adding reconstituted bsAbs diluted at 0.1 µM with terbium buffer, PBS pH 7.4 and 0.3% Tween-20 to each well. Strepdavidin-d2 (100 µg mL^{-1}) and IgG-Tb (10 µg mL^{-1}) was added to a final volume of 5 µL per well and incubated for 4 h. **(A)** BsAb reconstitution with biotinylated Fab Int^N and oaSEED Int^C attached to anti-human IgG-Tb cryptate. Successful reconstitution resulted in FRET signaling. **(B)** HPLC analysis of reconstituted bsAb at several time points quenched with H_2O_2 for cross validation. **(C)** HTRF fluorescence detection at several time points. Data reduction was performed by normalization of background noise of the donor for each well, minimizing well to well variations and normalization of the measurements, to minimize plate to plate variations. The fluorescence signal was measured at 620 nm and 665 nm. **(D)** Correlation between HPLC and HTRF analysis calculated as standard curve and coefficient of determination.

The fluorescent signal increase over time, indicated that energy transfer of the fluorophores will only occur if biotinylated Fab Int^N is in close proximity to anti-human IgG-Tb attached to the Fc portion of oaSEED Int^C. **Figure 33C** illustrates the fluorescence signal increase over time after reconstitution of both antibody fragments bringing both fluorophores to the demanded distance. The addition of TCEP and DHAA needed for antibody reconstitution was not influencing the HTRF assay system. A correlation between HPLC and HTRF data shows a high coefficient of determination with $R^2 = 0.992$, indicating that HTRF analysis displays comparable amounts of reconstituted bsAb and therefore suitable for reconstitution quantification and generation in a 1536 well format (**Figure 33D**).

Antibody reconstitution was conducted in 96 and 384 well plate format and could potentially be used in a 1536 well format revealed by HTRF quantification observations. Reproducibility and biologically functional anti-CD40 mAbs were generated in a high throughput manner and tested in functional assays. The ultimate goal is to address the reconstitution technology to screen for bsAb combinations to find a possible lead candidate out of a huge antibody repertoire. It is of importance to investigate the screening potential of this method, which is described in detail in the following chapter.

5.7. Combinatorial screening of reconstituted antibodies for possible lead candidate identification

Antibody reconstitution was proved to be amenable for fully automated HT (**Chapter 5.5**) and was further investigated with respect to combinatorial screening. Several bsAbs were reconstituted simultaneously, bearing different binding moieties, to demonstrate screening potential based on higher and lower affinity profiles (**Figure 34**). Reconstituted bsAbs were analyzed by BLI, flow cytometry or ELISA for retained binding properties. Reconstituted c-METxEGFR bsAbs B10v5xhu225L and B10v5xhu225H showed similar biophysical binding properties for B10v5 with a binding affinity of 0.8 nM against recombinant c-MET (**Figure S13**). Binding to recombinant EGFR of the hu225H Fab arm was detected with 0.18 nM and had considerably higher affinity compared to hu225L with 0.2 µM (**Figure S13**). Stepwise association to recombinant c-MET and EGFR using reconstituted bsAbs B10v5xhu225L and B10v5xhu225H, confirmed simultaneous binding of both antigens after BLI analysis. Monospecific B10v5 oaSEED was used to determine unspecific binding to EGFR, but only binding to c-MET was observed, as expected (**Figure S13**). Cellular binding of cell surface receptor antigens c-MET and EGFR was confirmed by incubating reconstituted bsAbs B10v5xhu225L, B10v5xhu225H and F06xhu225H with several cancer cell lines, offering moderate to high expression levels of antigen, as described previously (**Chapter 5.3.2, Figure 25**). ELISA was performed after reconstitution of bsAbs to illustrate differences in signal detection and therefore screening capability for different bispecific combinations. F06xhu225H showed lower signal absorbance after binding recombinant c-MET, compared to B10v5xhu225H after ELISA analysis based on a much lower affinity profile of F06 over B10v5 (**Figure 34**). No signal detection was observed with B10v5xhu225L, binding to recombinant EGFR based on the low affinity profile of 0.2 µM (**Figure 34**), which was confirmed by BLI analysis (**Figure S13**). High signal detection was achieved with B10v5xhu225H based on the high affinity to EGFR.

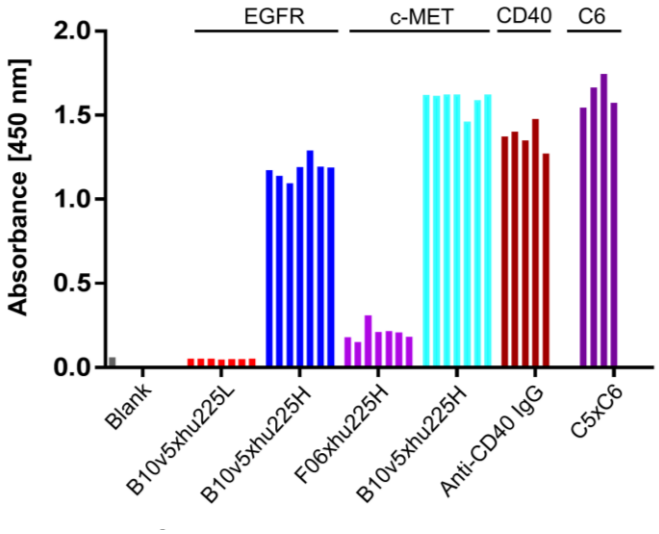

Figure 34: Antibody reconstitution using different formats and combinations to investigate screening feasibility.

Several bsAbs B10v5xhu225L, B10v5xhu225H, F06xhu225H, C5xC6 and mAbs anti-CD40 IgG1 were reconstituted simultaneously in 96 well plate format, according to previously described reconstitution conditions. The absorbance signal at 450 nm was measured after binding of bsAbs and mAbs to their respective recombinant antigens after detection with POD labeled anti-human Fc specific antibody. Reconstitution reproducibility was ensured by 4-7 replicants of each reconstituted variant.

Binding to recombinant CEACAM6 was successfully demonstrated by reconstituted bsAb C5xC6 exhibiting strong binding affinities against the recombinant antigen, as determined previously (**Chapter 5.3.1, Figure 23**). Furthermore, reconstituted anti-CD40 mAbs showed reproducible absorbance signals, when compared to above mentioned experiments (**Chapter 5.5**, **Figure 32A**). Reconstitution reproducibility was confirmed by 4-7 replicants as illustrated in **Figure 34**. Several in parallel reconstituted bsAbs and mAbs were showing expected signal detection after binding to their respective antigens, indicating that antibody reconstitution by PTS in different formats and combinations is feasible for HT.

6. Discussion

6.1. Generation of reconstituted antibodies in different formats mediated by PTS

The evaluation of complex NBEs such as bispecific antibodies for therapeutic development remains challenging due to extensive cloning steps followed by expression and purification until the optimal lead candidate is discovered. Furthermore, chain mispairings and homodimerization occurs during antibody expression, leading to low product quality and yields. In course of this study, the recombination of antigen binding arms is forced by the attachment of split intein parts introduced in the hinge region fused to their native exteins, activating PTS in a mild reducing environment. The split intein mediated bsAb reconstitution offers a way to bypass above mentioned limitations by fusing a single Fab fragment to a one-armed heterodimeric Fc fragment on the protein level *in vitro*. Split intein parts are fused N-or C-terminally within the hinge region and remain distal from the Fc portion and the paratope region of the Fab, providing no alteration of effector functions and antigen binding. Therefore, it is not surprising, that bsAb functionality is retained after reconstitution, as the split intein parts are excised out of the combination partners giving rise to stable bsAbs.

The relatively large distance between Fab arms and Fc portion due to separation by the hinge region allows for the most appropriate space and flexibility to perform PTS.[30,31] It was successfully demonstrated that the addition of TCEP in the nanomolar concentration range, as needed for PTS activation, does not lead to LC shuffling during generation of bsAb reconstitution with two different LCs. These observations were confirmed by the study of Han *et al.* To create a reducing environment, TCEP was used based on its properties to be compatible with Ni^{2+} IMAC affinity purification, unlike dithiothreitol (DTT), which was also been successfully tested and used for PTS ligation in this study and by others. Furthermore, TCEP is a milder reducing agent compared to DTT, primarily reducing interchain disulfide bonds.[148]

A re-oxidation step to recover disulfide bridging is usually carried out gently by dialysis over time to strip out the reducing agent and supply the antibody solution with fresh buffer. To make the reconstitution technology suitable for HTS, dialysis is not the first choice for re-oxidation, although several filters or desalting columns are available even for HT scale to perform buffer exchanges. In this study, TCEP is inhibited in its power by the addition of a 10-fold molar excess of DHAA over TCEP to avoid excessive desalting steps. Furthermore, TCEP is not very stable at neutral pH in phosphate buffers and tend to oxidate within 72 h which favors the re-oxidation process. Although studies have shown that DHAA can be reduced by TCEP as well and long-term stability investigations of reconstituted antibodies have to be performed to check intact disulfide bonds over time.[149] In addition, antibody oxidation can affect structural functionality (Methionine oxidation) and must be investigated. Reference antibody APX005M reached a higher signal level compared to reconstituted anti-CD40 mAbs conducting CD40 activation experiments. The addition of TCEP and DHAA might cause effects on cell viabilities during treatment with these reagents. Alternative split inteins, not dependent on reducing environments to perform PTS, could be a potential solution to bypass antibody re-oxidation. Similar splicing kinetics compared to the well characterized and fast split intein *Npu* DnaE were achieved and reported in several studies by using other split intein variants without the dependency on a reducing environment.[150] PTS is initiated by either a pH shift or a temperature shift and sufficient for high splicing efficiency. The cysteine-less

split intein Aes, recently engineered by Bhagawati *et al.*, combines optimal reaction conditions with good splicing properties and might be an alternative for reconstituted bsAbs, like T-cell engagers.[146] The effector cell recruitment, extracted from human blood, is very sensitive and might not be compatible with TCEP or DHAA during screening campaigns.[146]

Other groups like Alam *et al.*, described in an elegant way to reconstitute monospecific antibody fragments in different formats using a SpyTag/SpyCatcher protein ligase system.[107] The system can be extended by other ligase systems to generate bispecifics. However, the generation of bsAbs using the SpyTag/SpyCatcher technology is leaving a significant imprint of 23 amino acids within the molecule after protein ligation.[108,151]

T-cell engagers offer the ability to rearrange target and effector cells by simultaneous attachment through their binding moieties and therefore, the format matters in terms of flexibility and paratope distances, to achieve high potency engagement.[152] Reconstituted bsAbs using the SpyTag/SpyCatcher technology, would drastically increase the flexibility and the paratope distances compared to the naturally IgG format and alter the engagement potential. Reconstitution with split inteins leaves by far a decreased scar of 6 amino acids within the molecule after performing PTS. Furthermore, this scar can be reduced to $2-3$ amino acids at position $+1$ to $+3$, only leaving the C-terminal Extein "CFN" or "CF" respectively, inside the molecule. The N-terminal Extein "AEY" at position -1 to -3 seems to have no significant impact on splicing efficiency and recognition of the N-terminal split intein part.[153,154] Of note, altering the native extein sequences can lead to side reactions in terms of C- or N-terminal pre cleavage not able to achieve the desired product anymore.[138]

Therefore, antibody reconstitution mediated by split inteins allows for closer in-format bsAbs and improves the chance to efficiently engage target and effector cells. Reconstituted T-cell engagers mediated by split inteins are providing good or even better potency engagement compared to a classic produced reference, as investigated by Han *et al.*[66] Cytotoxic potential in the presence of tumor and T-cells initiating T-cell activation was reported and successfully demonstrated *in vitro* and *in vivo*. These observations support the aspect that cellular functional assays can be conducted using reconstituted antibodies resulting in high potencies. However, the addition of a non-native amino acid sequence in form of exteins attached to each split intein part must be considered and might cause molecular structural alteration and therefore modifications in biological functionality. Computational modeling could be used to define which amino acid residues could be omitted within the hinge region in order to achieve the same length and flexibility in screening with the required residues, as later in the genetically correctly fused molecule. This would allow for final format and functional screening of bsAbs. Furthermore, C-terminal fusions at the Fc portion commonly extended by GS-linkers would be conceivable.

Labrijn *et al.* 2013 published a technology to generate bsAbs efficiently by controlled Fab-arm exchange former known as DuoBodies.[43,44] Duobodies are forming full-length in format bispecific IgGs, but however they are restricted to a full-length IgG format. The split intein technology presented in this study, allows for reconstitution in several formats, changing the valency and specificity of bivalent IgGs, heterodimeric Fc bispecifics and IgG fusion with Fabs and VHHs. Split inteins are not limited to antibodies and furthermore, non-antibody Fc fusions like cytokine traps can be added to the format portfolio. Since the optimal format and combination for a new biological entity with a specific mode of action is unknown, split inteins offer the

possibility to screen not only for the best combination of paratope moieties but also for the best format itself to access the desired mode of action.

The manufacturability of antibody fragments fused to split intein parts as starting material for antibody reconstitution, more specifically the secretion yield after transfection of HEK293F cells, is comparable to antibody fragments lacking a split intein partner. Although it was observed that some antibody fragments, like hu225H Fab Int^N and other fragments attached to the N-terminal split intein part are lower in expression yield. The split intein parts Int^N and Int^C are not forming a conformational complex unless PTS is activated. The Int^N part exposes a high content of hydrophobic patches, which potentially could lead to aggregation or degradation because of the long unfolded protein structure of the split intein sequence, linker and purification tag. In case of a mis- or unfolded protein, several antibody fragments fused to Int^N and Int^C have been produced at higher concentrations ranging from 1 mg mL^{-1} up to 13 mg mL^{-1} to show robustness of the starting material. Aggregation was not observed for constructs used in this study and allowed for good yields with high monomeric content. However, the production of VHH or scFv fragments fused to Int^N in *E. coli* highly favors inclusion body formation (data not shown).

6.2. Evaluation of reconstitution efficiency, biophysical and functional characterization

Han *et al.* already demonstrated initial success in generating a bsAb reconstituted by split inteins. Therefore, the development of an HTS platform for bsAbs was the focus of this project and offers an advanced purification strategy optimized for automation. One of the main differences compared to the study of Han *et al.* is the construct design and therefore the purification strategy ensured by fused hexahistidine tags upstream and downstream of the respective split intein parts, which are removed again after PTS. Han and coworkers needed to purify their split intein constructs by two extensive purification steps via Protein A purification followed by IMAC to remove non-reconstituted antibody fragments. Here, a molecular design was described, allowing for a one step purification via IMAC by addition of Ni^{2+} beads, without buffer exchange or elution of the desired reconstituted antibody. The reconstituted antibody remains tag less after PTS, while spliced split inteins still carry the hexahistidine tag for purification. The purification of product related impurities during bsAb production remains a manufacturing challenge. Especially small-scale expressions for screening applications cannot be supported by extensive purification steps.[41,155] Therefore, non-reconstituted antibody fragments and processed split intein can be trapped with high affinity by Ni^{2+} beads. It was successfully demonstrated that non-reconstituted antibody fragments, as well as the spliced intein parts were removed after Ni^{2+} bead treatment, boosting the monomeric content of the desired reconstituted product to good quality and yield. A high monomeric content of reconstituted antibodies also depends on the correct molar ratio of the precursor antibody fragments. Especially for mAb reconstitution the molar ratio of 2:1 antibody fragments Int^N and Int^C respectively is important. If the molar ratio is unbalanced, the chance of half-bodies might occur, bearing only one Fab fragment fused to the Fc portion. With respect to HTS amenability, it is of importance to analyze byproducts and product related impurities like half-body formation, which might compromise functional screening assays. Choosing the optimal molar ratio of precursor antibody fragments fused to their intein parts showed quantitatively conversion as demonstrated in this study.

Furthermore, the long stretch of 26 amino acids containing a 4x G_4S-Linker plus hexahistidine tag attached to the Int^C, is not compromising the PTS reaction. Split intein parts still had enough space to form a conformational complex. However, *Npu* DnaE is known to complete splicing within minutes. In this study, antibody reconstitution was completed after 2 h yielding a high monomeric content of reconstituted antibody. The additional linker and purification tags might lead to a slower PTS reaction by disturbing the split inteins to form a fast-conformational structure. Despite of these potential drawbacks, high reconstitution yields, and more importantly correct final molecule assembly were confirmed by intensive biochemical characterization and mass spectrometry.

Reconstituted bsAbs and mAbs were generated in several formats and were further characterized in terms of their biophysical and biochemical properties compared to their previously reported parental antibodies[84,156], providing similar kinetic properties, thermostability, and biological functionality. Slight variations in thermostability were observed for reconstituted bsAb C5xC6 compared to reference C5xC6, likely through the modified hinge region based on remaining extein sequences. Inhibition of p-c-MET and p-EGFR, T-cell engagement, CD40 activation and bispecific binding was demonstrated for several reconstituted antibodies resulting in comparable functionalities compared to their references. The impact of used reagents TCEP and DHAA in several biophysical and biochemical experiments did not lead to a false positive signal increase or disturbance of the assays itself. The high dilution rates to picomolar or nanomolar concentrations used for reconstituted antibodies in functional cellular assay systems might extenuate the use of these reagents. Noteworthy, the concentrations used for reconstitution reagents TCEP and DHAA did not lead to a luminescence signal detection after conducting CD40 activation but may have an effect on cell viabilities of CD40 expressing HEK cells. The lower detected signal of reconstituted anti-CD40 mAbs compared to the APX005M reference antibody might result from insufficient cell levels based on these concentration ranges. Furthermore, the modified hinge region by an additional cysteine derived from the extein could potentially lead to newly formed disulfide bonds during the reduction and re-oxidation conditions after antibody reconstitution and therefore leading to a geometrically change and flexibility of the molecule compared to the natural unmodified IgG reference. Formation of byproducts with different HC-HC or HC-LC pairing might occur and account for the different maximum detection levels after CD40 activation. Further investigation of the potential influence of reconstituted anti-CD40 mAbs for CD40 activation or the used reagents TCEP and DHAA would be needed with critical look into byproduct formation. Various reconstituted bsAbs have confirmed the applicability of split inteins for bispecific functional HTS in various assays not specifically screened for compatibility. All conducted cell assays were suitable for reconstituted antibody functional screening not causing any obstruction.

6.3. Miniaturization and high throughput feasibility of antibody reconstitution

It is a growing trend to miniaturize biological assay systems and implement automated systems and robotic technology based on the rapidly growing repertoire of new promising therapeutic targets in pharmaceutical industry. The advantages of automated systems combined with HT feasibility are cost reducing and offer the possibility to screen for an increased number of hit candidates in less time. DNA and protein microarrays are

one of the best examples for assay miniaturization. Antibody reconstitution by split intein mediated PTS was miniaturized starting from manual low throughput to industrialized robotic HTS by applying the technology to 96, 384 and 1536 well formats. Downscaling the reaction volumes for each well format did not compromise the reconstitution efficiency and the reaction itself. It was successfully demonstrated that Ni^{2+} beads can be distributed in each well of a 384 well plate been able to trap non-reconstituted antibody fragments and spliced intein parts. The ELISA readout provided a minor signal variation throughout the plate, likely from concentration differences for each well upon automatic pipetting but delivers robust signal to noise ratio for broad HTS campaigns.

The one pot purification described for non-reconstituted antibody purification might be further applicable for unpurified antibody fragments directly after secretion with unknown concentrations. The split intein *Npu* DnaE is able to perform PTS in conditioned medium after antibody fragment expression without further purification (**Figure S17**). Potentially an already purified antibody fragment can be spiked into the expression of the counterpart antibody fragment for reconstitution or a combination of both antibody fragment expressions could be mixed for reconstitution without extensive preliminary purification steps. Non-reconstituted antibody fragments are removed by Ni^{2+} beads as discussed above. Small scale implementation for automated antibody fragment expression prior to antibody reconstitution could extend and improve the automation setup.

HTRF analysis offered a fast and efficient data set about antibody reconstitution rates in 1536 well format. Although not detecting impurities in form of non-reconstituted antibodies, HTRF experiments revealed that antibody reconstitution is amenable for 1536 well format. Adaption of the developed purification design to 1536 well format warrants further investigation of factors as Ni^{2+} beads addition potentially suffering from the well geometry, low volumes of maximum 12.5 µL, sample evaporation, inhomogeneous stirring of the beads and separating reconstituted antibodies from Ni^{2+} beads. A tradeoff between the enormous number of antibody combinations that can be screened in a 1536 well format and the loss of single antibody combinations through a higher content of non-reconstituted antibodies exists but seems acceptable based on the highly enlarged screening space. To get a better idea of the HTRF output, a cross validation was performed using SE-HPLC analysis correlating well with HTRF analysis. The low concentrations and volumes required for HTRF analysis describe a perfect analytical tool for 1536 well formats compared to SDS-PAGE and SE-HPLC analysis. However, precursor antibody fragments Fab Int^N have to be labeled with biotin, making it non-convenient to use HTRF as a standard analytical tool for reconstitution efficiency. A more elegant way would be a biotin labeled antigen directed against the reconstituted Fab arm to enable HTRF.

Implementation of a fully automated system for antibody reconstitution confirmed improved accuracy of reconstitution as measured by antigen binding ELISA signal, when compared to a manual conducted approach. In addition, more antibodies can be generated in a less amount of time. Over 330 reconstituted anti-CD40 mAbs were generated fully automated with high reproducibility in less than one day, providing functional CD40 activation as a proof for HTS compatible functional screening. Up to 40 000 reconstituted bsAbs could potentially be generated in one week and screened for functionality when applying a full extent industry scale screening approach.

6.4. Application of combinatorial high throughput screening

The investigation of a novel screening technology for a large set of potential combinations of paratope moieties provided in a bispecific format to bypass current screening limitations and broaden up the target screening space was the primary goal of this study. Pharmaceutical development of bsAbs is supplied by several screening methods during discovery for the best combinations out of two paratope binders. However, the target screening space is limited indebted by the tremendous amount of biological paratopes and combinations. Sampei *et al.* demonstrated an impressive screening approach to find the best combination for a FIXa/FX bsAbs. They screened 200 x 200 monoclonal antibodies separately against FIXa and FX, leading to 400 single cloning steps. Finally, they generated 40 000 different bispecific combinations with extensive expression and purification steps to discover the best hit candidate. Ten different byproducts in form of mispaired HC-HC or HC-LC species were observed during bsAb production, decreasing the yield of the desired product and demanding on a multistep purification strategy.[157,158] Currently HTS for bsAbs is very limited by cloning, expression and purification steps reducing the huge potential capacity of the screening space. The presented novel combinatorial HTS technology in this study opens the possibility to widen this major bottleneck in conventional screening approaches. The combination of antibody fragments *in vitro* allows for a combinatorial setup overcoming the need for individual expression and purification for each combination. Generating 40 000 individual bsAb combinations by fully automated antibody reconstitution in a 384 well plate format would significantly decrease the number of expressions from 40 000 to 400 variants. In addition, this method allows for a massive cut in time management and manufacturing costs during generation and screening of bsAbs. Screening of 40 000 variants could have potentially done within one week using the split intein approach.

Hit discovery and development of clinical candidates predominantly prefers a full-length IgG format. However, most of the formats derived from early stage screening campaigns are based on a scFv, VHH or Fab format selected by for example yeast surface display or phage display derived from bacterial hosts. A re-formatting step is obliged to achieve the final format but means a risk in losing or altering biological functionality like decreased affinity or biological potency. Re-formatting, re-testing and maybe re-engineering is needed, potentially reducing candidate numbers and increasing timelines and costs. Functional screening already in the desired full-length IgG format would bypass extensive reformatting steps and alteration of potential biological functionality. Generation of full-length IgG antibodies in bacterial hosts like *E. coli* is challenging and mostly results in misfolded protein or low yields without glycosylation compared to scFv, VHH or Fab fragments. Fusing these antibody fragments to split inteins prior to phage or yeast display selection would allow for the possibility to directly change the format by antibody reconstitution before hit identification and make these molecules accessible for modes of action, which are dependent on Fc mediated effector functions or bivalent binding. A re-formatting step into a bivalent or bispecific IgG-like format after hit candidate generation would bypass multiple cloning, expression and purification steps aside from the economy of time. Furthermore, re-engineering and optimizations to retain biological functionalities could be omitted. VHH fragments fused to Int^N and produced in *E. coli* followed by reconstitution to an oaSEED molecule or Fc portion was demonstrated in this study and affirmed the above-mentioned hypothesis.

The investigation of two distinct split inteins without cross reactivity to each other during PTS, provides the possibility for orthogonal reconstituted antibody variants originated from multiple antibody building blocks.[159,160] Undesired combinatorial ligation can be avoided by finding a split intein pair offering simultaneous orthogonal PTS activity leading to a dual split intein screening approach for either multifunctional antibody formats or the discovery of bispecific antibody-drug-conjugate (ADC) variants. The opportunity to generate antibodies out of three antibody building blocks increases the combinatorial screening setup for bispecific or trispecific formats in parallel. In addition, Fc portions could be potentially linked to toxins with a fixed DAR and reconstituted with Fab fragments to generate and screen for bispecific ADCs. Pizer *et al.* has demonstrated that split inteins are suitable for the ligation of immunotoxins C-terminally to Fc antibody portions.[161]

In conclusion, antibody reconstitution mediated by split inteins provides a powerful combinatorial and functional screening tool for the generation of bsAbs in a fully automated setup. In future, this technology could be used in pharmaceutical antibody discovery to support a fast and efficient identification of optimal binder combinations in a bispecific format or other complex formats to address the desired mode of action.

6.5. Outlook

The technical proof of concept for industry scaled automated HT generation of bsAb variants supported by potential combinatorial functional screening was successfully demonstrated. Next development steps should include the methodology application for a combinatorial full binder repertoire bsAb discovery campaign for broad coverage of the large screening space. Furthermore, functional screenings could be extended to additional bsAb formats such as VHH-IgG fusions or non-IgG architectures to broaden up the application range. Of note, Weber *et al.* successfully demonstrated that the natural IgG antibody architecture is not necessarily the best option to achieve a unique mode of action, which is still undiscovered.[162] In their study, they generated a brain shuttle mAb by fusing a brain shuttle module to the C-terminal constant region of the Fc portion, still retaining bivalent antigen binding against beta-amyloid. This unnatural design offered improved target engagement and efficacy and furthermore the molecule was able to become fully active through an inverted binding mode.[163] These observations show that it is highly important to screen not only for the best combination on the one hand but simultaneously screen for the optimal format, always keeping in mind that the natural antibody structure might not be the best option for the desired mode of action. The split intein reconstitution technology potentially allows to screen for the best combination of two binding moieties and compares different formats at the same time to find the best architecture for a unique mode of action.

Further implementation of small-scale expression prior to antibody reconstitution and HTS would power up the whole set up. A critical look into products, product related impurities, and the amounts of undesired products upon reconstitution is needed as well as further development of suitable HT analytical tools. The conducted cell assays illustrated the suitability of intein mediated reconstitution for functional interrogation of envisioned specific modes of action. A closer look into assay compatibilities would be desirable especially with regard to T-cell engagers. The antibody HTS platform could be extended with a dual split intein approach screening for functional screening of selectivity optimized bispecific ADCs,[84] or trispecific antibodies.[164,165] With a plethora of potential applications in future therapeutic antibody discovery, the method described in this thesis could enable

bispecific antibody high throughput functional screenings for enhanced probability of identifying optimal combinations and formats, which could ultimately lead to the generation of better biotherapeutics.

7. References

1. Moore GL, Chen H, Karki S, Greg A. Engineered Fc variant antibodies with enhanced ability to recruit complement and mediate effector functions. MAbs. 2, 181–189 (2010).
2. Medzhitov R, Janeway CA. Innate immunity: Impact on the adaptive immune response. Jr. Heal. San Fr. 9, 4–9 (1997).
3. Akira S, Hemmi H. Recognition of pathogen-associated molecular patterns by TLR family. Immunol. Lett. 85, 85–95 (2003).
4. Iwasaki A, Medzhitov R. Regulation of adaptive immunity by the innate immune system. Science. 327, 291–295 (2010).
5. Seda V, Mraz M. B-cell receptor signalling and its crosstalk with other pathways in normal and malignant cells. Eur. J. Haematol. 94, 193–205 (2015).
6. Redman J, Hill E, AlDeghaither D, Weiner L. Mechanisms of Action of Therapeutic Antibodies for Cancer. Mol Immunol 67, 28–45 (2015).
7. Strome SE, Sausville EA, Mann D. A Mechanistic Perspective of Monoclonal Antibodies in Cancer Therapy Beyond Target-Related Effects. Oncologist 12, 1084–1095 (2007).
8. Muralidharan S, Mandrekar P. Cellular stress response and innate immune signaling: Integrating pathways in host defense and inflammation. J. Leukoc. Biol. 94, 1167–1184 (2013).
9. Milstein C, Alerts E. Pillars Article: Continuous cultures of fused cells secreting antibody of predefined. Nature 256, 495–497 (1975).
10. Kuhn C, Weiner HL. Therapeutic anti-CD3 monoclonal antibodies: From bench to bedside. Immunotherapy 8, 889–906 (2016).
11. Masharani UB, Becker J. Teplizumab therapy for type 1 diabetes. Expert Opin Biol Ther 10, 459–465 (2010).
12. Baker MP, Reynolds HM, Lumicisi B, Bryson CJ. Immunogenicity of protein therapeutics: The key causes, consequences and challenges. Immune Recognit. Signal. 1, 314–322 (2010).
13. Kuriakose A, Chirmule N, Nair P. Immunogenicity of Biotherapeutics: Causes and Association with Posttranslational Modifications. J. Immunol. Res. 10, 1-18 (2016).
14. Kashmiri SVS, Iwahashi M, Tamura M, Padlan EA, Milenic DE, Schlom J. Development of a minimally immunogenic variant of humanized anti-carcinoma monoclonal antibody CC49. Crit. Rev. Oncol. Hematol. 38, 3–16 (2001).
15. Newsome BW, Ernstoff MS. The clinical pharmacology of therapeutic monoclonal antibodies in the treatment of malignancy: Have the magic bullets arrived? Br. J. Clin. Pharmacol. 66, 6–19 (2008).
16. Smith MR. Rituximab (monoclonal anti-CD20 antibody): Mechanisms of action and resistance. Oncogene 22, 7359–7368 (2003).
17. Burger RA, Mark MD, Brady MF, Bookman MA, Fleming GF, Monk BJ, et al. Incorporation of bevacizumab in the primary treatment of ovarian cancer. Obstet. Gynecol. Surv. 67, 289–290 (2012).
18. Chang JH, Garg NK, Lunde E, Han KY, Jain S, Azar DT. Corneal Neovascularization: An Anti-VEGF Therapy Review. Surv. Ophthalmol. 57, 415–429 (2012).
19. Reichert JM, Rosensweig CJ, Faden LB, Dewitz MC. Monoclonal antibody successes in the clinic. Nat. Biotechnol. 23, 1073–1078 (2005).
20. Psimadas D, Georgoulias P, Valotassiou V, Loudos G. Antibody structure instability and formulation. J. Pharm. Sci. 101, 2271–2280 (2012).

21. Schroeder HW, Cavacini L. Structure and function of immunoglobulins. J. Allergy Clin. Immunol. 125, 41–52 (2010).

22. Davies DR, Chacko S. Antibody Structure. Acc. Chem. Res. 26, 421–427 (1993).

23. Brezski RJ, Jordan RE. Cleavage of IgGs by proteases associated with invasive diseases: An evasion tactic against host immunity? MAbs 2, 212–220 (2010).

24. Brady LJ. Antibody-mediated immunomodulation: A strategy to improve host responses against microbial antigens. Infect. Immun. 73, 671–678 (2005).

25. Desjarlais JR, Lazar GA. Modulation of antibody effector function. Exp. Cell Res. 317, 1278–1285 (2011).

26. Saxena A, Wu D. Advances in therapeutic Fc engineering - modulation of IgG-associated effector functions and serum half-life. Front. Immunol. 7, 580 (2016).

27. Nimmerjahn F, Ravetch JV. Fcγ receptors: Old friends and new family members. Immunity 24, 19–28 (2006).

28. Vidarsson G, Dekkers G, Rispens T. IgG subclasses and allotypes: From structure to effector functions. Front. Immunol. 5, 1–17 (2014).

29. Leighton PA, Morales J, Harriman WD, Ching KH. V(D)J rearrangement is dispensable for producing CDR-H3 sequence diversity in a gene converting species. Front. Immunol. 9, 11–13 (2018).

30. Doroftei D. Generation of antibody diversity. Intech. doi:10.5772/intechopen.69483 (2017).

31. Briney BS, Crowe JE. Secondary mechanisms of diversification in the human antibody repertoire. Front. Immunol. 4, 1–7 (2013).

32. Sedykh SE, Prinz VV, Buneva, VN, Nevinsky GA. Bispecific antibodies: Design, therapy, perspectives. Drug Des. Devel. Ther. 12, 195–208 (2018).

33. Spiess C, Zhai Q, Carter PJ. Alternative molecular formats and therapeutic applications for bispecific antibodies. Mol. Immunol. 67, 95–106 (2015).

34. Chelius D, Ruf P, Gruber P, Plöscher M, Liedtke R, Gansberger E, Hess J, et al. Structural and functional characterization of the trifunctional antibody catumaxomab Structural and functional characterization of the trifunctional antibody catumaxomab. Landes Bioscience. 0862, 309–319 (2016).

35. Labrijn AF, Janmaat ML, Reichert JM, Parren PWHI. Bispecific antibodies: a mechanistic review of the pipeline. Nat. Rev. Drug Discov. 18, 585-608 (2019).

36. Baeuerle PA, Reinhardt C. Bispecific T-cell engaging antibodies for cancer therapy. Cancer Res. 69, 4941–4944 (2009).

37. Krishnamurthy A, Jimeno A. Bispecific antibodies for cancer therapy: A review. Pharmacol. Ther. 185, 122–134 (2018).

38. Gauthier L, Morel A, Anceriz N, Morel Y, Narni-Mancinelli E, Vivier E. Multifunctional Natural Killer Cell Engagers Targeting NKp46 Trigger Protective Tumor Immunity. Cell 177, 1701-1713 (2019).

39. Vivier E, Nunès JA, Vély F. Natural killer cell signaling pathways. Science. 306, 1517–1519 (2004).

40. Pahl J, Cerwenka A. Tricking the balance: NK cells in anti-cancer immunity. Immunobiology 222, 11–20 (2017).

41. Husain B, Ellerman D. Expanding the Boundaries of Biotherapeutics with Bispecific Antibodies. BioDrugs 32, 441–464 (2018).

42. Kong YCM, Flynn JC. Opportunistic autoimmune disorders potentiated by immune-checkpoint inhibitors anti-CTLA-4 and anti-PD-1. Front. Immunol. 5, 1–8 (2014).

43. Kontermann RE, Brinkmann U. Bispecific antibodies. Drug Discov. Today 20, 838–847 (2015).

44. Mazor Y, Hansen A, Yang C, Chowdhury PS, Wang J, Stephens G, et al. Insights into the molecular basis of a bispecific antibody's target selectivity. MAbs 7, 461–469 (2015).

45. Wang Q, Chen Y, Park J, Liu X, Hu Y, Wang T, McFarland K, Betenbaugh MJ. Design and Production of Bispecific Antibodies. Antibodies 8, 43 (2019).

46. Knight T, Callaghan MU. The role of emicizumab, a bispecific factor IXa- and factor X- directed antibody, for the prevention of bleeding episodes in patients with hemophilia A. Ther. Adv. Vaccines 5, 39–47 (2017).

47. Scott MJ, Lee JA, Wake MS, Batt KV, Wattam TA, Hiles ID, Batuwangala TD, et al. 'In-Format' screening of a novel bispecific antibody format reveals significant potency improvements relative to unformatted molecules. MAbs 9, 85–93 (2017).

48. Brinkmann U, Kontermann RE. The making of bispecific antibodies. MAbs 9, 182–212 (2017).

49. Krah S, Sellmann C, Rhiel L, Schröter C, Dickgiesser S, Beck J, Zielonka S, Toleikis L, et al. Engineering bispecific antibodies with defined chain pairing. N. Biotechnol. 39, 167–173 (2017).

50. Milstein C, Cuello AC. Hybrid hybridomas and their use in immunohistochemistry. Nature 305, 5–8 (1983).

51. Huehls AM, Coupet TA, Sentman CL. Bispecific T-cell engagers for cancer immunotherapy. Immunol. Cell Biol. 93, 290–296 (2015).

52. Ridgway JBB, Presta LG, Carter P. 'Knobs-into-holes' engineering of antibody C(H)3 domains for heavy chain heterodimerization. Protein Eng. 9, 617–621 (1996).

53. Crick FHC. The packing of α-helices: simple coiled-coils. Acta Crystallogr. 6, 689–697 (1953).

54. Merchant AM, Zhu Z, Yuan JQ, Goddard A, Adams CW, Presta LG, Carter P. An efficient route to human bispecific IgG. Nat. Biotechnol. 16, 677–681 (1998).

55. Liu H, Saxena A, Sidhu SS, Wu D. Fc engineering for developing therapeutic bispecific antibodies and novel scaffolds. Front. Immunol. 8, 1–15 (2017).

56. Moriyama H. Stable Heterodimers From Remodeling the Domain Interface of Homodimer using Phage Display Library. Jibi Inkoka Tembo 24, 465–480456 (1981).

57. Gunasekaran K, Pentony M, Shen M, Garrett L, Forte C, Woodward A, Ng SB, Born T. Enhancing antibody Fc heterodimer formation through electrostatic steering effects: Applications to bispecific molecules and monovalent IgG. J. Biol. Chem. 285, 19637–19646 (2010).

58. Liu Z, Leng E, Gunasekaran K, Pentony M, Shen M, Howard M, Stoops J, Manchulenko K, et al. A novel antibody engineering strategy for making monovalent bispecific heterodimeric IgG antibodies by electrostatic steering mechanism. J. Biol. Chem. 290, 7535–7562 (2015).

59. Labrijn AF, Meesters JI, Bart E, de Goeij CG, van den Bremer ETJ, Neijssen J, van Kampen MD, et al. Efficient generation of stable bispecific IgG1 by controlled Fab-arm exchange. Proc. Natl. Acad. Sci. 110, 5145–5150 (2013).

60. Strop P, Ho W, Boustany LM, Abdiche YN, Lindquist KC, Farias SE, Rickert M, et al. Generating bispecific human IgG1 and IgG2 antibodies from any antibody pair. J. Mol. Biol. 420, 204–219 (2012).

61. Davis JH, Aperlo C, Li Y, Kurosawa E, Lan Y, Lo KM, Huston JS. SEEDbodies: Fusion proteins based on strand-exchange engineered domain (SEED) CH3 heterodimers in an Fc analogue platform for asymmetric binders or immunofusions and bispecific antibodies. Protein Eng. Des. Sel. 23, 195–202 (2010).

62. Fan G, Wang Z, Hao M, Li J. Bispecific antibodies and their applications. J. Hematol. Oncol. 8, 130 (2015).

63. Garber K. Bispecific antibodies rise again. Nat. Rev. Drug Discov. 13, 799–801 (2014).

64. Klein C, Schaefer W, Regula JT, Dumontet C, Brinkmann U, Bacac M, Umana P. Engineering therapeutic bispecific antibodies using CrossMab technology. Methods 154, 21–31 (2019).

65. Spiess C, Merchant M, Huang A, Zhong Z, Yang NY, Peng J, Ellerman D, et al. Bispecific antibodies with natural architecture produced by co-culture of bacteria expressing two distinct half-antibodies. Nat. Biotechnol. 31, 753–758 (2013).

66. Han L, Chen J, Ding K, Zong H, Xie Y, Jiang H, Zhang B, Lu H, et al. Efficient generation of bispecific IgG antibodies by split intein mediated protein trans-splicing system. Sci. Rep. 7, 8360 (2017).

67. Han L, Zong H, Zhou Y, Pan Z, Chen J, Ding K, Xie Y, Jiang H, et al. Naturally split intein *Npu* DnaE mediated rapid generation of bispecific IgG antibodies. Methods 154, 32-37 (2018).

68. Kügler J, Wilke S, Meier D, Tomszak F, Frenzel A, Schirrmann T, Dübel S, Garritsen H, et al. Generation and analysis of the improved human HAL9/10 antibody phage display libraries. BMC Biotechnol. 15, 10 (2015).

69. Bradbury A, Velappen N, Verzillo V, vecka M, Chasteen L, Sblattero D, Marzari R, Lou J, et al. Antibodies in proteomics II: Screening, high-throughput characterization and downstream applications. Trends Biotechnol. 21, 312–317 (2003).

70. Fitzgerald V, Leonard P. Single cell screening approaches for antibody discovery. Methods 116, 34–42 (2017).

71. Schmitz U, Versmold A, Kaufmann P, Frank HG. Phage display: A molecular tool for the generation of antibodies - A review. Placenta 21, 106–112 (2000).

72. Jones ML, Seldon T, Smede M, Linville A, Chin DY, Barnard R, Mahler SM, Munster D, et al. A method for rapid, ligation-independent reformatting of recombinant monoclonal antibodies. J. Immunol. Methods 354, 85–90 (2010).

73. Jostock T, Vanhove M, Brepoels E, van Gool R, Daukandt M, Wehnert A, van Hegelsom R, et al. Rapid generation of functional human IgG antibodies derived from Fab-on-phage display libraries. J. Immunol. Methods 289, 65–80 (2004).

74. Xiao X, Douthwaite JA, Chen Y, Kemp B, Kidd S, Percival-Alwyn J, Smith A, et al. A high-throughput platform for population reformatting and mammalian expression of phage display libraries to enable functional screening as full-length IgG. MAbs 9, 996–1006 (2017).

75. Chames P, Van Regenmortel M, Weiss E, Baty D, Therapeutic antibodies: Successes, limitations and hopes for the future. Br. J. Pharmacol. 157, 220–233 (2009).

76. Wu G, Doberstein SK. HTS technologies in biopharmaceutical discovery. Drug Discov. Today 359, 718–720 (2006).

77. Szymański P, Markowicz M, Mikiciuk-Olasik E. Adaptation of high-throughput screening in drug discovery-toxicological screening tests. Int. J. Mol. Sci. 13, 427–452 (2012).

78. Dunne A, Jowett M, Rees S. High Throughput Screening. Methods 565, 239–257 (2009).

79. Mayr LM, Bojanic D. Novel trends in high-throughput screening. Curr. Opin. Pharmacol. 9, 580–588 (2009).

80. Hertzberg RP, Pope AJ. High-throughput screening: New technology for the 21st century. Curr. Opin. Chem. Biol. 4, 445–51 (2000).

81. Sundberg S. A. High-throughput and ultra-high-throughput screening: solution- and cell-based approaches. Curr. Opin. Chem. Biol. 11, 47–53 (2000).

82. Bleicher KH, Böhm HJ, Müller K, Alanine AI. Hit and lead generation: beyond high-throughput screening. Nat. Rev. Drug Discov. 2, 369–78 (2003).

83. Muda M, Gross AW, Dawson JP, He C, Kurosawa E, Schweickhardt R, Dugas M, Soloviev M, et al. Therapeutic assessment of SEED: A new engineered antibody platform designed to generate mono- and

bispecific antibodies. Protein Eng. Des. Sel. 24, 447–454 (2011).

84. Sellmann C, Doerner A, Knuehl C, Rasche N, Sood V, Krah S, Rhiel L, et al. Balancing Selectivity and Efficacy of Bispecific Epidermal Growth Factor Receptor (EGFR) × c-MET Antibodies and Antibody-Drug Conjugates. J. Biol. Chem. 291, 25106–25119 (2016).

85. Chen CG, Fabri LJ, Wilson M.J, Panousis C. One-step zero-background IgG reformatting of phage-displayed antibody fragments enabling rapid and high-throughput lead identification. Nucleic Acids Res. 42, (2014).

86. Mazor Y, Sachsenmeier KF, Yang C, Hansen A, Filderman J, Mulgrew K, Wu H, Dall´Acqua WF. Enhanced tumor-targeting selectivity by modulating bispecific antibody binding affinity and format valence. Sci. Rep. 7, 1–11 (2017).

87. Steinwand M, Droste P, Frenzel A, Hust M, Dübel S, Schirrmann T. The influence of antibody fragment format on phage display based affinity maturation of IgG. MAbs 6, 204–218 (2013).

88. Robinson MP, Ke N, Lobstein J, Peterson C, Szkodny A, Mansell TJ, Tuckey C, et al. Efficient expression of full-length antibodies in the cytoplasm of engineered bacteria. Nat. Commun. 6, (2015).

89. Miller BR, Demarest S, Lugovskoy A, Huang F, Wu X, Snyder WB, Croner LJ, et al. Stability engineering of scFvs for the development of bispecific and multivalent antibodies. Protein Eng. Des. Sel. 23, 549–557 (2010).

90. Perez HL, Cardarelli PM, Deshpande S, Gangwar S, Schroeder GM, Vite GD, Borzilleri RM. Antibody-drug conjugates: Current status and future directions. Drug Discov. Today 19, 869–881 (2014).

91. Debelouchina GT, Muir TW. A molecular engineering toolbox for the structural biologist. Q. Rev. Biophys. 50, (2017).

92. Yao H, Jiang F, Lu A, Zhang G. Methods to design and synthesize antibody-drug conjugates (ADCs). Int. J. Mol. Sci. 17, (2016).

93. Strop P, Liu SH, Dorywalska M, Delaria K, Dushin RG, Tran TT, Ho WH, Farias S, et al. Location matters: Site of conjugation modulates stability and pharmacokinetics of antibody drug conjugates. Chem. Biol. 20, 161–167 (2013).

94. Griffin M, Casadio R, Bergamini CM. Transglutaminases: Nature's biological glues. Biochem. J. 368, 377–396 (2002).

95. Yokoyama MK. Properties and applications of microbial transglutaminase. Appl. Microbiol. Biotechnol. 64, 447–454 (2004).

96. Ando H, Adachi M, Umeda K, Matsuura A, Nonaka M, Uchio R, Tanaka H, Motoki M. Purification and characteristics of a novel transglutaminase derived from microorganisms. Agric. Biol. Chem. 53, 2613–2617 (1989).

97. Luisa A, Gaspar C, Góes-favoni SP. De. Action of microbial transglutaminase (MTGase) in the modification of food proteins : A review. FOOD Chem. 171, 315–322 (2015).

98. Kieliszek M, Misiewicz A. Microbial transglutaminase and its application in the food industry. A review. Folia Microbiol. 59, 241–250 (2014).

99. Nonaka M, Matsuura Y, Motoki M. Incorporation of Lysine- and Lysine Dipeptides into αs1-Casein by Ca2+-independent Microbial Transglutaminase. Biosci. Biotechnol. Biochem. 60, 131–133 (1996).

100. Strop P. Versatility of microbial transglutaminase. Bioconjug. Chem. 25, 855–862 (2014).

101. Falck G. Enzyme-Based Labeling Strategies for Antibody–Drug Conjugates and Antibody Mimetics. Antibodies 7, 4 (2018).

102. Dennler P, Chiotellis A, Fischer E, Bregeon D, Belmant C, Gauthier L, Lhospice F, et al. Transglutaminase-based chemo-enzymatic conjugation approach yields homogeneous antibody-drug conjugates. Bioconjug. Chem. 25, 569–578 (2014).

103. Kline T, Steiner AR, Penta K, Sato AK, Hallam TJ, Yin G. Methods to Make Homogenous Antibody Drug Conjugates. Pharm. Res. 32, 3480–3493 (2015).

104. Ohtsuka T, Sawa A, Kawabata R, Nio N, Motoki M. Substrate specificities of microbial transglutaminase for primary amines. J. Agric. Food Chem. 48, 6230–6233 (2000).

105. Sutherland AR, Alam MK, Geyer CR. Post-translational Assembly of Protein Parts into Complex Devices by Using SpyTag/SpyCatcher Protein Ligase. ChemBioChem 20, 319–328 (2019).

106. Reddington SC, Howarth M. Secrets of a covalent interaction for biomaterials and biotechnology: SpyTag and SpyCatcher. Curr. Opin. Chem. Biol. 29, 94–99 (2015).

107. Alam K, Gonzales C, Hill W, El-Sayed A, Fonge H, Barreto K, Geyer CR. Synthetic Modular Antibody Construction by Using the SpyTag/SpyCatcher Protein-Ligase System. ChemBioChem 18, 2217–2221 (2017).

108. Yumura K, Akiba H, Nagatoishi S, Kusano-Arai O, Iwanari H, Hamakubo T, Tsumoto K. Use of SpyTag/SpyCatcher to construct bispecific antibodies that target two epitopes of a single antigen. J. Biochem. 162, 203–210 (2017).

109. Li L, Fierer JO, Rapoport TA, Howarth M. Structural analysis and optimization of the covalent association between SpyCatcher and a peptide tag. J. Mol. Biol. 426, 309–317 (2014).

110. Alam K, El-Sayed A, Barreto K, Bernhard W, Fonge H, Geyer CR. Site-Specific Fluorescent Labeling of Antibodies and Diabodies Using SpyTag/SpyCatcher System for In Vivo Optical Imaging. Mol. Imaging Biol. 21, 54–66 (2019).

111. Siegmund V, Piater B, Zakeri B, Eichhorn T, Fischer F, Deutsch C, Becker S, Toleikis L, et al. Spontaneous Isopeptide Bond Formation as a Powerful Tool for Engineering Site-Specific Antibody-Drug Conjugates. Sci. Rep. **6**, 1–9 (2016).

112. Popp MW, Antos JM, Grotenbreg GM, Spooner E, Ploegh HL. Sortagging: A versatile method for protein labeling. Nat. Chem. Biol. 3, 707–708 (2007).

113. Ritzefeld M. Sortagging: A robust and efficient chemoenzymatic ligation strategy. Chem. - A Eur. J. 20, 8516–8529 (2014).

114. Antos JM, Truttmann MC, Ploegh HL. Recent advances in sortase-catalyzed ligation methodology. Curr. Opin. Struct. Biol. 38, 111–118 (2016).

115. Hirakawa H, Ishikawa S, Nagamune T. Ca^{2+}-independent sortase-A exhibits high selective protein ligation activity in the cytoplasm of Escherichia coli. Biotechnol. J. 10, 1487–1492 (2015).

116. Huang X, Aulabaugh A, Ding W, Kapoor B, Alksne L, Tabei K, Ellestad G. Kinetic Mechanism of *Staphylococcus aureus* Sortase SrtA. Biochemistry 42, 11307–11315 (2003).

117. Schmohl L, Schwarzer D. Sortase-mediated ligations for the site-specific modification of proteins. Curr. Opin. Chem. Biol. 22, 122–128 (2014).

118. Zhou Q. Site-specific antibody conjugation for ADC and beyond. Biomedicines 5, (2017).

119. Kane PM, Yamashiro CT, Stevens TH. Biochemical characterization of the yeast vacuolar H^+-ATPase. J. Biol. Chem. 264, 19236–19244 (1989).

120. Hirata R. Ohsumi Y, Nakano A, Kawasaki H, Suzuki K, Anraku Y. Molecular structure of a gene, VMA1, encoding the catalytic subunit of H^+-translocating adenosine triphosphatase from vacuolar membranes of Saccharomyces cerevisiae. J. Biol. Chem. 265, 6726–6733 (1990).

121. Gogarten JP, Senejani AG, Zhaxybayeva O, Olendzenski L, Hilario E. Inteins: Structure, Function, and Evolution. Annu. Rev. Microbiol. 56, 263–287 (2002).

122. Aranko AS, Volkmanna G. Protein trans-splicing as a protein ligation tool to study protein structure and function. Biomol. Concepts 2, 183–198 (2011).

123. Appleby-Tagoe JH, Thiel IV, Wang Y, Wang Y, Mootz HD, Liu XQ. Highly efficient and more general cis- and trans-splicing inteins through sequential directed evolution. J. Biol. Chem. 286, 34440–34447 (2011).

124. Mills KV, Johnson MA, Perler FB. Protein splicing: How Inteins escape from precursor proteins. J. Biol. Chem. 289, 14498–14505 (2014).

125. Miraula M, Enculescu C, Schenk G, Mitić N. Inteins—A Focus on the Biotechnological Applications of Splicing-Promoting Proteins. Am. J. Mol. Biol. 5, 42–56 (2015).

126. Perler FB. Protein splicing mechanisms and applications. IUBMB Life 57, 469–476 (2005).

127. Tori K, Dassa B, Johnson MA, Southworth MW, Brace LE, Ishino Y, Pietrokovski S, Perler FB. Splicing of the mycobacteriophage bethlehem DnaB intein: Identification of a new mechanistic class of inteins that contain an obligate block f nucleophile. J. Biol. Chem. 285, 2515–2526 (2010).

128. Friedel K, Popp MA, Matern JCJ, Gazdag EM, Thiel IV, Volkmann G, Blankenfeldt W, Mootz HD. Chemical Science A functional interplay between intein and extein sequences in protein splicing compensates for the essential block B histidine. Chem. Sci. 10, 239–251 (2019).

129. Ramirez M, Valdes N, Guan D. Engineering split intein DnaE from Nostoc punctiforme for rapid protein purification. Prot. Eng. 26, 215–223 (2013).

130. Wu Q, Gao Z, Wei Y, Ma G, Zheng Y, Dong Y, Liu Y. Conserved residues that modulate protein *trans* -splicing of *Npu* DnaE split intein. Biochem. J. 461, 247–255 (2014).

131. Topilina NI, Mills KV. Recent advances in in vivo applications of intein-mediated protein splicing. Mob. DNA 5, 5 (2014).

132. Xu Y, Zhang L, Ma B, Hu L, Lu H, Dou T, Chen J, Zhu J. Intermolecular disulfide bonds between unpaired cysteines retard the C-terminal trans-cleavage of *Npu* DnaE. Enzyme Microb. Technol. 118, 6–12 (2018).

133. Badalà F, Nouri-mahdavi K, Raoof DA. Inteins: Nature´s Gift to Protein Chemists. Computer. 144, 724–732 (2008).

134. Minteer CJ, Siegart NM, Colelli KM, Liu X, Linhardt R, Wang C, Gomez A, et al. Intein-Promoted Cyclization of Aspartic Acid Flanking the Intein Leads to Atypical N-Terminal Cleavage. Biochemistry 56, 1042–1050 (2017).

135. Shah NH, Eryilmaz E, Cowburn D, Muir TW. Extein residues play an intimate role in the rate-limiting step of protein trans -splicing. J. Am. Chem. Soc. 135, 5839–5847 (2013).

136. Wu H, Hu Z, Liu XQ. Protein frans-splicing by a split intein encoded in a split DnaE gene of Synechocystis sp. Proc. Natl. Acad. Sci. 95, 9226–9231 (1998).

137. Iwai H, Züger S, Jin J, Tam PH. Highly efficient protein trans-splicing by a naturally split DnaE intein from Nostoc punctiforme. FEBS Lett. 580, 1853–1858 (2006).

138. Carvajal-Vallejos P, Palliss R, Mootz HD, Schmidt SR. Unprecedented rates and efficiencies revealed for new natural split inteins from metagenomic sources. J. Biol. Chem. 287, 28686–28696 (2012).

139. Zettler J, Schütz V, Mootz HD. The naturally split *Npu* DnaE intein exhibits an extraordinarily high rate in the protein trans-splicing reaction. FEBS Lett. 583, 909–914 (2009).

140. Wood DW, Camarero JA. Intein applications: From protein purification and labeling to metabolic control methods. J. Biol. Chem. 289, 14512–14519 (2014).

141. Vila-Perello M, Liu Z, Shah NH, Willis JA, Idoyaga J, Muir TW. Streamlined Expressed Protein Ligation Using Split Inteins. J. Am. Chem. Soc. 135, 286-292 (2013).

142. Möhlmann S, Bringmann P, Greven S, Harrenga A. Site-specific modification of ED-B-targeting antibody using intein-fusion technology. BMC Biotechnol. 11, 76 (2011).

143. Wong S, Mosabbir AA, Truong K. An engineered split intein for photoactivated protein trans-splicing. PLoS One 10, 1–16 (2015).

144. Böcker JK, Dörner W, Mootz HD. Light-control of the ultra-fast Gp41-1 split intein with preserved stability of a genetically encoded photo-caged amino acid in bacterial cells. Chem. Commun. 55, 1287–1290 (2019).

145. Di Ventura B, Mootz HD. Switchable inteins for conditional protein splicing. Biol. Chem. 0, 467–475 (2018).

146. Bhagawati M, Terhorst TME, Füsser F, Hoffmann S, Pasch TA. Mesophilic cysteine-less split intein for protein trans - splicing applications under oxidizing conditions. PNAS. 116, 22164-22172 (2019).

147. Stevens, A. J. *et al.* Design of a Split Intein with Exceptional Protein Splicing Activity. *J. Am. Chem. Soc.* 138, 2162–2165 (2016).

148. Agarwal P., Bertozzi CR. Site-specific antibody-drug conjugates: The nexus of bioorthogonal chemistry, protein engineering, and drug development. Bioconjug. Chem. 26, 176–192 (2015).

149. Wechtersbach L, Cigić B. Reduction of dehydroascorbic acid at low pH. J. Biochem. Biophys. Methods 70, 767–772 (2007).

150. Carvajal-vallejos P, Pallissé R, Mootz HD, Schmidt SR. Unprecedented Rates and Efficiencies Revealed for New Natural Split Inteins from Metagenomic Sources. Biol. Chem. 27, 266-96 (2013).

151. Sutherland AR, Alam MK, Geyer CR. Post-translational Assembly of Protein Parts into Complex Devices by Using SpyTag/SpyCatcher Protein Ligase. ChemBioChem 20, 319–328 (2019).

152. Bluemel C, Hausmann S, Fluhr P, Sriskandarajah M, Stallcup WB, Baeuerle PA, Kufer P. Epitope distance to the target cell membrane and antigen size determine the potency of T cell-mediated lysis by BiTE antibodies specific for a large melanoma surface antigen. Cancer Immunol. Immunother. 59, 1197–1209 (2010).

153. Cheriyan M, Pedamallu CS, Tori K, Perler F. Faster protein splicing with the nostoc punctiforme DnaE intein using non-native extein residues. J. Biol. Chem. 288, 6202–6211 (2013).

154. Stevens AJ, Sekar G, Shah NH, Mostafavi AZ, Cowburn D, Muir TW. A promiscuous split intein with expanded protein engineering applications. Proc. Natl. Acad. Sci. 114, 8538–8543 (2017).

155. Xu Y, Lee J, Tran C, Heibeck TH, Wang WD, Yang J, Stafford RL, Steiner AR, et al. Production of bispecific antibodies in 'knobs-into-holes' using a cell-free expression system. MAbs 7, 231–242 (2015).

156. Krah S, Schröter C, Eller C, Rhiel L, Rasche N, Beck J, Sellmann C, Günther Ralf, et al. Generation of human bispecific common light chain antibodies by combining animal immunization and yeast display. Protein Eng. Des. Sel. 30, 291–301 (2017).

157. Sampei Z, Igawa T, Soeda T, Okuyama-Nishida Y, Moriyama C, Wakabayashi T, et al. Identification and Multidimensional Optimization of an Asymmetric Bispecific IgG Antibody Mimicking the Function of Factor VIII Cofactor Activity. PLoS One 8, (2013).

158. Kitazawa T, Igawa T, Sampei Z, Muto A, Kojima T, Soeda T, Yoshihashi K, et al. A bispecific antibody to factors IXa and X restores factor VIII hemostatic activity in a hemophilia A model. Nat. Med. 18, 1570–1574 (2012).

159. Aranko AS, Oeemig JS, Iwa H. Structural basis for protein trans -splicing by a bacterial intein-like domain – protein ligation without nucleophilic side chains. FEBS J. 280, 3256–3269 (2013).

160. Aranko AS, Oeemig JS, Zhou D, Kajander T, Wlodawer A, Iawai H. Structure-based engineering and comparison of novel split inteins for protein ligation. Mol. Biosyst. 10, 1023 (2014).

161. Pirzer T, Becher KS, Rieker M, Meckel T, Mootz HD, Kolmar H. Generation of Potent Anti-HER1/2 Immunotoxins by Protein Ligation Using Split Inteins. ACS Chem. Biol. 13, 2058–2066 (2018).

162. Weber F, Bohrmann B, Niewoehner J, Fischer JAA, Rueger P, Tiefenthaler, Moelleken J, Bujotzek A, et al. Brain Shuttle Antibody for Alzheimer's Disease with Attenuated Peripheral Effector Function due to an Inverted Binding Mode. Cell Rep. 22, 149–162 (2018).

163. Niewoehner J, Borhmann B, Collin L, Urich E, Sade H, Maier P, Rueger P, Stracke JO, Lau W, et al. Increased Brain Penetration and Potency of a Therapeutic Antibody Using a Monovalent Molecular Shuttle. Neuron 81, 49–60 (2014).

164. Runcie K, Budman DR, John V, Seetharamu N. Bi-specific and tri-specific antibodies- the next big thing in solid tumor therapeutics. Mol. Med. 24, 1–15 (2018).

165. Klein C, Schaefer W, Regula JT. The use of CrossMAb technology for the generation of bi- and multispecific antibodies. MAbs 8, 1010–1020 (2016).

8. Appendix

8.1. Protein sequences

Amino acid sequences of used antibody-intein fusions and parental reference antibodies based on commercially available antibodies or in house generated antibodies are shown below. DNA sequences of antibody-intein fragments for plasmid generation in pTT5 vector backbone were codon optimized for mammalian expression systems and obtained from GeneArt (Life Technologies).

IgG1 Fc Int^{C}

HHHHHHGGGGSGGGGSGGGGSGGGGSMIKIATRKYLGKQNVYDIGVERDHNFALKNGFIASNCFN
THTCPPCPAPELLGGPSVFLFPPKPKDTLMISRTPEVTCVVVDVSHEDPEVKFNWYVDGVEVHNAK
TKPREEQYNSTYRVVSVLTVLHQDWLNGKEYKCKVSNKALPAPIEKTISKAKGQPREPQVYTLPPSR
DELTKNQVSLTCLVKGFYPSDIAVEWESNGQPENNYKTTPPVLDSDGSFFLYSKLTVDKSRWQQGN
VFSCSVMHEALHNHYTQKSLSLSPG

IgG2 Fc Int^{C}

HHHHHHGGGGSGGGGSGGGG SGGGGSMIKIATRKYLGKQNVYDIGVERDHNFALKNGFIASNCF
NTHTCPPCPAPPVAGPSVFLFPPKPKDTLMISRTPEVTCVVVDVSHEDPEVQFNWYVDGVEVHNAK
TKPREEQFNSTFRVVSVLTVVHQDWLNGKEYKCKVSNKGLPAPIEKTISKTKGQPREPQVYTLPPSR
EEMTKNQVSLTCLVKGFYPSDIAVEWESNGQPENNYKTTPPMLDSDGSFFLYSKLTVDKSRWQQG
NVFSCSVMHEALHNHYTQKSLSLSPG

APX Fab Int^{N} HC

QVQLVESGGGVVQPGRSLRLSCAASGFSFSSTYVCWVRQAPGKGLEWIACIYTGDGTNYSASWAKG
RFTISKDSSKNTVYLQMNSLRAEDTAVYFCARPDITYGFAINFWGPGTLVTVSSASTKGPSVFPLAPS
SKSTSGGTAALGCLVKDYFPEPVTVSWNSGALTSGVHTFPAVLQSSGLYSLSSVVTVPSSSLGTQTYI
CNVNHKPSNTKVDKRVEPKSCDKAEYCLSYETEILTVEYGLLPIGKIVEKRIECTVYSVDNNGNIYTQ
PVAQWHDRGEQEVFEYCLEDGSLIRATKDHKFMTVDGQMLPIDEIFERELDLMRVDNLPNAAAEQ
KLISEEDLSHHHHHH

APX Fab Int^{N} LC

DIQMTQSPSSLSASVGDRVTIKCQASQSISSRLAWYQQKPGKPPKLLIYRASTLASGVPS RFSGSGSGT
DFTLTISSLQPEDVATYYCQCTGYGISWPIGGGTKVEIKRTVAAPSVFIFP PSDEQLKSGTASVVCLL
NNFYPREAKVQWKVDNALQSGNSQESVTEQDSKDSTYSLSSTLTLSKADYEKHKVYACEVTHQGLSS
PVTKSFNRGEC

CEACAM5 (AG) SEED

EVQLVESGGGLVKPGGSLRLSCAASGFTFDDYAMHWVRQAPGKGLEWVSGISWNSGSIGYADSVK
GRFTISRDNAKNSLYLQMNSLRAEDTALYYCAKETIPTYLAAVVPFDYWGQGTLVTVSSASTKGPSV
FPLAPSSKSTSGGTAALGCLVKDYFPEPVTVSWNSGALTSGVHTFPAVLQSSGLYSLSSVVTVPSSSLG
TQTYICNVNHKPSNTKVDKRVEPKSCDKTHTCPPCPAPELLGGPSVFLFPPKPKDTLMISRTPEVTCV
VVDVSHEDPEVKFNWYVDGVEVHNAKTKPREEQYNSTYRVVSVLTVLHQDWLNGKEYKCKVSNKA
LPAPIEKTISKAKGQPFRPEVHLLPPSREEMTKNQVSLTCLARGFYPKDIAVEWESNGQPENNYKTT
PSRQEPSQGTTTFAVTSKLTVDKSRWQQGNVFSCSVMHEALHNHYTQKTISLSPGK

CEACAM6 (GA) SEED

EMQLVQSGAEVKKPGASVKVSCKASGYTFTGFYIHWVRQAPGQGLEWMGRINLNSGVRNYVQKFQ
GRVTMTRDTSIGTAYMELSGLRSDDTAVYYCATPTYYDILTGPFDYWGQGTLVTVSSASTKGPSVF
PLAPSSKSTSGGTAALGCLVKDYFPEPVTVSWNSGALTS GVHTFPAVLQSSGLYSLSSVVTVPSSSLG
TQTYICNVNHKPSNTKVDKRVEPKSCDKTHTCPPCPAPELLGGPSVFLFPPKPKDTLMISRTPEVTCV
VVDVSHEDPEVKFNWYVDGVEVHNAKTKPREEQYNSTYRVVSVLTVLHQDWLNGKEYKCKVSNKA
LPAPIEKTISKAKGQPREPQVYTLPPPSEELALNELVTLTCLVKGFYPSDIAVEWLQGSQELPREKYL
TWAPVLDSDGSFFLYSILRVAAEDWKKGDTFSCSVMHEALHNHYTQKSLDRSPGK

cLC

EIVMTQSPATLSVSPGERATLSCRASQSVSSNLAWYQQKPGQAPRLLIYGASTRATGIPARFSGSGSG
TEFTLTISSLQSEDFAVYYCQQYNNWPWTFGQGTKVEIKRTVAAPSVFIFPPSDEQLKSGTASVVCLL
NNFYPREAKVQWKVDNALQSGNSQESVTEQDSKDSTYSLSSTLTLSKADYEKHKVYACEVTHQGLSS
PVTKSFNRGEC

huFc Int^{C} (GA) SEED

HHHHHHGGGGSGGGGSGGGGSGGGGSMIKIATRKYLGKQNVYDIGVERDHNFALKNGFIASNCFN
THTCPPCPAPELLGGPSVFLFPPKPKDTLMISRTPEVTCVVVDVSHEDPEVKFNWYVDGVEVHNAK
TKPREEQYNSTYRVVSVLTVLHQDWLNGKEYKCKVSNKALPAPIEKTISKAKGQPREPQVYTLPPPS
EELALNELVTLTCLVKGFYPSDIAVEWLQGSQELPREKYLTWAPVLDSDGSFFLYSILRVAAEDWKK
GDTFSCSVMHEALHNRFTQKSLDRSPG

CEACAM6 Fab IntN

EMQLVQSGAEVKKPGASVKVSCKASGYTFTGFYIHWVRQAPGQGLEWMGRINLNSGVRNYVQKFQ
GRVTMTRDTSIGTAYMELSGLRSDDTAVYYCATPTYYDILTGPFDYWGQGTLVTVSSASTKGPSVF
PLAPSSKSTSGGTAALGCLVKDYFPEPVTVSWNSGALTSGVHTFPAVLQSSGLYSLSSVVTVPSSSLGT
QTYICNVNHKPSNTKVDKRVEPKSCDKAEYCLSYETEILTVEYGLLPIGKIVEKRIECTVYSVDNNGNI
YTQPVAQWHDRGEQEVEYCLEDGSLIRATKDHKFMTVDGQMLPIDEIFERELDLMRVDNLPNAAA
EQKLISEEDLSHHHHHH

hOKT3 Fab (AG) SEED

QVQLVQSGGGVVQPGRSLRLSCKASGYTFTRYTMHWVRQAPGKGLEWIGYINPSRGYTNYNQKVK
DRFTISRDNSKNTAFLQMDSLRPEDTGVYFCARYYDDHYCLDYWGQGTPVTVSSASTKGPSVFPLA
PSSKSTSGGTAALGCLVKDYFPEPVTVSWNSGALTSGVHTFPAVLQSSGLYSLSSVVTVPSSSLGTQT
YICNVNHKPSNTKVDKRVEPKSCDKTHTCPPCPAPELLGGPSVFLFPPKPKDTLMISRTPEVTCVVVD
VSHEDPEVKFNWYVDGVEVHNAKTKPREEQYNSTYRVVSVLTVLHQDWLNGKEYKCKVSNKALPA
PIEKTISKAKGQPFRPEVHLLPPSREEMTKNQVSLTCLARGFYPKDIAVEWESNGQPENNYKTTPSR
QEPSQGTTTFAVTSKLTVDKSRWQQGNVFSCSVMHEALHNHYTQKTISLSPG

hOKT3 LC

DIQMTQSPSSLSASVGDRVTITCSASSSVSYMNWYQQTPGKAPKRWIYDTSKLASGVPSRFSGSGSGT
DYTFTISSLQPEDIATYYCQQWSSNPFTFGQGTKLQITRTVAAPSVFIFPPSDEQLKSGTASVVCLLN
NFYPREAKVQWKVDNALQSGNSQESVTEQDSKDSTYSLSSTLTLSKADYEKHKVYACEVTHQGLSSP
VTKSFNRGEC

Trastuzumab Fab Int^{N}

EVQLVESGGGLVQPGGSLRLSCAASGFNIKDTYIHWVRQAPGKGLEWVARIYPTNGYTRYADSVKG
RFTISADTSKNTAYLQMNSLRAEDTAVYYCSRWGGDGFYAMDYWGQGTLVTVSSASTKGPSVFPL
APSSKSTSGGTAALGCLVKDYFPEPVTVSWNSGALTSGVHTFPAVLQSSGLYSLSSVVTVPSSSLGTQ
TYICNVNHKPSNTKVDKRVEPKSCDKAEYCLSYETEILTVEYGLLPIGKIVEKRIECTVYSVDNNGNIY
TQPVAQWHDRGEQEVFEYCLEDGSLIRATKDHKFMTVDGQMLPIDEIFERELDLMRVDNLPNAAA
EQKLISEEDLSHHHHHH

Trastuzumab LC

DIQMTQSPSSLSASVGDRVTITCRASQDVNTAVAWYQQKPGKAPKLLIYSASFLYSGVPSRFSGSRSG
TDFTLTISSLQPEDFATYYCQQHYTTPPTFGQGTKVEIKRTVAAPSVFIFPPSDEQLKSGTASVVCLL
NNFYPREAKVQWKVDNALQSGNSQESVTEQDSKDSTYSLSSTLTLSKADYEKHKVYACEVTHQGLSS
PVTKSFNRGEC

c-MET B10v5 (AG) SEED

EVQLVQSGGGLVQPGGSLRLSCAASGFTFSSYAMSWVRQAPGKGLEWVSAISGSGGSTYYADSVKG
RFTISRDNSKNTLYLQMNSLRAEDTAVYYCAKDRRITHTYWGQGTLVTVSSASTKGPSVFPLAPSSK
STSGGTAALGCLVKDYFPEPVTVSWNSGALTSGVHTFPAVLQSSGLYSLSSVVTVPSSSLGTQTYICN
VNHKPSNTKVDKRVEPKSCDKTHTCPPCPAPELLGGPSVFLFPPKPKDTLMISRTPEVTCVVVDVSH
EDPEVKFNWYVDGVEVHNAKTKPREEQYNSTYRVVSVLTVLHQDWLNGKEYKCKVSNKALPAPIE
KTISKAKGQPFRPEVHLLPPSREEMTKNQVSLTCLARGFYPKDIAVEWESNGQPENNYKTTPSRQEP
SQGTTTFAVTSKLTVDKSRWQQGNVFSCSVMHEALHNHYTQKTISLSPGK

c-MET B10v5 LC

EPVLTQPPSVSVAPGETATIPCGGDSLGSKIVHWYQQRPGQAPLLVVYDDAARPSGIPERFSGSKSGT
TATLTISSVEAGDEADYFCQVYDYHSDVEVFGGGTKLTVLGQPKAAPSVTLFPPSSEELQANKATLV
CLISDFYPGAVTVAWKADSSPVKAGVETTTPSKQSNNKYAASSYLSLTPEQWKSHKSYSCQVTHEGS
TVEKTVAPTECS

c-MET F06 AG SEED

QVQLQQSGAEVKKPGSSAKVSCKASGGTFSSYAISWVRQAPGQGLEWMGGIIPIFGTANYAQKFQGR
VTITADESTSTAYMELSSLRSEDTAVYYCARDQRGYDYYYYYGMDVWGQGTTVTVSSASTKGPSV
FPLAPSSKSTSGGTAALGCLVKDYFPEPVTVSWNSGALTSGVHTFPAVLQSSGLYSLSSVVTVPSSSLG
TQTYICNVNHKPSNTKVDKRVEPKSCDKTHTCPPCPAPELLGGPSVFLFPPKPKDTLMISRTPEVTCV
VVDVSHEDPEVKFNWYVDGVEVHNAKTKPREEQYNSTYRVVSVLTVLHQDWLNGKEYKCKVSNKA
LPAPIEKTISKAKGQPFRPEVHLLPPSREEMTKNQVSLTCLARGFYPKDIAVEWESNGQPENNYKTT
PSRQEPSQGTTTFAVTSKLTVDKSRWQQGNVFSCSVMHEALHNHYTQKTISLSPGK

c-MET F06 LC

QLVLTQSPSVSVAPGKTARITCGGNNIRNVGVHWYQKKPGQAPILVVYDDDDRPSGVPERFSGSNSG
NTATLTISRVEAGDEADYYCQVWDSATDQRVFGGGTKLTVLGQPKAGPSVTLFPPSSEELQANKAT
LVCLISDFYPGAVTVAWKADSSPVKAGVETTTPSKQSNNKYAASSYLSLTPEQWKSHRSYSCQVTHE
GSTVEKTVAPTEC

hu225H Fab Int^{N}

EVQLVQSGAEVKKPGASVKVSCKASGFSLTNYGVHWMRQAPGQGLEWIGVIWRGGNTDYNTPFTS
RVTITSDKSTSTAYMELSSLRSEDTAVYYCARALTYYDYEFAYWGQGTLVTVSSASTKGPSVFPLAP
SSKSTSGGTAALGCLVKDYFPEPVTVSWNSGALTSGVHTFPAVLQSSGLYSLSSVVTVPSSSLGTQTYI
CNVNHKPSNTKVDKRVEPKSCDKAEYCLSYETEILTVEYGLLPIGKIVEKRIECTVYSVDNNGNIYTQ
PVAQWHDRGEQEVFEYCLEDGSLIRATKDHKFMTVDGQMLPIDEIFERELDLMRVDNLPNAAAEQ
KLISEEDLSHHHHHH

hu225H LC

DIQMTQSPSSLSASVGDRVTITCRASQSIGTNIHWYQQKPGKAPKLLIKYASESISGVPSRFSGSGYGT
DFTLTISSLQPEDVATYYCQQNNNWPTTFGQGTKVEIKRTVAAPSVFIFPPSDEQLKSGTASVVCLL
NNFYPREAKVQWKVDNALQSGNSQESVTEQDSKDSTYSLSSTLTLSKADYEKHKVYACEVTHQGLSS
PVTKSFNRGEC

hu225L Fab Int^{N}

EVQLVQSGAEVKKPGASVKVSCKASGFSLTNYGVHWMRQAPGQGLEWIGVIWSGGNTDYNTPFTS
RVTITSDKSTSTAYMELSSLRSEDTAVYYCARALDYYDYEFAYWGQGTLVTVSSASTKGPSVFPLAP

SSKSTSGGTAALGCLVKDYFPEPVTVSWNSGALTSGVHTFPAVLQSSGLYSLSSVVTVPSSSLGTQTYI
CNVNHKPSNTKVDKRVEPKSCDKAEYCLSYETEILTVEYGLLPIGKIVEKRIECTVYSVDNNGNIYTQ
PVAQWHDRGEQEVFEYCLEDGSLIRATKDHKFMTVDGQMLPIDEIFERELDLMRVDNLPNAAAEQ
KLISEEDLSHHHHHH

hu225L LC

DIQMTQSPSSLSASVGDRVTITCRASQSIGTNIHWYQQKPGKAPKLLIKYASESISGVPSRFSGSGYGT
DFTLTISSLQPEDVATYYCQQNNEWPNTFGQGTKVEIKRTVAAPSVFIFPPSDEQLKSGTASVVCLLN
NFYPREAKVQWKVDNALQSGNSQESVTEQDSKDSTYSLSSTLTLSKADYEKHKVYACEVTHQGLSSP
VTKSFNRGEC

Int^{C}

SGGGGSMIKIATRKYLGKQN VYDIGVERDH NFALKNGFIASNCFN

Int^{N}

AEYCLSYETEILTVEYGLLPIGKIVEKRIECTVYSVDNNGNIYTQPVAQWHDRGEQEVFEYCLEDGS
LIRATKDHKFMTVDGQMLPIDEIFERELDLMRVDNLPN

8.2. Supplemental Figures

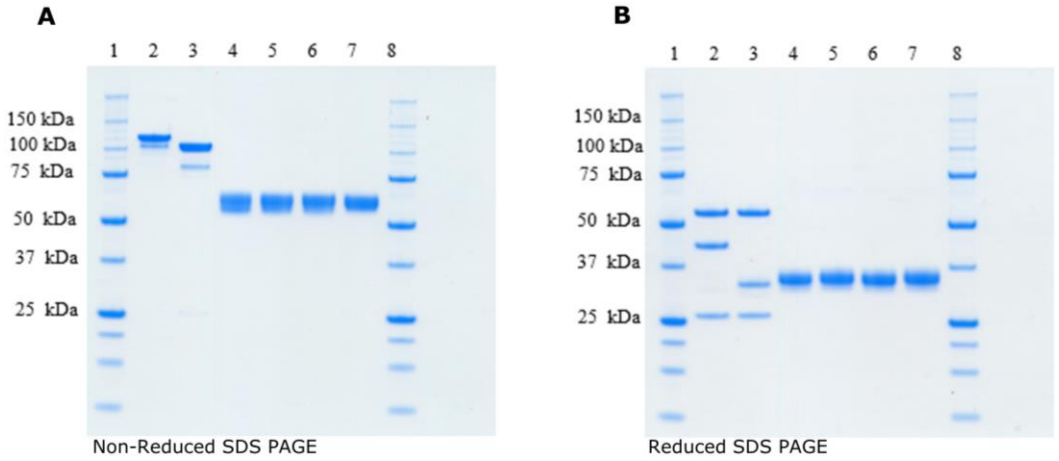

Figure S 1: SDS-PAGE analysis of precursor antibody fragments fused to the respective intein part after final purification step via SEC.

(A) Non-reduced SDS-PAGE analysis of precursor fragments. Lane 1: Marker; Lane 2: hOKT3 Fab (AG) aHer2 VHH (GA) SEED; Lane 3: hOKT3 Fab (AG) huFc Int^{C} (GA) SEED; Lane 4: huFc IgG1 Int^{C}; Lane 5: huFc IgG1.4 Int^{C}; Lane 6: huFc IgG1.6 Int^{C}; Lane 7: huFc IgG2 Int^{C}. **(B)** Reduced SDS-PAGE analysis of precursor fragments for HC and LC detection. Lane 1: Marker; Lane 2: hOKT3 Fab (AG) aHer2 VHH (GA) SEED; Lane 3: hOKT3 Fab (AG) huFc Int^{C} (GA) SEED; Lane 4: huFc IgG1 Int^{C}; Lane 5: huFc IgG1.4 Int^{C}; Lane 6: huFc IgG1.6 Int^{C}; Lane 7: huFc IgG2 Int^{C}.

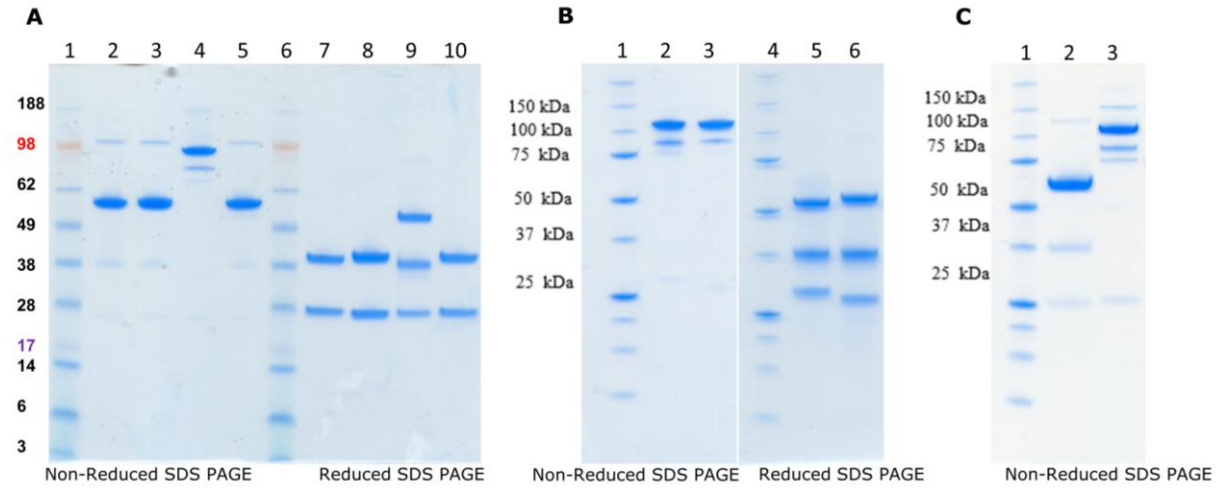

Figure S 2: SDS-PAGE analysis of precursor antibody fragments fused to the respective intein part after final purification step via SEC.

(A) Non-reduced SDS-PAGE analysis Lane 1: Marker; Lane 2: hu225H Fab Int^N; Lane 3: hu225L Fab Int^N; Lane 4: oaC5 SEED Int^C; Lane 5: C6 Fab Int^N; Lane 6: Marker; Reduced SDS-PAGE analysis: Lane 7: hu225H Fab Int^N; Lane 8: hu225L Fab Int^N; Lane 9: oaC5 SEED Int^C; Lane 10: C6 Fab Int^N **(B)** Non-reduced SDS-PAGE analysis: Lane 1: Marker; Lane 2: oa B10v5 SEED Int^C ; Lane 3: oa F06 SEED Int^C ; Reduced SDS-PAGE analysis: Lane 4: Marker; Lane 5: oa B10v5 SEED Int^C ; Lane 6: oa F06 SEED Int^C . **(C)** Non-reduced SDS-PAGE analysis: Lane 1: Marker; Lane 2: Trastuzumab Fab Int^N ; Lane 3: oa Trastuzumab SEED Int^C;

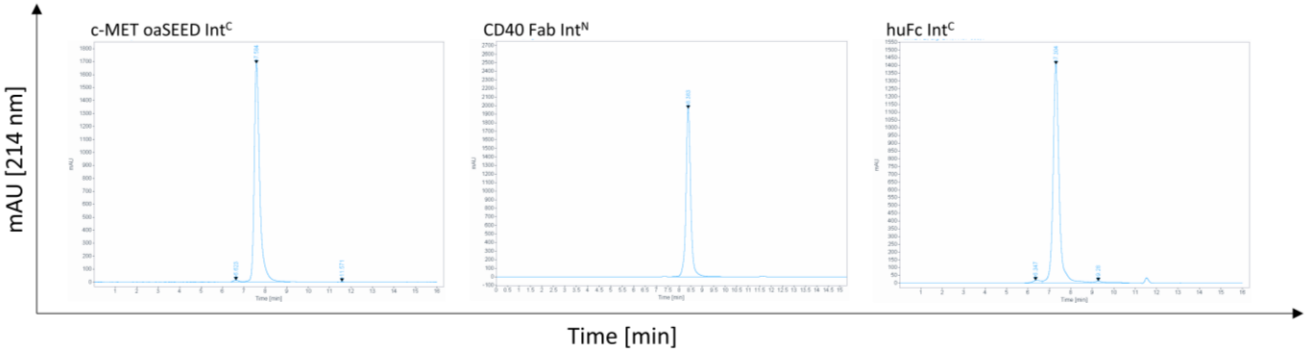

Figure S 3: Analytical size exclusion chromatography (SE-HPLC) of precursor antibody fragments in different formats fused to split inteins.

Purified antibody fragments were concentrated to 1 mg mL^{-1} and analyzed by HPLC using 10 µg of protein and a TSKgel Super SW3000 analytical size exclusion column. High monomeric content of B10v5 oaSEED Int^C, CD40 Fab Int^N and huFc Int^C was achieved with 98.9%, 96.4% and 96.0% respectively.

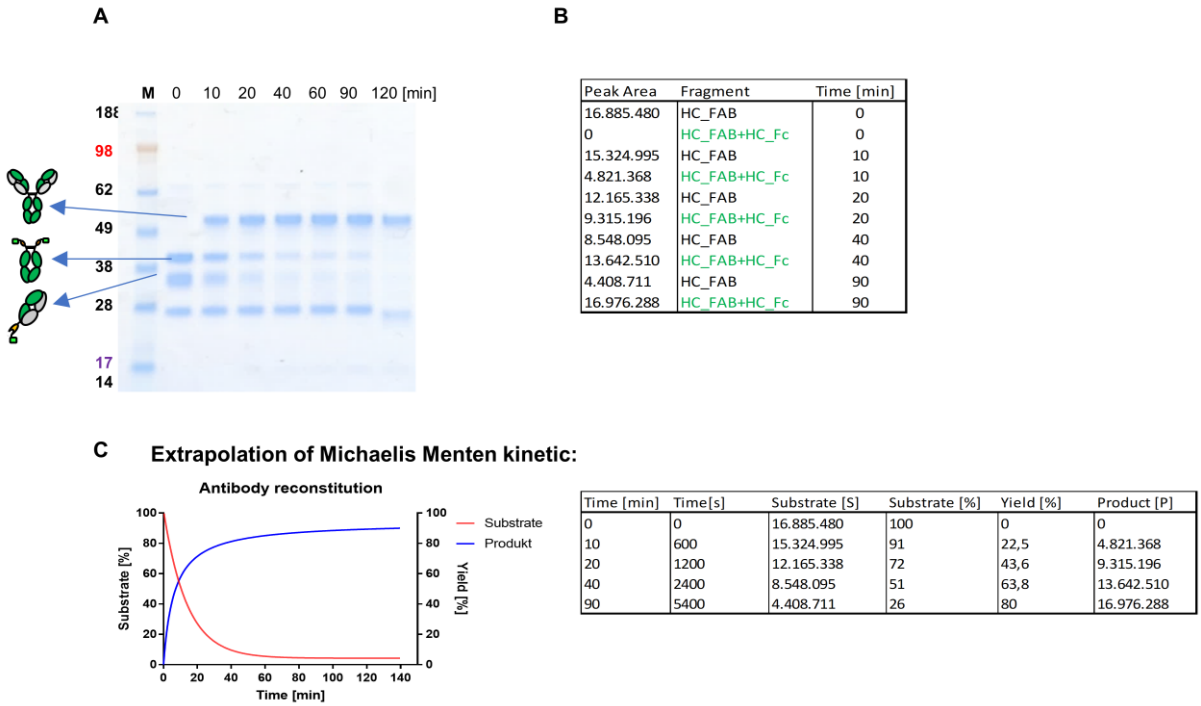

Peak Area	Fragment	Time [min]
16.885.480	HC_FAB	0
0	HC_FAB+HC_Fc	0
15.324.995	HC_FAB	10
4.821.368	HC_FAB+HC_Fc	10
12.165.338	HC_FAB	20
9.315.196	HC_FAB+HC_Fc	20
8.548.095	HC_FAB	40
13.642.510	HC_FAB+HC_Fc	40
4.408.711	HC_FAB	90
16.976.288	HC_FAB+HC_Fc	90

Time [min]	Time[s]	Substrate [S]	Substrate [%]	Yield [%]	Product [P]
0	0	16.885.480	100	0	0
10	600	15.324.995	91	22,5	4.821.368
20	1200	12.165.338	72	43,6	9.315.196
40	2400	8.548.095	51	63,8	13.642.510
90	5400	4.408.711	26	80	16.976.288

Figure S 4: Antibody reconstitution over time and efficiency determination.

(**A**) Precursor antibody fragments anti-CD40 Fab Int^N and huFc Int^C were mixed in a molar ratio of 2:1 and PTS was activated by the addition of 0.5 mM TCEP followed by incubation for 2 h at 37°C. (**B**) Peak areas of precursor antibody fragments (substrate) and reconstituted antibody product were determined over time by pixel analysis using ImageJ. Highest peak point of precursor antibody fragments at 0 h were considered as 100%. Conversion of antibody fragments into reconstituted anti-CD40 product mediated by PTS was observed over time and depletion of antibody fragments was almost completed after 120 min. **(C)** Peak areas were used to generate an extrapolated Michaelis Menten kinetic by GraphPad Prism v7 analysis. A reconstitution efficiency of around 90% was achieved.

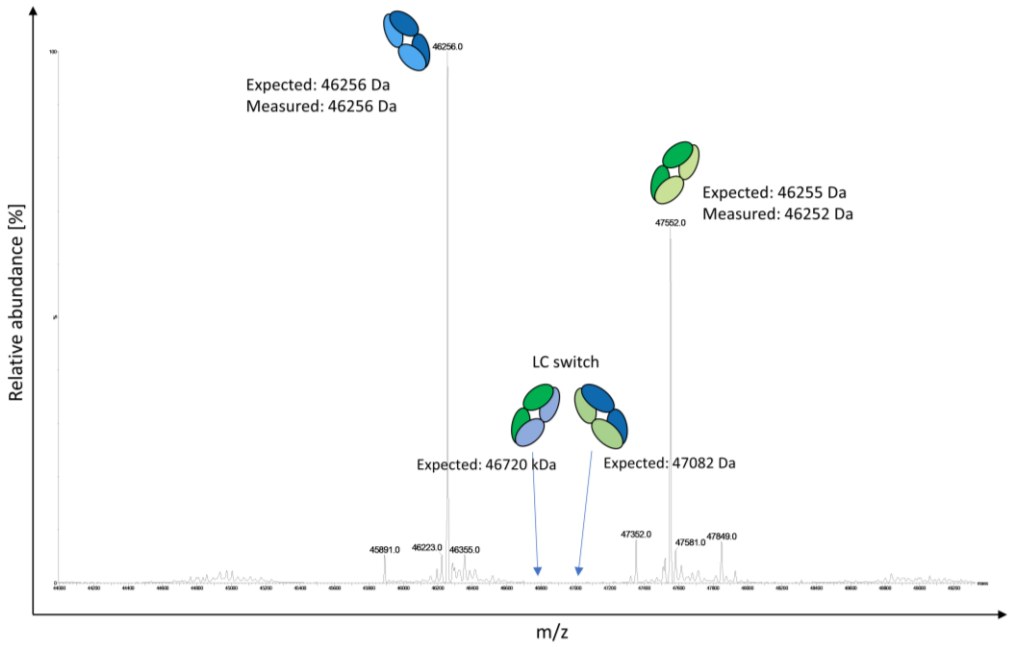

Figure S 5: Papain digestion of reconstituted c-METxEGFR bsAb B10v5xhu225H for Fab release and LC shuffling investigation by MS analysis.

Reconstituted bsAb B10v5xhu225H was treated with Papain and incubated for 3 h at 37°C under shaking conditions for Fab release. Fabs were further analyzed by ESI-MS. The expected mass of B10v5 (c-MET) Fab as well as hu225H (EGFR) Fab correlates with the measured mass. The expected masses for both Fabs with an LC switch was depicted in the spectrum but was not detected.

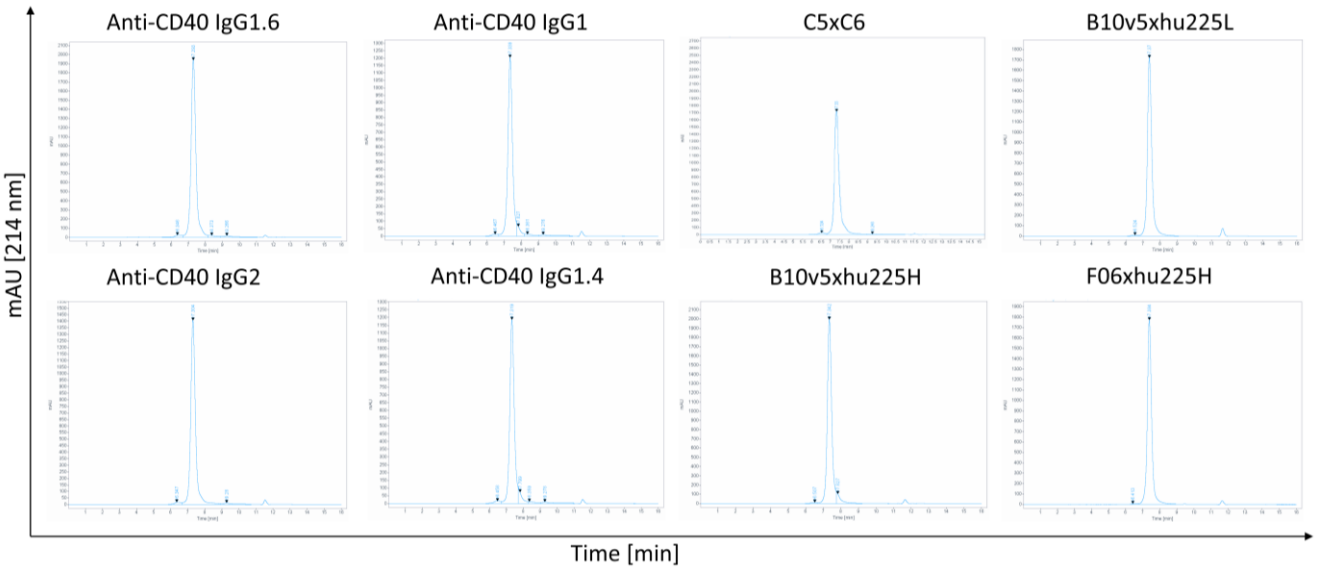

Figure S 6: Analytical size exclusion chromatography (SE-HPLC) of different reconstituted bsAbs and mAbs.

Reconstituted antibody samples were diluted to 1 mg mL^{-1} in PBS and 10 µg of protein sample was injected onto a TSKgel Super SW3000 analytical size exclusion column. Monomeric content of reconstituted bsAbs and mAbs are listed in **Table 3**.

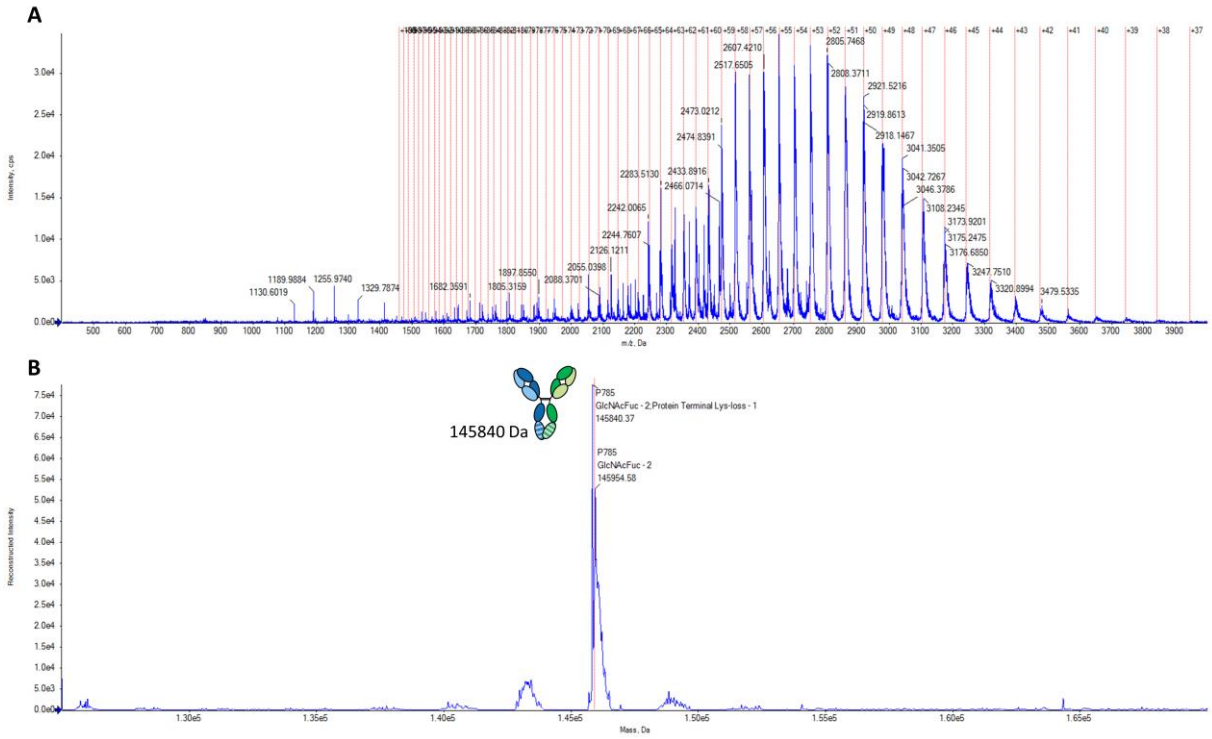

Figure S 7: Intact mass determination of reconstituted bsAb B10v5xhu225L by TOF-MS analysis under non-reduced conditions.

(A) Illustration of a full m/z spectrum for reconstituted bsAb B10v5xhu225L. **(B)** Intact reconstruction spectrum of reconstituted bsAb B10v5xhu225L.

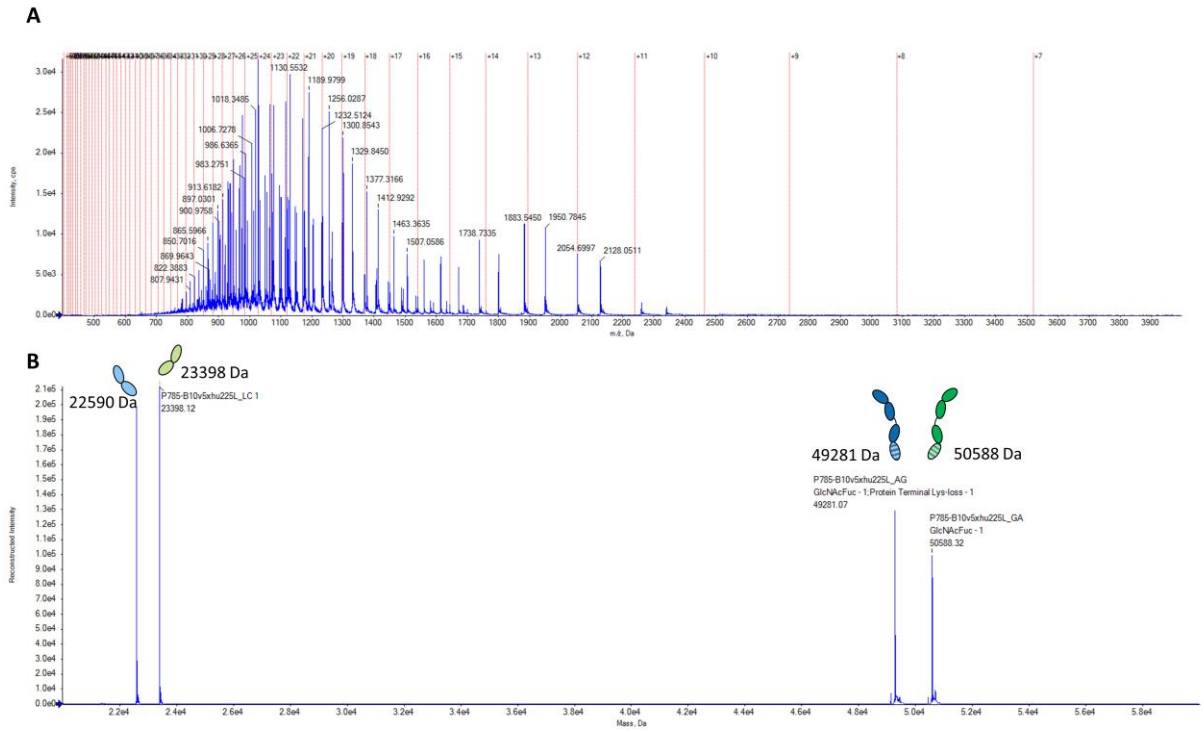

Figure S 8: Intact mass determination of reconstituted bsAb B10v5xhu225L by TOF-MS analysis under reduced conditions.

(A) Illustration of a full m/z spectrum for reconstituted bsAb B10v5xhu225L. **(B)** Intact reconstruction spectrum of reconstituted bsAb B10v5xhu225L.

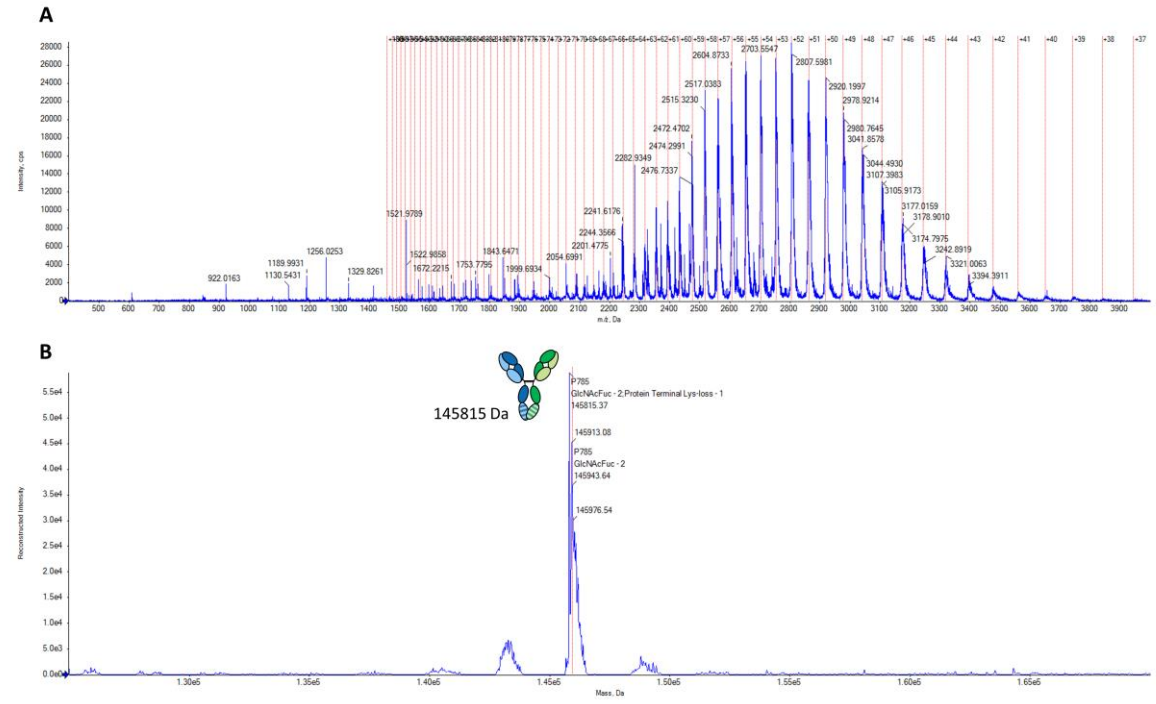

Figure S 9: Intact mass determination of reconstituted bsAb B10v5xhu225H by TOF-MS analysis under non-reduced conditions.

(A) Illustration of a full m/z spectrum for reconstituted bsAb B10v5xhu225H. **(B)** Intact reconstruction spectrum of reconstituted bsAb B10v5xhu225H.

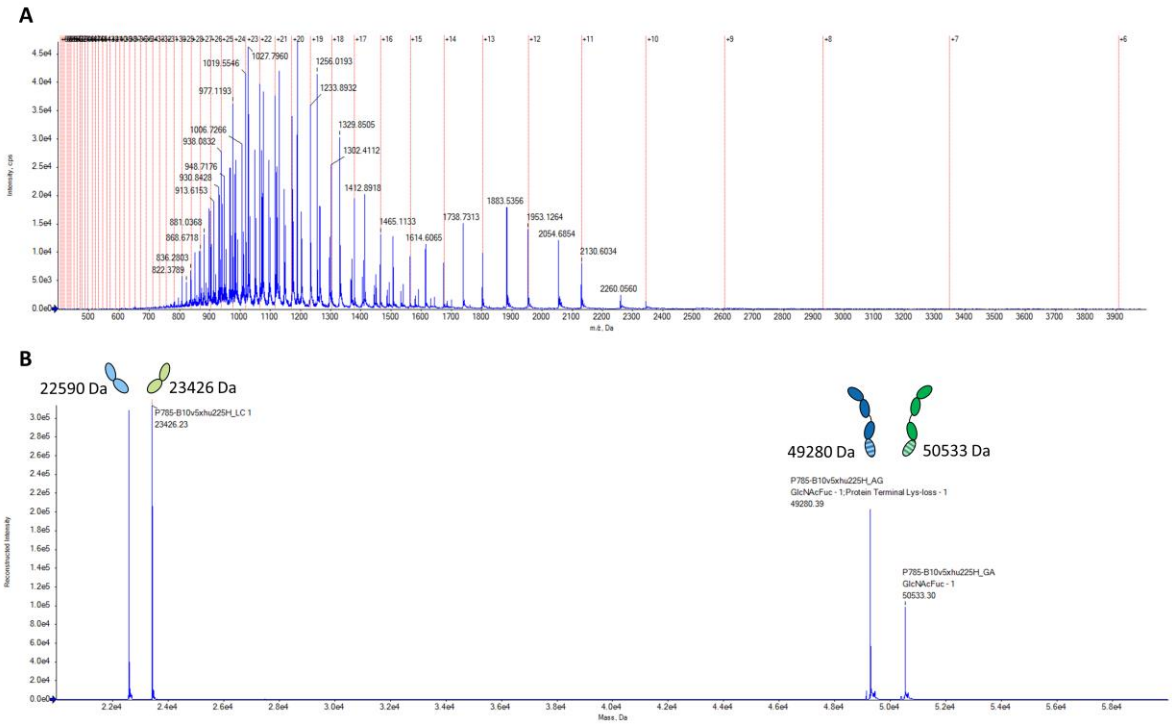

Figure S 10: Intact mass determination of reconstituted bsAb B10v5xhu225H by TOF-MS analysis under reduced conditions.

(A) Illustration of a full m/z spectrum for reconstituted bsAb B10v5xhu225H. **(B)** Intact reconstruction spectrum of reconstituted bsAb B10v5xhu225H.

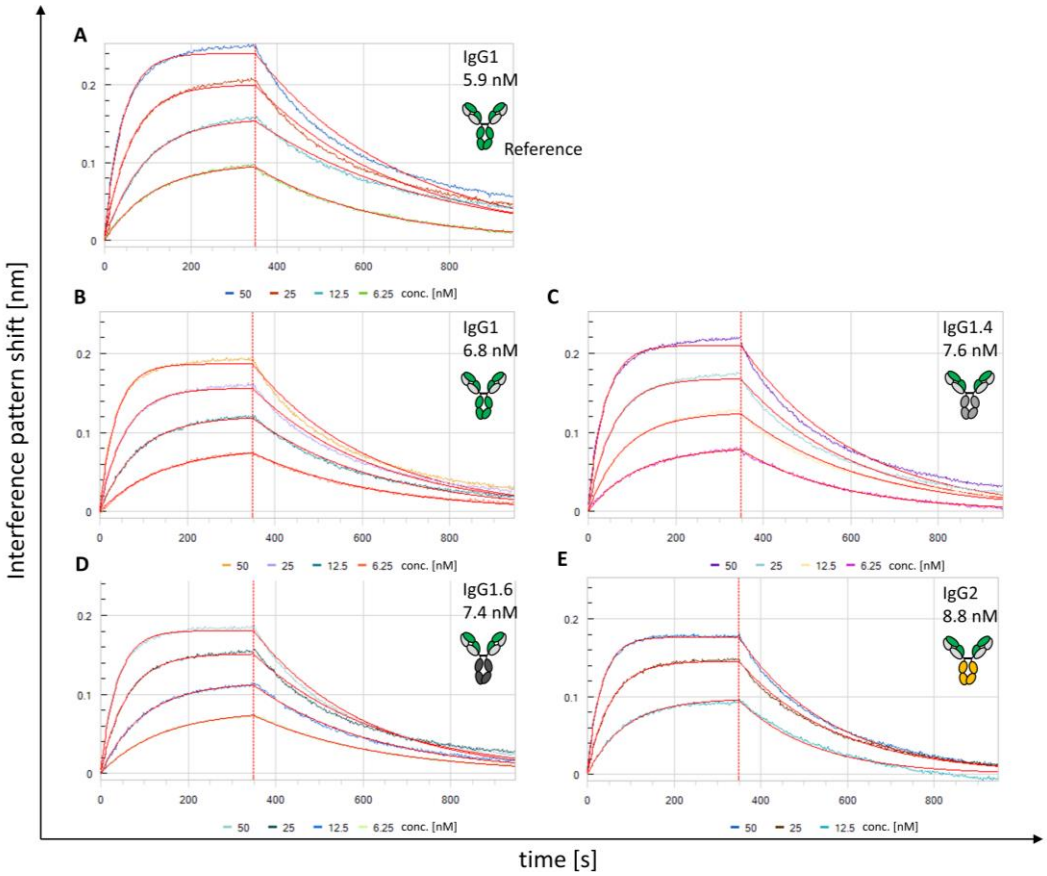

Figure S 11: Affinity comparison between reconstituted anti-CD40 mAbs and reference anti-CD40 (APX005M) binding to soluble recombinant human CD40 by BLI analysis.

Antibodies were analyzed with ProteinA biosensors. K_D was determined after 300 s association and 600 s dissociation with recombinant human CD40 and monitored with varying concentration of analyte antigen over time resulting in an interference pattern shift (nm). (**A**) K_D determination of reference antibody APX005M. (**B**) K_D determination of reconstituted anti-CD40 IgG1. (**C**) K_D determination of reconstituted anti-CD40 IgG1.4. (**D**) K_D determination of reconstituted anti-CD40 IgG1.6. (**E**) K_D determination of reconstituted anti-CD40 IgG2. All reconstituted anti-CD40 mAbs showed similar kinetic parameters to reference antibody APX005M.

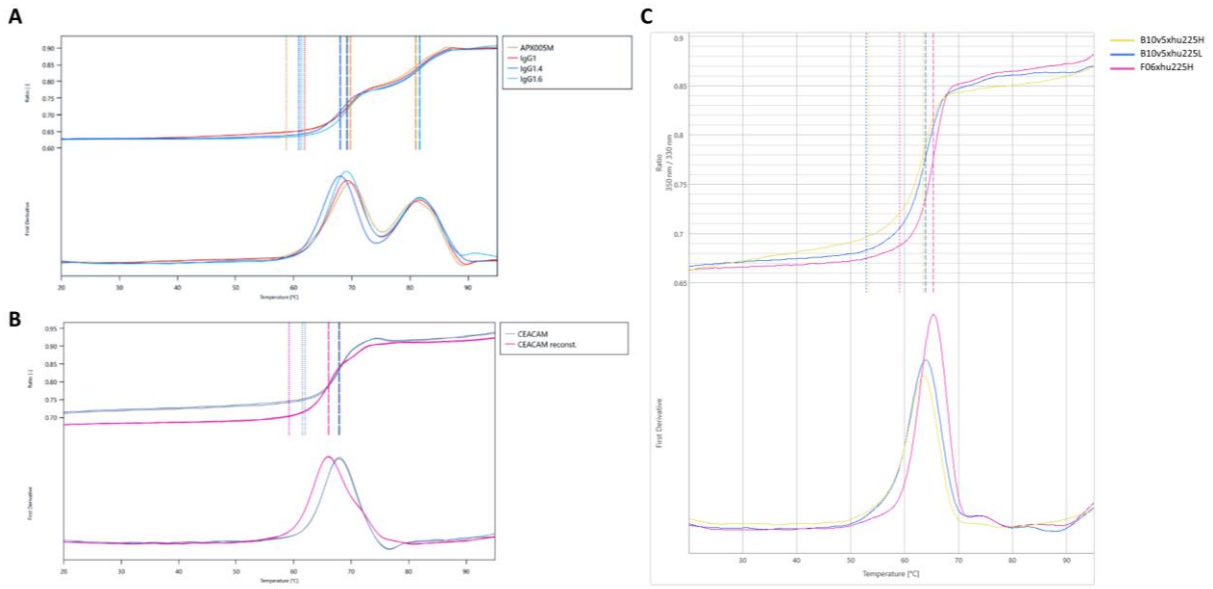

Figure S 12: DSF analysis of several reconstituted antibodies.

(A) Melting points of reconstituted anti-CD40 mAbs, reconstituted bsAb C5xC6 (**B**) and reconstituted bsAbs B10v5xhu225H and B10v5xhu225L (**C**) were determined by the maximum of the first peak at F330nm/F350nm ratio and compared to their reference antibodies.

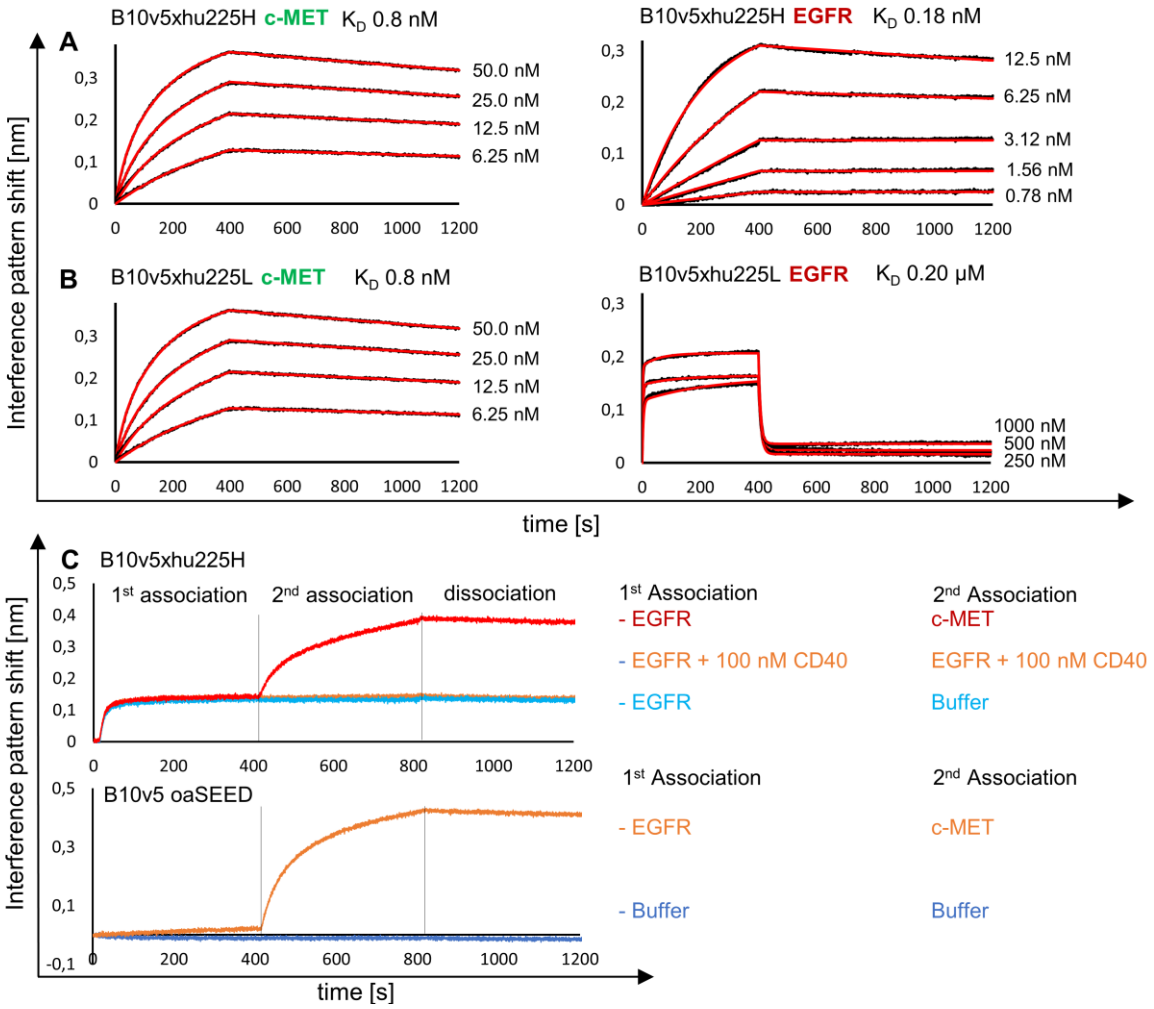

Figure S 13: Affinity determination of reconstituted c-METxEGFR antibodies B10v5xhu225H and B10v5xhu225L binding to soluble recombinant c-MET and EGFR by BLI analysis.

BsAbs were analyzed with ProteinA biosensor tips. K_D was determined after 400 s association and 1200 s dissociation of the respective antigens and monitored with varying concentration of analyte over time resulting in an interference pattern shift (nm). (**A**) K_D determination for reconstituted B10v5xhu225H bsAb binding to respective recombinant antigens. (**B**) K_D determination for reconstituted B10v5xhu225L bsAb binding to respective recombinant antigens. (**C**) Simultaneous binding of soluble recombinant c-MET and EGFR by reconstituted bsAb B10v5xhu225H. Both antigens c-MET and EGFR are associated stepwise. Reference antigen recombinant CD40 was used as a negative control in high concentration of 100 nM, to test unspecific binding response. No binding to recombinant EGFR was observed by monovalent oa B10v5 SEED.

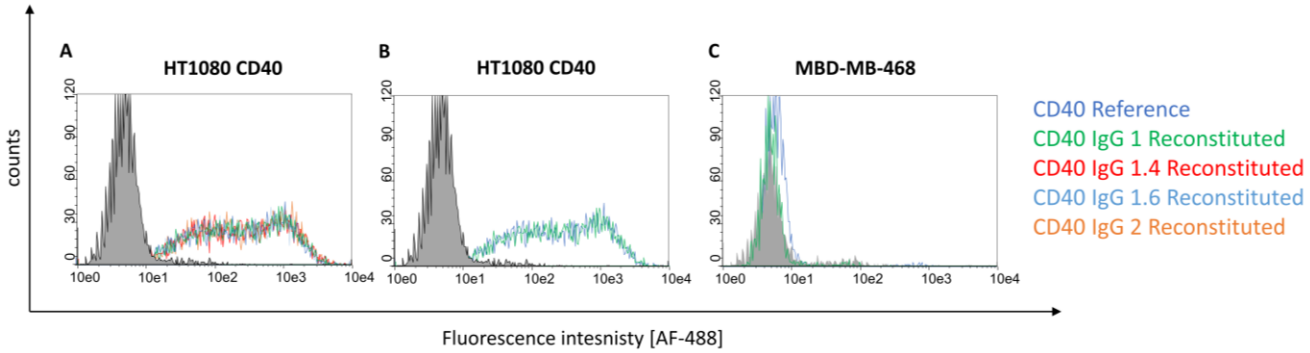

Figure S 14: Cellular binding of reconstituted anti-CD40 mAbs and anti-CD40 reference antibody (APX005M).

CD40 expressing cancer cell lines HT1080 and negative cell line MBD-MB-468 were incubated with 10 µg mL^{-1} antibodies for 1 h. Antibodies were detected with Alexa Fluor 488-conjugated anti-human IgG (H+L) Fab via FACS analysis. **(A)** Binding was observed with several reconstituted anti-CD40 mAbs. **(B)** Comparison of binding levels between reconstituted anti-CD40 IgG1 and reference anti-CD40 (APX005M). **(C)** Determination of unspecific binding for reconstituted antibodies on negative cell line MBD-MB-468. Analysis was conducted using the green fluorescent channel with adjusted forward and side scatter (Guava easyCyte HT cytometer). Blue: Reference anti-CD40 IgG (APX005M); Green: Reconstituted anti-CD40 IgG1; Red: Reconstituted anti-CD40 IgG1.4; Light blue: Reconstituted anti-CD40 IgG1.6; Orange: Reconstituted anti-CD40 IgG2.

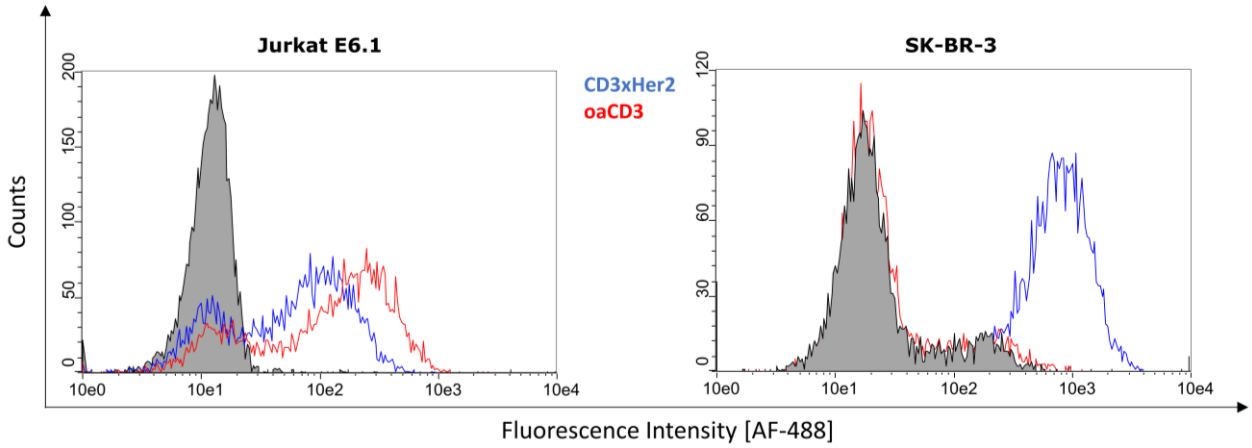

Figure S 15: Cellular binding of reconstituted bsAb CD3xHer2 TCE and monovalent oa CD3 SEED.

Her2 positive SK-BR-3 cancer cells and CD3 expressing Jurkat E6.1 cells were incubated with 10 µg mL^{-1} antibodies for 1h. Antibodies were detected with Alexa Fluor 488-conjugated anti-human IgG (H+L) Fab via FACS analysis. Binding was observed with reconstituted bsAb CD3xHer2 TCE on both antigens expressed on SK-BR-3 cancer cells and Jurkat E6.1 cells, while monovalent oa CD3 SEED was only binding to CD3 on Jurkat E6.1. Analysis was conducted using the green fluorescent channel with adjusted forward and side scatter (Guava easyCyte HT cytometer). Blue: Reconstituted CD3xHer2; Red: oa CD3 SEED; Black: Non-related isotype control (anti-HEL).

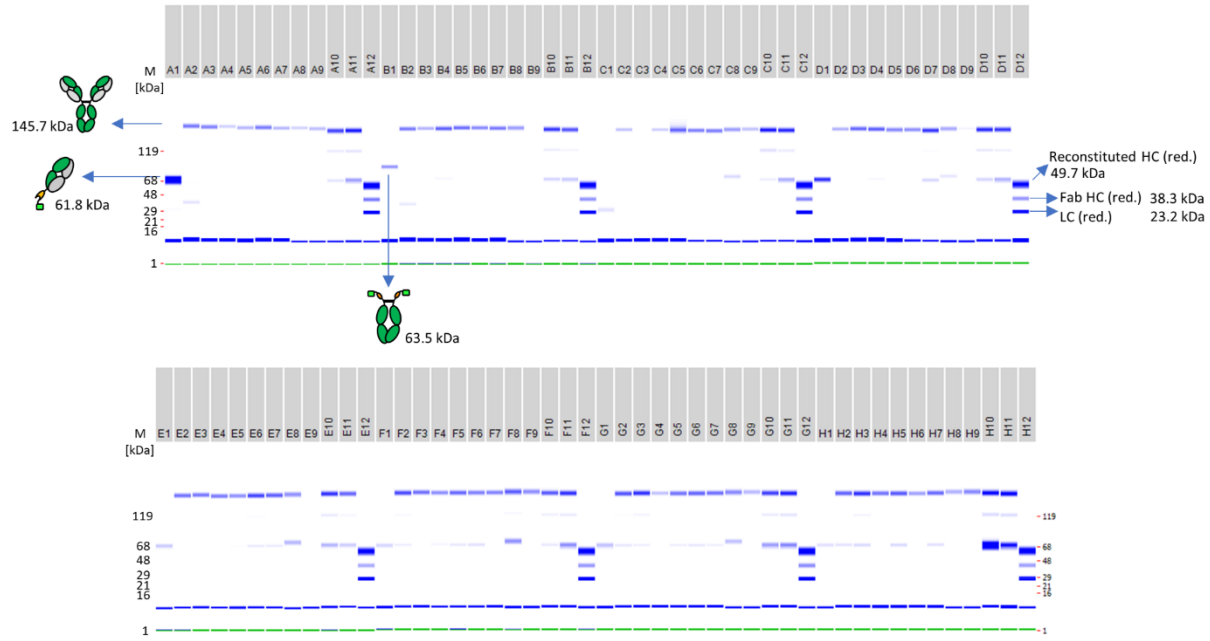

Figure S 16: Miniaturization of antibody reconstitution in 96 well format and demonstration of one-pot purification strategy.

A surplus of anti-CD40 Fab Int^N is used in a ratio 3:1 over huFc Int^C. Example for Panel A: A1: Single anti-CD40 Fab Int^N (61.5 kDa). B1: single huFc Int^C (63.5 kDa). A2 to A9: Antibody fragments anti-CD40 Int^N and huFc Int^C were mixed in a ratio 3:1 and 0.5 mM TCEP was added for PTS activation. Reconstituted antibodies were isolated from non-reconstituted antibodies anti-CD40 Fab Int^N and huFc Int^C by addition of 25 µL Ni^{2+} beads with a binding capacity of 40 µg 25 $µL^{-1}$ and further treated with a 10-fold molar excess of DHAA over TCEP for re-oxidation. Gel bands for reconstituted anti-CD40 antibodies were observed at 145.7 kDa under non-reduced conditions. A10-A11: Not treated with Ni^{2+} beads after reconstitution reaction, resulting in reconstituted anti-CD40 antibody as well as antibody fragments anti-CD40 Int^N and huFc Int^C. A12: Antibody fragments anti-CD40 Int^N and huFc Int^C after TCEP treatment without the addition of Ni^{2+} beads and DHAA (control). Gel panels B to H contain the same molecules compared to panel A. Gel band at 1 kDa (green): Lower Marker (LM). Blue band below 16 kDa: System Peak.

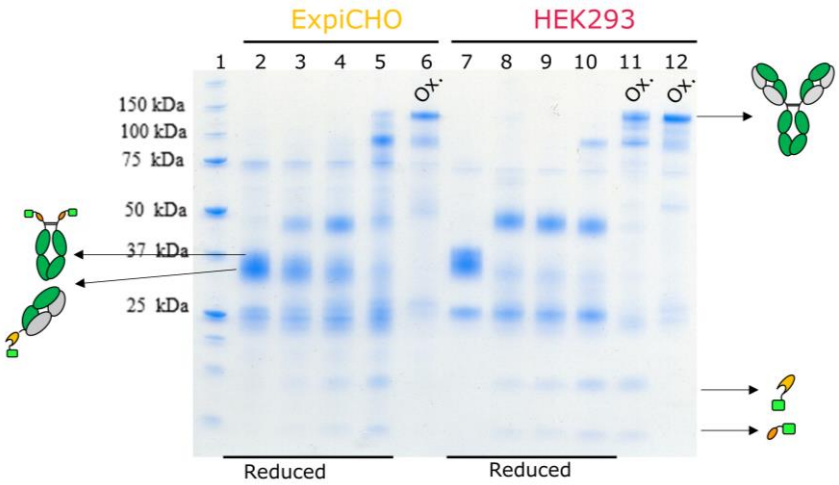

Figure S 17: Reconstitution determination directly during antibody fragment expression in conditioned HEK293 and ExpiCHO expression medium.

Purified antibody fragment anti-CD40 Fab Int^N was spiked into huFc Int^C expression after 5 days and treated with 2 mM TCEP to activate PTS. **Spiking into conditional ExpiCHO expression medium**: Lane 1: Marker; Lane 2: Antibody fragments anti-CD40 Fab Int^N and huFc Int^C at 0 h after TCEP addition. Lane 3: 1 h after TCEP addition; Lane 4: 2 h after TCEP addition; Lane 5: 24 h after TCEP addition; Lane 6: Treatment with 10 fold molar excess of DHAA over TCEP for 2h (re-oxidation); **Spiking into conditional HEK293 expression medium**: Lane 7: Antibody fragments anti-CD40 Fab Int^N and huFc Int^C at 0 h after TCEP addition. Lane 8: Reconstitution after 1 h; Lane 9: Reconstitution after 2 h; Lane 10: Reconstitution after 24 h; Lane 11: Treatment with 10-fold molar excess of DHAA over TCEP for 1h (re-oxidation); Lane 12: Treatment with 10-fold molar excess of DHAA over TCEP for 2 h (re-oxidation).

8.3. Supplemental Tables

Table S 1: Reconstituted mAbs and bsAbs and antibody fragments fused to their N-terminal or C-terminal split intein part were analyzed by mass spectrometry.

Antibody	Conditions	Theoretical mass [Da]	Measured mass [Da]
C5xC6 Reconstituted	Intact	147919	147926
B10v5xhu225L	Intact	145837	145840
B10v5xhu225H	Intact	145810	145815
F06xhu225L	Intact	146888	146891
Anti-CD40 IgG1 Reconstituted	Intact	146462	146461
Anti-CD40 IgG1.4	Intact	146184	146184
Reconstituted	Intact	146004	146006
Anti-CD40 IgG1.6 Reconstituted			
oa C5 Int^C GA	Reduced	32474	32475
oa C5 Int^C AG	Reduced	50084	50084
oa C5 Int^C LC	Reduced	23390	23390
C6 Fab Int^N HC	Reduced	38951	38951
C6 Fab Int^N LC	Reduced	23390	23390
oa F06 Int^C GA	Reduced	32474	32475
oa F06 Int^C AG	Reduced	50208	50208
oa F06 Int^C LC	Reduced	22711	22711
oa B10v5 Int^C GA	Reduced	32474	32474
oa B10v5 Int^C AG	Reduced	49278	49278
oa B10v5 Int^C LC	Reduced	22590	22590
hu225H Fab Int^N HC	Reduced	38411	38411
hu225H Fab Int^N LC	Reduced	23425	23425
hu225L Fab Int^N HC	Reduced	38465	38466
hu225L Fab Int^N LC	Reduced	23397	23397
CD40 Fab Int^N HC	Reduced	38288	38288
CD40 Fab Int^N LC	Reduced	23226	23226
huFc IgG1 Int^C HC	Reduced	32078	32079

8.4. List of Figures

8.5. List of Tables

8.6. Abbreviations

aa	Amino acid
ADC	Antibody-drug conjugate
ADCC	Antibody-dependent cellular cytotoxicity
AF488	Alexa Fluor 488
Amp	Ampicillin
APC	Antigen presenting cell
Asn	Asparagin
BCA	Bicinchoninic acid
BCR	B-cell receptor
BiTE	Bispecific T-cell engager
BLI	Biolayer interferometry
BSA	Bovine serum albumin
BsAb	Bispecific antibody
C225	Cetuximab
CDC	Complement-dependent cytotoxicity
CDR	Complementarity determining region
cFAB	Controlled Fab arm exchange
c-MET	Tyrosine protein kinase / hepatocyte growth factor
C5	CEACAM5; Carcinoembryonic antigen-related cell adhesion molecule
C6	CEACAM6
CD3	Cluster of differentiation
CD40	Cluster of differentiation
CH1-3	Constant domain 1-3 of the heavy chain
CIP	Antarctic phosphatase
cLC	Common light chain
CnaB2	Collagen adhesion domain
CTLA4	Cytotoxic T lymphocyte-associated antigen 4
CV	Column volume
Da	Dalton
DAR	Drug-to-antibody ratio
dH_20	Distilled water
DNA	Deoxyribonucleic acid
DnaE	Catalytic α subunit of DNA polymerase III
DTT	Dithiothreitol
ECD	Extracellular domain
E. coli	*Escherichia coli*
EGFR	Epidermal growth factor receptor

ELISA	Enzyme-linked immunosorbent assay
EPL	Expressed Protein Ligation
EpCAM	Epithelial cell adhesion molecule
Fab	Fragment antigen binding
FACS	Fluorescence activated cell sorting
FbaB	Fibronectin binding protein
Fc	Fragment crystallizable
FcRn	Neonatal Fc receptor
FcγR	Fcγ receptor
FCS	Fetal calf serum
FDA	Food and Drug Administration
FR	Framework
HAMA	human anti-mouse antibodies
h	Hour
HC	Heavy chain
HCC	Hepatocellular carcinoma
HER	Human epidermal growth factor receptor
HGF	Hepatocyte growth factor
HIC	Hydrophobic interaction chromatography
His-tag	Histidine tag, usually composed of six histidines
HPLC	High performance liquid chromatography
HRP / POD	Horseradish peroxidase
HT	High throughput
HTS	High throughput screening
HTRF	Homogenous Time Resolved Fluorescence
hu	Human
Ig	Immunoglobulin
IMAC	Immobilized metal ion affinity chromatography
Int^N	N-terminal split intein part
Int^C	C-terminal split intein part
ka	Association rate constant
KB	Kinetics buffer
KD	Equilibrium dissociation constant
kd	Dissociation rate constant
KiH	Knobs into holes
LB medium	Luria-Bertani medium
LC	Light chain
LDS	Lithium dodecyl sulfate

mAb / pAb	Monoclonal antibody / polyclonal antibody
MALDI-TOF	Matrix-assisted laser desorption/ionization time of flight mass spectrometry
MS	Mass spectrometry
MCS	Multiple cloning site
mTGase	Microbial transglutaminase
mu	Murine, mus musculus
MWCO	Molecular weight cut-off
NBE	New biological entity
n.d.	Not determined
NC	Nitrocellulose
nCL	Native chemical ligation
NEAA	Non-essential amino acids
NK	Natural killer cells
Npu	Cyanobacterium Nostoc punctiforme
oa	One-armed
OD	Optic density
OKT3	Orthoclone; Muromonab-CD3
PAMPs	Pathogen-associated molecular patterns
PBS	Phosphate buffered saline
PCR	Polymerase chain reaction
PD-1	Programmed cell death protein 1
PD-L1	Programmed cell death protein ligand 1
PDB	Protein Data Bank
PVDF	Polyvinylidene fluoride
PTS	Protein-trans-splicing
RFU	Relative fluorescence units
RIPA buffer	Radioimmunoprecipitation assay buffer
rpm	Revolutions per minute
RT	Room temperature
scFv	Single-chain variable fragment
s.d.	Standard deviation
SDS	Sodium dodecylsulfate
SEC	Size exclusion chromatography
s	second
SEED	Strand exchange engineered domain
Srt	Sortase
Ssp	Cyanobacterium synechocystis

TCEP	Tris(2-Carboxyethyl) phosphine
TCR	T-cell receptor
TG	Transglutaminase
TFF	Tangential Flow Filtration
TLR	Toll-like receptor
Tm	Melting temperature
TME	Tumor microenvironment
Tris	Tris(hydroxymethyl)aminomethane
US	United States
v/v	Volume per volume
VDJ	Somatic recombination
VEGF	Vascular endothelial growth factor
VH	Variable domain of the heavy chain
VL	Variable domain of the light chain
w/v	Weight per volume
wt	Wild type

8.7. Acknowledgment

I would like to use the opportunity to thank several people who deserve to be mentioned explicitly during the last years of my PhD venture. First, I am indebted to my Doktorvater and academic supervisor Prof. Dr. Harald Kolmar for giving me the opportunity to be part of his group at the biochemical Institute in Darmstadt. I highly appreciate the scientific discussions and the support throughout the last years, as well as the seminars and excursions I was able to participate.

Likewise, I want to express my gratitude to Dr. Lars Toleikis, who welcomed me in the Protein Engineering and Antibody Technology group at Merck to conduct my experiments in his laboratories and for the admission to his team and the constant support within the scope of my PhD. I thank him for also giving me opportunities to promote my work at several conferences.

Furthermore, I want to thank Prof. Dr. Michael Hust for taking over the part as the second reviewer and thank him for scientific advice and discussions. I thank Prof. Dr. Siegfried Neumann and Prof. Dr. Johannes Kabisch for their willingness to serve as expert examiners. I also extent my gratitude to Prof. Dr. Prechtl as the chairperson of my dissertation committee.

I would particularly like to thank Dr. Mark Schütte for taking care of my supervision and his time and guidance at work and beyond and for always be willing to offer unceasing encouragement, support and assist until submission of my masterpiece. On the same token, I'd like to thank my supervisor Dr. Achim Doerner for fruitful scientific discussions and creative ideas to make this project become as outstanding as it is now. In addition, I would like to extend my thanks to Thomas Rysiok and Dr. Stefan Becker for taking over my supervision and supporting me throughout the last period of my PhD. Especially my gratitude belongs to Thomas Rysiok as my former boss and mentor at Merck. Everything started in his group and I am more than happy that he joined my journey until the end of this project. Exceeding gratitude goes to Dr. Janis Rosskopf and Oliver Edler for proofreading my thesis and for scientific input.

I would also like to thank all the people from the PEAT and ADC department at Merck and my work group at the technical university of Darmstadt. Many people have directly or indirectly supported this project enormously by introducing new methods or providing materials or instruments. The lab of Jan-Carsten Pieck, Elke Ciesielski and Johannes Schmidt for introducing me into the robotic world and supporting me to automate my methods. I like to thank the group of Dr. Stefan Becker, especially Kerstin Hallstein for teaching me to master BLI experiments. I appreciate Dominik Reitz and Ramona Gaa for their experimental contribution to my PhD project.

Very special thanks to my former colleagues from the upstream development group of Thomas Rysiok, Oliver Edler, Marion Sauer and Elvira Meißen for their outstanding support in antibody expression during my PhD and beyond. I felt always welcomed and appreciated in your group and will miss working and hanging out with

you. In addition, I want to thank the entire "Expressionisten-Gedächntisgruppe" extended by Gernot Musch, Ulrike Bode and Beatrix Böckler for cheerful events, support and still making me feel as a part of the group. Sincere thanks to Jacqueline Buttler for her support throughout my PhD, listening to my concerns, volunteering to offer me her office space and helping me out to make the right decisions. Dirk Müller-Pompalla, Stephan Keller, Alexander Müller and Sigrid Auth for exceeding support in antibody purification and analytics. A major part of my project was conducted in this laboratory and tremendously improved the quality of this work. I was able to extend my skill repertoire and it was really a pleasure to work there. Especially I thank Stephan and Alexander for always taking care, creating an outstanding work environment and planning hilarious events.

The laboratory of Dr. Nicolas Rasche, especially Jens Hannewald as my local TCEP and DHAA dealer. Without his support antibody reconstitution never would have been a success.

The group of Dr. Roland Kellner, including Claudia Kubis, Dr. Jason Tonillo, Amanda Vanselow and Jennifer Schanz for their support in mass spectrometry analysis. Marion Wetter and Pia Stroh, I would like to thank for their support and patience of my never-ending requests for HEK cells.

I thank Dr. Friedrich Rippmann for advice in computational and molecular design of my antibody constructs. My collaborators Oliver Rammo and Bianca Edelmann for fruitful scientific discussions about Inteins and experimental support. Dr. Carolin Sellmann, Dr. Simon Krah and Dr. Stefan Zielonka for their scientific input in antibody engineering and construct design.

I would like to thank my PhD compassionate colleagues and former colleagues Dr. Janis Rosskopf, Sebastian Jäger, Marie Quillmann, Anna Kaempffe and Lukas Pekar for their encouragement, support, advice and the calm work environment. You really made this journey worthwhile. Dr. Marcel Rieker for his creative mind and ideas, interesting discussions, guidance and support in HTRF analysis. Dr. Jean Wakim and Dr. Dmitry Zabeszhinsky for interesting conversations, advice and support. I wish we would have got in touch earlier.
I thank all the members and alumni members of the AK Kolmar group for scientific discussions, seminars and excursions and several events. Especially Arturo Macarron, Steffen Hinz, Adrian Elder, as well as Sandra Müller, Markus Lubda, Martina Zimmermann and Gregory Som from the Merck side.

My sincerest thanks and appreciation to my entire Canadian family, especially to John, Lucila, Alvin and "The Beatles" for their support, energy and constant encouragement over the last years. I thank my girlfriend Swantje for her unconditional support and understanding during my educational career in the last years. You always gave me strength and new courage to realize my goals. Finally, I would like to thank my mom Astrid who sacrificed everything to enable me my studies and finally my PhD. Thank you for your endless support, guidance and inspiration throughout my life. I dedicate this doctoral degree to you.

9. Affirmations

Tim Lothar Hofmann

_____
(Datum)

Erklärung
Ich erkläre hiermit, dass ich meine Dissertation selbstständig
und nur mit den angegebenen Hilfsmitteln angefertigt habe.

_____
(Tim Hofmann)

Tim Lothar Hofmann

_____
(Datum)

Erklärung
Ich erkläre hiermit, noch keinen Promotionsversuch unternommen zu haben.

_____
(Tim Hofmann)

Tim Lothar Hofmann

_____
(Datum)

Erklärung

Ich erkläre hiermit, dass die elektronische Version der Doktorarbeit mit der schriftlichen Version übereinstimmt. Die elektronische Version liegt dem Prüfungssekretariat vor.

_____
(Tim Hofmann)